The Dissertation Committee for Kaci Leigh Erwin Certifies that this is the approved version of the following Dissertation:

Investigation of the Ring-Cleaving Dioxygenase and Hydratase-Aldolase Reactions in the *Mycobacterium vanbaalenii* PYR-1 Catabolic Pathways

Committee:

Christian P. Whitman, Supervisor

Walter L. Fast

David W. Hoffman

Hung-wen (Ben) Liu

Yan (Jessie) Zhang

Investigation of the Ring-Cleaving Dioxygenase and Hydratase-Aldolase Reactions in the *Mycobacterium vanbaalenii* PYR-1 Catabolic Pathways

by

Kaci Leigh Erwin

Dissertation

Presented to the Faculty of the Graduate School of

The University of Texas at Austin

in Partial Fulfillment

of the Requirements

for the Degree of

Doctor of Philosophy

The University of Texas at Austin

August 2018

Abstract

Investigation of the Ring-Cleaving Dioxygenase and Hydratase-Aldolase Reactions in the *Mycobacterium vanbaalenii* PYR-1 Catabolic Pathways

Kaci Leigh Erwin, Ph.D.

The University of Texas at Austin, 2018

Supervisor: Christian P. Whitman

Polycyclic aromatic hydrocarbons (PAHs) are ubiquitous environmental pollutants made of fused aromatic rings. The improper disposal of petrochemicals is a major source of PAHs in the environment. They are generally recalcitrant due to their stability and poor water solubility. Degradation of PAHs by bacteria and other microorganisms is one way to remove PAHs from contaminated environments. *Mycobacterium vanbaalenii* PYR-1 is the first identified bacterium with the ability to completely degrade pyrene. In addition, *M. vanbaalenni* PYR-1 can degrade a variety of PAHs and, in this regard, is the most nutritionally versatile bacteria isolated so far. The degradation of PAHs by *M. vanbaalenni* PYR-1 has been extensively studied with many proposed avenues leading to useful cellular intermediates. However, there is very little biochemical evidence for many of these pathways.

The degradative pathways for naphthalene, phenanthrene, pyrene, and fluoranthene were examined. Within the naphthalene catabolic pathway, no enzymes have been assigned to the ring-opening of 1,2-dihydroxynaphthalene or the hydration and retro-aldol cleavage

of *trans*-*o*-hydroxybenzylidenepyruvate. Within the phenanthrene catabolic pathway, 1-hydroxy-2-naphtoate and *trans*-*o*-carboxybenzylidenepyruvate are thought to be processed by the enzymes designated PhdI and PhdJ, respectively. The results show that PhdI ring-opens 1-hydroxy-2-naphthoate but not 1,2-dihydroxynaphthalene. The hydratase-aldolase PhdJ processes both *trans*-*o*-hydroxybenzylidenepyruvate and *trans*-o-carboxybenzylidenepyruvate but prefers *trans*-o-carboxybenzylidenepyruvate. Ring-opening of both 3,4-dihydroxyphenanthrene and 9,10-dihydroxyphenanthrene, intermediates in the phenanthrene catabolic pathway, have previously been assigned to PhdF. However, the results show that PhdF catalyzes the ring-opening of 3,4-dihydroxyphenanthrene but not 9,10-dihydroxyphenanthrene. We also show that the product of the PhdF-catalyzed reaction using 3,4-dihydroxyphenanthrene is processed by PhdG, the enzyme proposed to do this reaction. Finally, PhdF was reported to catalyze all ring-opening reactions in the upper catabolic pathways for pyrene and fluoranthene. We find that PhdF does not catalyze any of these proposed reactions in the pyrene pathway and investigations in the fluoranthene pathway are ongoing.

The sum of our observations clarifies the reaction pathways for the degradation of naphthalene, phenanthrene, pyrene, and fluoranthene in *M. vanbaalenii* PYR-1. This work sets the stage for detailed mechanistic studies of the individual enzymes. This knowledge, combined with the considerable body of literature on PAH degradation pathways, could guide the development and optimization of bioremediation technologies.

Table of Contents

List of Tables

List of Figures

List of Schemes

Chapter 1: Introduction

1.1 Pollutants

a. General

A pollutant is defined as a harmful substance with an unnatural presence or elevated concentration in an environment or organism (Mathew, 2017). Pollutants impact all environments, including air through greenhouse gases and particulate matter, soil through pesticide use, improper disposal of toxic chemicals, and non-biodegradable material, and water through oil spills and runoff from contaminated soils (Gavrilescu, 2010). The pollutants with the highest impact are consequences of an increase over the last century in human activities such as urbanization, transportation, industry, and agriculture (Gavrilescu, 2010). By 2000, the global chemical production reached 400 million tons per year, with 50% of these chemicals considered environmentally harmful (World Wide Fund, 2018). The toxic, persistent, and pervasive characteristics of pollutants can originate from the parent pollutant or from a byproduct during pollutant degradation (Mathew, 2017). The Stockholm Convention of the United Nations Environment Program labels the most toxic of pollutants as persistent organic pollutants (POPs) (UNEP, 2001). POPs are defined as organic substances that are persistent in the environment by remaining intact for many years, capable of traveling long ranges through air, soil, or water, capable of bioaccumulation, and toxic to humans and wildlife (UNEP, 2001). A list of these compounds can be found in Table 1.1 (Megson, 2016). Unfortunately, pollution remains a threat due to the lack of risk assessment for many human processes and the lack of proper and adequate prevention or remediation methods (Gavrilescu, 2015).

Annex	Priority Pollutant	
Original List 2001	Chlordane	Toxaphene
	Dieldrin	DDT
	Endrin	Polychlorinated biphenyls
	Heptachlor	Polychlorinated dibenzo-p-dioxins
	Hexachlorobenzene	Polychlorinated dibenzofurans
	Mirex	
Added May 2009	Hexachlorocyclohexane	Pentchlorobenzene
	Chlordecone	Tetrabromodiphenyl ether
	Hexabromobiphenyl	Pentabromodiphenyl ether
	Hexabromodihpenyl ether	Perfluorooctanesulfonic acid
	Heptabromodiphenyl ether	Perfluorooctanesulfonyl fluoride
	Lindane	
Added May 2011	Endosulfan	
Added May 2013	Hexabromocyclododecane	
Added May 2015	Hexachlorobutadiene	
	Pentachlorophenol	
	Polychlorinated naphthalenes	
Under Review	Decabromodiphenyl ether	
	Dicofol	
	Short-chain chlorinated paraffins	
	Pentadecafluorooctanoic acid	

Table 1.1: POPs list from the Stockholm convention (adapted from Megson, 2016).

b. Polycyclic Aromatic Hydrocarbons

Polycyclic aromatic hydrocarbons (PAHs) are ubiquitous, carcinogenic pollutants made up of fused aromatic rings (Kaushik, 2006). PAHs are created through incomplete combustion of fuels such as coal, petroleum, oil, and wood. Natural exposure occurs through forest fires, oil seeps, and volcanic eruptions, but most environmental exposure is the result of human processes (Kaushik, 2006; Goldberg, 1971). A list of these processes is given in Table 1.2 (Duan, 2015).

Industrial Activities	Predominant PAHs
Gasification/liquefaction of fossil fuels	Fluoranthene, pyrene, chrysene, benzo(a)pyrene
Coke production	Anthracene, phenanthrene, benzo(a)pyrene
Catalytic cracking	Fluoranthene, pyrene, benzo(b)fluoranthene, benzo(k)fluoranthene, thiophene compounds
Carbon-black production/use	Fluoranthene, benzo(a)pyrene
Asphalt production/use	Fluoranthene, pyrene, chrysene, benzo(a)pyrene
Coal-tar/coal-tar-pitch production/use	Fluoranthene, phenanthrene, pyrene
Crude oil refining/distillation	Pyrene, benzo(a)pyrene
Wood-preservative/combustion	Fluoranthene, benzo(a)pyrene
Fuel/oil storage, transportation, processing, use, disposal	Fluoranthene, pyrene, benzo(b)fluoranthene, benzo(k)fluoranthene, thiophene compounds
Open burning	Phenanthrene, anthracene
Incineration	Fluoranthene, phenanthrene, pyrene

Table 1.2: Industrial activities associated with PAH production (adapted from Duan, 2015).

Human exposure occurs primarily through inhalation of automobile exhaust, tobacco smoke, wood smoke, and consumption of charcoal-broiled foods or foods that have bioaccumulated the toxin (U.D.H.H., 1995). PAHs share characteristics with POPs and the two pollutant groups are often jointly monitored and regulated (EPA POP; Farrington, 2014). PAHs account for 16 of the 129 compounds on the EPA's priority pollutant list subject to regulation and testing (EPA Priority). A list of the PAHs on the priority pollutant list is given in Table 1.3 (Louvado, 2015). Of the 1408 waste sites that are classified as hazardous and targeted for long-term cleanup by the EPA in 2016, at least 600 are contaminated with various forms of PAHs (EPA Priorities).

EPA Priority PAH		Half-life (days)	EPA Priority PAH		Half-life (days)
Naphthalene		5.56	Pyrene	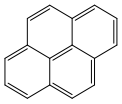	283.4
Acenaphthene		18.77			
Acenaphthylene		30.7	Benzo(a)pyrene	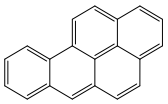	421.6
Anthracene	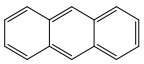	123	Benzo(b)fluoranthene	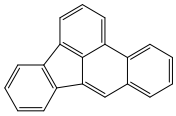	284.7
Phenanthrene	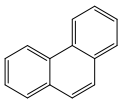	14.97	Benzo(k)fluoranthene	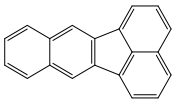	284.7
Fluorene	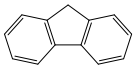	15.14	Dibenzo(a,h)anthracene	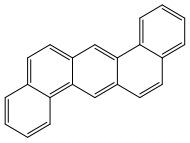	511.4
Fluoranthene	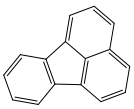	191.4			
Benzo(a)anthracene	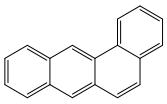	343.8	Benzo(g,h,i)perylene	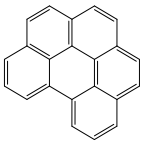	517.1
Chrysene	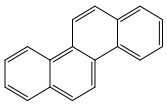	343.8	Indeno(1,2,3-c,d)pyrene	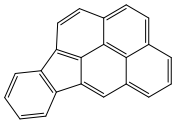	349.2

Table 1.3: PAHs on the EPA's priority pollutant list with estimated half-lives in soil (Adapted from Louvado, 2015).

PAHs with 3 or fewer rings are considered low molecular weight (LMW) while those with 4 or more rings are considered high molecular weight (HMW). The LMW PAHs have high toxicity, volatility and solubility while those with HMW have low volatility, low solubility and are carcinogenic. When exposed to mammals, cytochrome p450 as well as other mammalian monooxygenases can convert PAHs to highly reactive epoxides that are capable of binding DNA with the potential to cause mutations (Nesnow, 2000). When exposed to the environment, PAHs undergo several fates that include photooxidation, chemical oxidation, hydrolysis, bioaccumulation, biodegradation, volatilization, and adsorption (DiBlasi, 2008). LMW PAHs are lost through volatization, processing by organisms (bacteria, fungus, plants), or oxidation while HMW PAHs adhere to soil particulates due to their hydrophobic nature. Adsorption of HMW PAHs leads to low bioavailability and increased recalcitrance that results in accumulation. For example, a 3-ring PAH will typically have a half-life in soil of 12 to 126 days while a 5-ring PAH can have a half-life of up to 1400 days (Shuttleworth, 1995). Almost 90% of PAH contamination is present in soil, but contamination in oceans does occur due to run off from contaminated rivers, seepage at deep sea vents, and oil spills at ocean surfaces (Wild, 1995). After the Deepwater Horizon oil spill in 2010, HMW PAHs represented 31% of the total PAH contamination while HMW PAHs represented only 8% of PAHs in crude oils (Boehm, 2011). Due to their recalcitrance, HMW PAHs constitute over 80% of PAH pollution at contaminated sites (Kuppusamy, 2017).

1.2 Polycyclic Aromatic Hydrocarbon Bioremediation

a. Whole-Cell Bioremediation

Excavation and filling of contaminated sites were the major route of remediation until the late 1990s (Kuppusamy, 2017). The development of alternative technologies resulted in physical remediation through washing and fixation, chemical remediation through extraction and dechlorination, thermal remediation through incineration and desorption, photooxidation, and bioremediation (Ghosal, 2016; Lamichhane, 2017). Bioremediation is preferred over chemical and physical remediation methods because it is a more efficient and environmentally-friendly option (Lamichhane, 2017). Owing to these benefits, research on microbes capable of degrading PAHs for the end-purpose of bioremediation has increased (Lamichhane, 2017).

Through 3.5 billion years of evolution, microbes have acquired the genetic and functional diversity to adapt to almost any environment, even those unsuitable for most other organisms (Sogin, 2006). Microbes make up 60% of Earth's biomass and are found in the most extreme environments (Nikolaivits, 2017). It is fitting that the task of not only surviving but of interacting and altering environments deemed toxic to most organisms would fall to microbes. Upon exposure of an environment to a foreign, toxic compound, the distribution of microbes shifts to become dominated by those with the ability to degrade or accumulate the toxin (Vila, 2010). As the toxin level decreases, the composition of the microbial community shifts back towards its natural balance (Vila, 2010). While microbes will naturally adapt to and alter a contaminated environment, this process is usually slow and allows for the accumulation of toxic intermediates that other, less-resilient organisms cannot tolerate. Bioremediation is a process that takes advantage of a microbe's

natural ability to restore an environment to pre-contaminated conditions by either supplying necessary nutrients that are limited in the environment (biostimulation) or by introducing exogenous microorganisms already optimized for degradation of the specific contaminant (bioaugmentation) (Mohan, 2006). Bioremediation may be performed at the site of contamination (*in-situ*), or the contaminated medium may be relocated for processing (*ex-situ*). *In-situ* processes are preferred because they are more environmentally- and economically-friendly, but they require more time for complete treatment (Perpetuo, 2011). Figure 1.1 gives examples of bioremediation techniques (Azubuike, 2016). When choosing a bioremediation technique, it is important to consider location, cost, environment type, pollutant characteristics, and the degree of pollution (Azubuike, 2016).

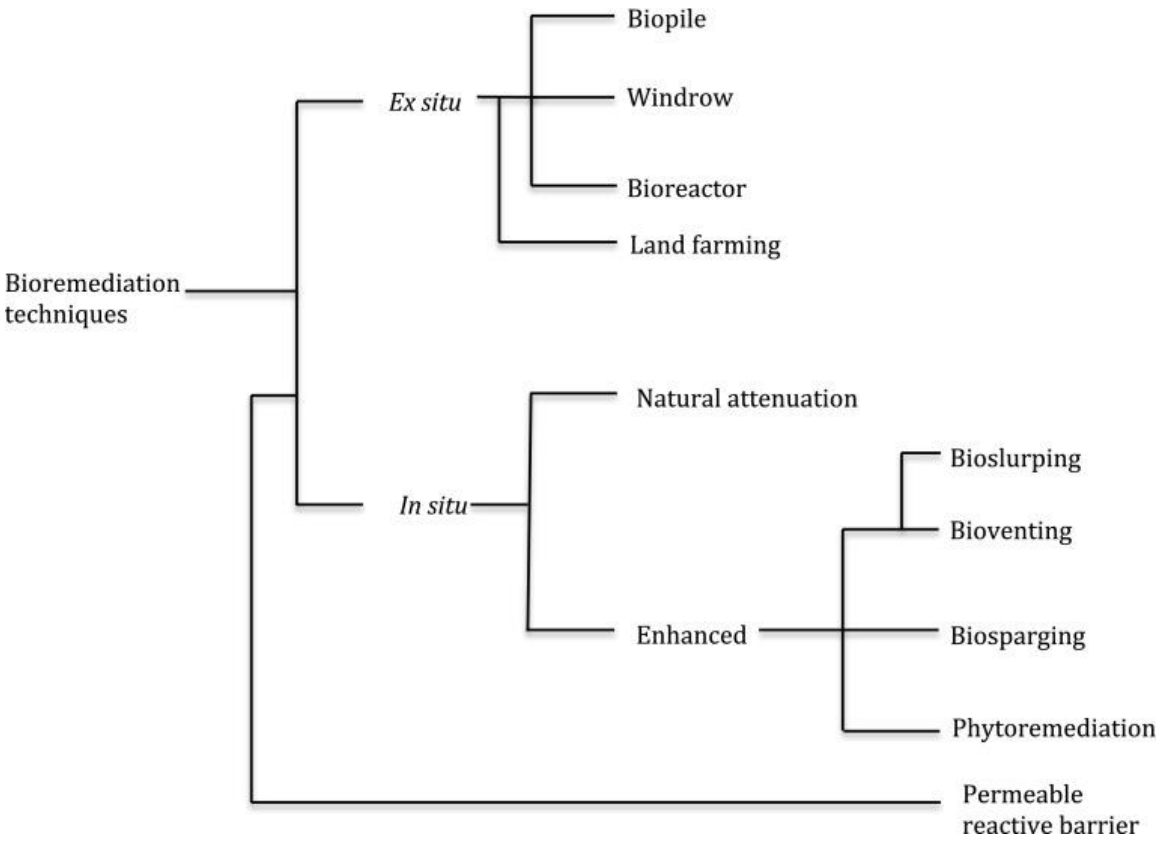

Figure 1.1: Bioremediation techniques (Azubuike, 2016).

Biostimulation is used when the contaminated environment is inhabited by microorganisms capable of PAH degradation. Nutrients to stimulate growth, cofactors required for the degradation process, or surfactants to solubilize contaminants are added to increase the rate of remediation. Sun et al. showed that the addition of nitrogen and phosphate to soil from a contaminated coking plant in Beijing increased overall PAH degradation by 10% after 175 days when compared to degradation from the unadulterated soil (Sun, 2012). Bioaugmentation is used when PAH-degrading bacteria are not present in these contaminated sites or when bioavailability is a limiting factor for remediation (Kuppusamy, 2017). The microbial species used for bioaugmentation is dependent on the microbe's nutrient, oxygen, pH, and temperature requirements (Liu, 2017). Marine bacteria are commonly used for bioaugmentation because of their ability to thrive in a wide range of environmental conditions (low temperatures, high pressures, variable light intensities) (Nikolaivits, 2017). When bioavailability is a limiting factor, microbial strains able to produce biosurfactants capable of solubilizing and therefore increasing the bioavailability of PAHs may be used (Pedetta, 2013). When the biosurfactant-producing *Pseudomonas aeruginosa* organism was added to PAH-contaminated soil from a wood preservation factory in the U.S., the overall degradation of PAH increased 5 times that of the control soil-only sample after 14 days (Straube, 1999). A mix of microbial species may be used to provide necessary nutrients or minimize the accumulation of toxic intermediates through crossfeeding (Bouchez, 1999). The highest degradation rate of PAHs recorded was achieved using a mixture of *Pseudomonas*, *Cupriavidus*, and *Bacillus* strains isolated from a contaminated manufactured gas plant site in Australia (Kuppusamy, 2016). This mixture degraded PAHs 44% faster than a sample of control soil. While bioaugmentation is an effective process, the remediation rate for HMW PAHs is typically still slow

compared to LMW PAHs. In a study by Kuppusamy (2016), complete degradation of both LMW and HMW PAHs was achieved using a consortium of microbes, but the degradation of the HMW PAHs benzo[a]pyrene and pyrene took 17 and 4 times longer respectively than that of the LMW PAH phenanthrene.

b. Genetically Modified Microorganisms in Bioremediation

Most contamination sites are polluted with multiple compounds which presents a challenge. While it is possible for microbes present at contaminated sites to evolve the ability to degrade the mixture, the evolution process is frequently slow and may not occur at all (Cases, 2005). Bioaugmentation may not be feasible in some environments due to competition and lack of available resources (Cases, 2005). Identification of catabolic gene clusters and knowledge of their regulation as well as a sufficient understanding of the function, regulation, and stability of their associated enzymes allows for the construction of genetically modified microorganisms (GMMs) that can be used to enhance bioaugmentation (Wasilkowski, 2012). GMMs are used for optimized multi-toxin degradation without accumulation of toxic intermediates or energy loss due to increase in biomass (Kuppusamy, 2017). GMMs used in bioremediation will have new catabolic pathways, optimized inherent catabolic activities, or biosensing abilities (Kuppusamy, 2017; Wasilkowski, 2012; Timmis, 1999). GMMs used for bioaugmentation will typically have catabolic genes and gene clusters capable of complete degradation of a contaminant incorporated into the genome of an indigenous microbe under the control of a strong promoter (Cases, 2005). The use of GMMs for degradation of PAHs was first demonstrated by Gunsalus and Chakrabarty in 1981 with the development of the first patented living organisms (US Patent #425944), *Pseudomonas aeruginosa*

(NRRL B-5472) and *Pseudomonas putida* (NRRL B-5473). These two organisms were genetically modified by incorporation of genes for naphthalene, salicylate, octane, and camphor degradation and these organisms demonstrated the acquired ability to degrade those compounds.

The use of an indigenous microbe eliminates the need for acclimation and increases the chances of survival. Genetic modifications can be used to optimize the natural degradation capabilities of an indigenous microbe through modification of transcription regulation of catabolic operons or through enhanced enzyme activation. Operon transcriptional regulation is typically achieved through a positive response from a regulatory protein after interaction with a contaminant or an intermediate of contaminant degradation (Ramos, 1997). Regulatory proteins can be mutated to give a stronger response, have a lower threshold of activation, or respond to an alternative stimulus. Coupling transcriptional regulation to an unnatural stimulus allows greater flexibility in the control of the catabolic response (Timmis, 1999; Cebolla, 1997). For example, placing the trichloroethylene (TCE) catabolic operon under the control of a starvation promoter allows the expression of the TCE catabolic genes in nutrient-limited environments like that of contaminated sites (Martin, 1995). Catabolic optimization through mutation of catabolic enzymes is achieved by altering enzyme stability, substrate specificity, or kinetic properties (Timmis, 1999). For example, in a study by Ge and Eltis, replacement of the substrate-determining subunit of benzoate dioxygenase from *Acinetobacter calcoaceticus* ADP1 with that from toluate dioxygenase of *Pseudomonas putida* mt-2 resulted in a broader substrate range for the *Acinetobacter* dioxygenase (Ge, 2003). Enhanced catalytic activity is typically accomplished through site-directed mutations of enzyme active sites but requires that the structure of the enzyme or analogous enzymes be

known. The use of enzyme modification in optimization of catabolic activity is limited by the small number of structures known for enzymes acting within catabolic pathways (Timmis, 1999).

The use of biosensors is important in remediation to detect and monitor toxin levels throughout the process. A marker gene, such as *lacZ, lux,* or *GFP,* will be fused with the operon containing the desired gene to be monitored (Wasilkowski, 2012). When transcription of that operon is active, the marker gene will be expressed and the amount of transcription can be monitored. The use of a GMM as a biosensor was demonstrated initially using the first GMM approved for field application, *Pseudomonas fluorescens* HK44 (Sayler, 2000). This strain has a luminescent reporter gene linked to the naphthalene catabolic gene cluster and is used in the field to detect the presence of naphthalene as a reporter for enhanced PAH contamination (Sayler, 2000).

c. Purified Enzymes in Bioremediation

While the use of whole-cell microbes in bioremediation has had some success, there are limitations for this technique, including low viability of exogenous microbes due to incompatibility with the local environment, high toxicity and low bioavailability of contaminants, and the requirement for aeration, excess nutrients, or required cofactors for microbial growth (Eibes, 2015). If exogenous microbes can survive the contaminated environment, they may alter the natural microbial balance by remaining long after contaminant levels have returned to normal. The use of purified wild-type or genetically modified enzymes for bioremediation has several advantages over whole-cell bioremediation including higher toxin specificity, little to no unwanted by-product formation, greater stability in the presence of high toxin concentrations, and greater

stability under various environmental conditions, such as wide pH, temperature, and redox potential ranges (Eibes, 2015). Also, enzymes will be degraded naturally and will not alter the environment by remaining in the soil over a long period of time. Directed evolution and enzyme engineering techniques may be used to broaden substrate specificity and enhance the kinetic properties of purified enzymes. The development of nanotechnologies for immobilization of enzymes can increase enzyme stability and prolong enzyme lifetime (Rayu, 2012). For example, Acevedo et al. showed that manganese peroxidase immobilized onto nanoclay had an increased stability at high temperatures and high pH and a longer storage life than free purified enzyme without a decrease in catalytic activity. This immobilized manganese peroxidase was capable of degrading 90% of anthracene present in a contaminated soil within 24 hours (Acevedo, 2010). As stability and catalytic efficiency increase, smaller scale production of enzymes will be required for bioremediation leading to reduced costs compared with whole-cell techniques.

The number of enzymatic bioremediation experiments in the field is limited, but there are many examples of small-scale laboratory tests (Table 1.4) (Eibes, 2015). One of the few field experiments was performed in 2000 at an Air Base in Greenland for the degradation of waste fuel. A combination of free enzymes extracted from hydrocarbon-degrading cultures was used to enhance degradation by a bacterial consortium. The study resulted in complete degradation of LMW PAHs after 60 days and of HMW PAHs after 90 days (Vinson, 2000). In 2008, Wu et al. tested the ability of laccase isolated from *Trametes* sp. to degrade various PAHs in contaminated soil. Laccase showed moderate total PAH degradation after 14 days (32% degradation) but

completely degraded anthracene and benzo(a)pyrene after only 24 hours. Results like these are promising for the future of enzymatic bioremediation.

Technology	Matrix	Enzyme	Pollutant	Time	Removal (%)
Free enzyme	Soil	TPH-degrading multienzyme complex	Light hydrocarbons	30 days	>95
			Heavy hydrocarbons	90 days	>95
Free enzyme	Soil	Landguard™ OP-A	Diazinon	1 h	77
Free enzyme	Soil	Laccase	DDT	25 days	69
Free enzyme	Soil	Laccase	DDT	15 days	51
Free enzyme	Soil	Laccase	15 PAHs	24 h	23, 86, 90
Free enzyme	Soil	Laccase	4-Methylphenol	2 days	91
			DCP	14 days	88
Free enzyme	Soil	HRP (horseradish roots)	2,4-DCP	0.5 h	92
Free enzyme	Soil	HRP	Phenol	7 days	40-75
			o-Cresol		
			DCP		
Free enzyme	Soil	HRP (shepherd's purse root)	2,4-DCP	3 h	95
Free enzyme	Soil	HRP	2,4-DCP	24 h	90
Free enzyme	Soil	Laccase	Estradiol	264h	95
Free enzyme	Soil	HRP	DCP	30 min	85
Immobilized	Soil	Laccase	DCP	1 day	88
Immobilized	Soil	MnP	Anthracene	24 h	86-90
Immobilized	Soil	*Arthrobacter* sp. HB-5	Atrazine	144 h	90
Immobilized	Soil	*Arthrobacter* sp. DNS10	Atrazine	21 days	90
Immobilized	Soil	Laccase	Naphthalne	14 days	82
			Phenanthrene		
Slurry bioreactor	Soil slurry	Laccase	PFC	15 days	72-91
Slurry bioreactor	Soil slurry	Laccase	Phenanthrene	6 h	95
			Fluoranthene		93
			Benz(a)anthracene		79
			Benzo(a)pyrene		73
Slurry bioreactor	Soil slurry	Laccase	Octylphenol	8 h	85
			Nonylphenol		90
			Bisphenol A		95
			Ethinylestradiol		80
Single phase bioreactor	Acetone:water	MnP	Anthracene	3 days	28
Single phase bioreactor	Acetone:water	MnP	Anthracene	7 h	>95
			Dibenzothiophene	24 h	95
			Pyrene	24 h	61
Single phase bioreactor	Acetone:water	MnP	Anthracene	11.5 h	90
Single phase bioreactor	Acetone:DMF:water	BGP	Anthracene	7 h	99

Table 1.4: Reported enzyme technologies for bioremediation by 2015 (adapted from Eibes, 2015). TPH: total petroleum hydrocarbon; OP-A: phosphoesterase; HRP: horseradish peroxidase; MnP: manganese peroxidase; BGP: bitter gourd peroxidase; DDT: dichlorodiphenyltrichloroethane; DCP: dichlorophenol; PFC: perfluoroalkyl compounds.

1.3 Mycobacteria and PAH Bioremediation

a. Mycobacteria Characteristics

Mycobacteria are aerobic, rod-shaped bacteria belonging to the Gram-positive Actinobacteria group that are found in diverse environments (Primm, 2004). Mycobacteria have been extensively studied for their ability to degrade a wide range of PAHs. Studies using HMW PAHs as the sole carbon and energy sources typically result in the isolation of *Mycobacterium* spp (Kim, 2010). Although Mycobacteria are slow growers they survive and even outcompete other fast-growing bacteria when PAHs are present in soil (Kim, 2010). After being the first isolated bacteria capable of degrading pyrene, much attention has been given to *Mycobacterium vanbaalenii* PYR-1. *M. vanbaalenii* PYR-1 was isolated in 1986 from a contaminated estuary near the Harbor Island oil tank at Redfish Bay, Texas (Heitkamp, 1988). Genomic, metabolomic, and proteomic data from *M. vanbaalenii* PYR-1 have been combined to elucidate degradation pathways for multiple PAHs, including naphthalene, phenanthrene, anthracene, fluoranthene, pyrene, benz[a]anthracene, and benzo[a]pyrene (Kim, 2010). Analysis of the *M. vanbaalenii* PYR-1 genomic sequence annotates 194 genes as having roles in PAH catabolism (Kim, 2010). Most PAH catabolic genes are limited to two catabolic regions within the genome, region A at 494-643 kb and region B at 4,711-4,741 kb, with others spread throughout the *M. vanbaalenii* PYR-1 genome (Figure 1.2). Region A is specialized for HMW PAH degradation and contains all the genes necessary for HMW PAH catabolism. These genes are not organized into operons, as is typical for catabolic microbes. Instead, genes involved in a catabolic pathway are scattered among several gene clusters. For example, the genes responsible for the first three steps in pyrene degradation are found across 70 kb of DNA and 3 different gene clusters within region A and the

27 genes needed for complete pyrene degradation are found within 4 gene clusters. Analysis of the *M. vanbaalenii* PYR-1 genome shows redundancy in genes encoding enzymes for every step in PAH catabolism. For the first three steps in PAH catabolism there are 21 ring hydroxylating oxygenases (RHOs) (step 1), 50 cytochrome P450s (CYPs) (step 1), 5 dihydrodiol dehydrogenases (step 2), and 10 ring-cleaving dioxygenases (step 3). Many of these gene copies are found within the catabolic regions. The unstructured locations and redundancy of catabolic genes are likely caused by the presence of mobile genetic elements found throughout the catabolic regions. Due to the complex arrangement and duplication of genes, a sophisticated regulatory system is required to coordinate an appropriate response in the presence of a contaminant or catabolic intermediate (Kim, 2009). For example, the ring hydroxylating oxygenases NidAB and NidA3B3 are both capable of processing pyrene and fluoranthene *in vivo* but proteomic studies show that NidAB is upregulated only in the presence of pyrene while NidA3B3 is upregulated only in the presence of fluoranthene (Kim, 2006). Some genes have been identified that may be responsible for catabolic regulation, but their functions have not been confirmed (Kweon, 2010). The presence of multiple isozymes allows variation in processing of a PAH that creates branched metabolic pathways.

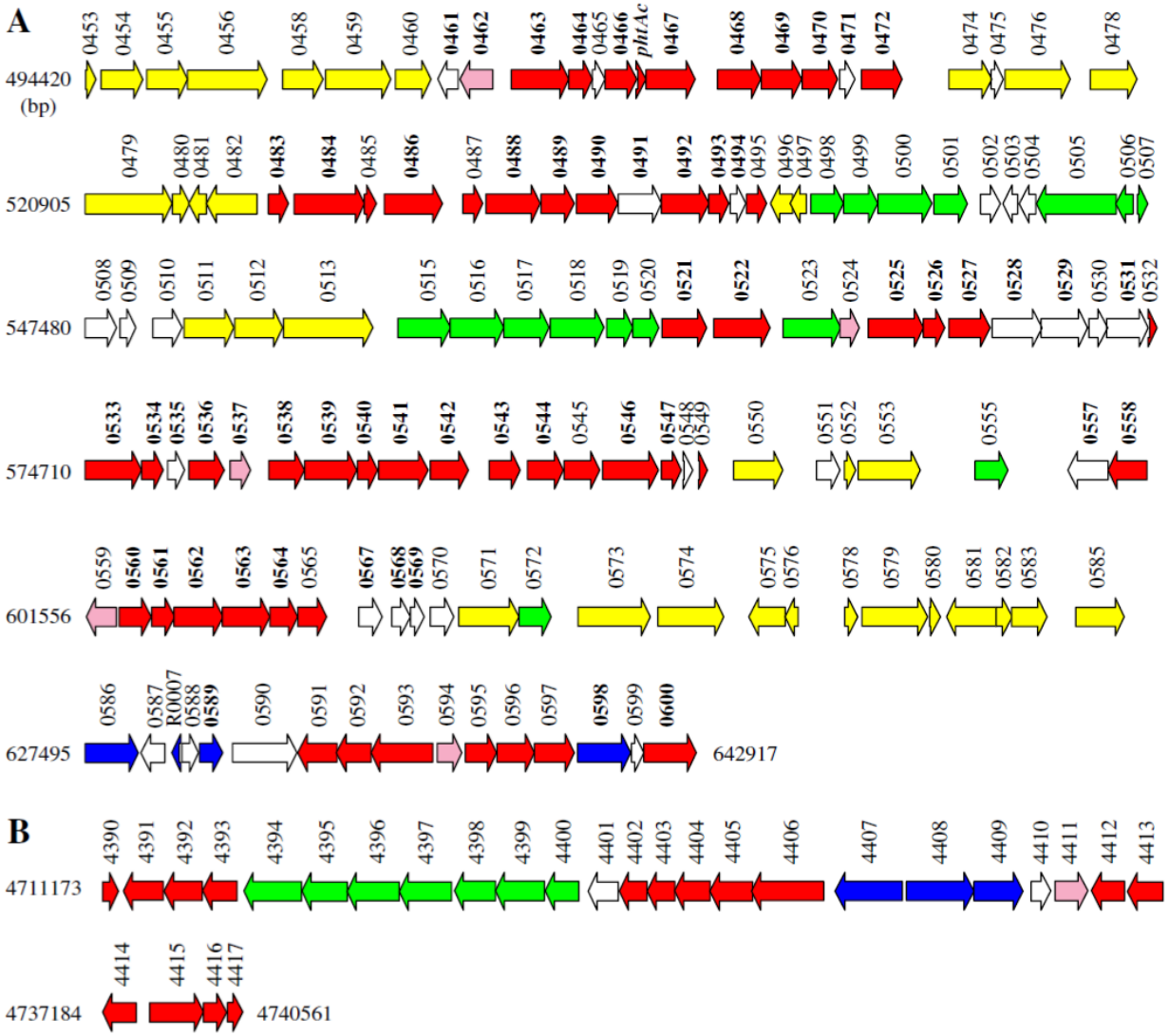

Figure 1.2: PAH catabolic regions from *Mycobacterium vanbaalenii* PYR-1. Arrows indicate the direction of transcription and numbers above the arrows correspond to ORFs. Bold numbers signify genes expressed in the presence of pyrene and fluoranthene. Arrows are colored as follows: red: PAH catabolism, pink: transcriptional regulation, yellow: DNA mobilization, green: membrane transport system, blue: function outside of PAH degradation, white: no predicted function (Kim, 2008).

b. *Mycobacterium vanbaalenii* PYR-1 Catabolism of PAHs

When exposed to a PAH, *Mycobacterium vanbaalenii* PYR-1 follows a central catabolic pathway that converts the PAH to intermediates of the tricarboxylic acid (TCA) cycle or a peripheral pathway that results in a dead-end product (Kweon, 2011). The general pathway for the degradation of PAH by *M. vanbaalenii* PYR-1 with the most support by experimental evidence is shown in Figure 1.3 (Kim, 2008). Catabolism using the central pathway begins with activation by the addition of one oxygen molecule by cytochrome P450 (CYP) followed by hydrolysis of the resulting epoxide or the addition of two oxygen molecules by ring hydroxylating oxygenases (RHOs). Dehydrogenation of the resulting dihydrodiols forms dihydroxylated, rearomatized intermediates that are cleaved by ring-cleaving dioxygenases. The products are then processed by hydratase-aldolases. For PAHs with 3 or more rings the cycle is repeated until a single ring remains. The single-ring product is then processed to intermediates of the TCA cycle, ultimately being used for cellular energy production.

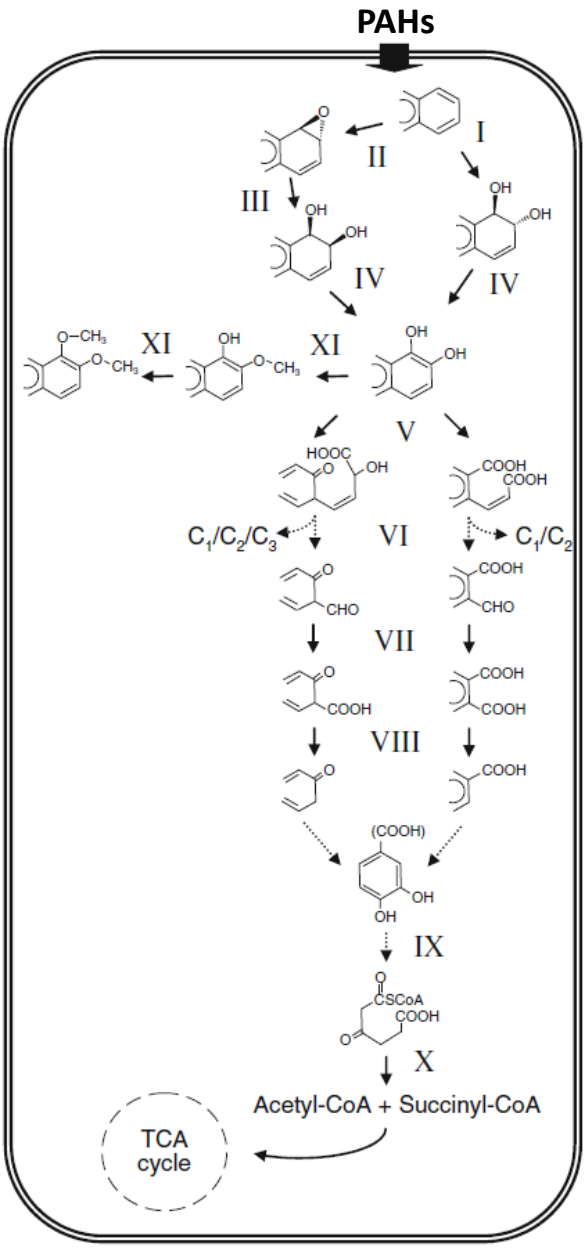

- Transport system

I. Ring-hydroxylating oxygenase: 21
II. P450 monooxygenase: 50
III. Epoxide hydrolase: 4

IV. Dihydrodiol dehydrogenase: 5

V. Ring-cleavage dioxygenase: 10

VI. *meta*-Cleavage product hydrolase: 8
Hydratase-aldolase: 3
Hydratase: 4
Aldolase:2
Alcohol dehydrogenase: 7

VII. Aldehyde dehydrogenase: 2

VIII. Decarboxylase: 2

IX. Protocatechuate 3,4-dioxygenase α subunit: 2
Protocatechuate 3,4-dioxygenase β subunit: 1
β-Carboxy-*cis*,*cis*-muconate cycloisomerase: 1
γ-Carboxymuconolactone decarboxylase/
β-ketoadipate enol-lactone hydrolase: 1
β-Ketoadipate CoA-transferase α subunit: 2
β-Ketoadipate CoA-transferase β subunit: 2

X. β-Ketoadipyl CoA thiolase : 5

XI. Catechol *O*-methyltransferase: 2

Figure 1.3: General PAH catabolism by *Mycobacterium vanbaalenii* PYR-1. Roman numerals represent the enzymatic steps. The number of enzymes associated with each step found within the *M. vanbaalenii* PYR-1 genome are given. (Adapted from Kim, 2008)

Additional catabolic pathways in *M. vanbaalenii* PYR-1 are necessary when PAH levels are higher than can be processed through the central pathway or when central pathway intermediates spontaneously form toxic compounds (Kweon, 2010). Catechol compounds created after the first two steps may spontaneously oxidize to form genotoxic quinone species. Quinone reductases, such as catalase peroxidase and superoxide dismutase, can reduce these reactive species back to catechols that can feed back into the central degradative pathway (Kweon, 2010). The highly reactive hydroxylated intermediates may also be methylated by O-methyltransferases to less reactive methoxy compounds through a peripheral detoxification pathway (Kim, 2008). Products of the peripheral detoxification pathways cannot be used by the microbe for energy production, so they are typically eliminated through transport out of the cell (Kweon, 2010). The pyrene catabolic pathway provides examples of both the central and detoxification pathways (Scheme 1.1). The central pathway begins with hydroxylation at C-4 and C-5 (**1**) and follows a catabolic route like that described above. The detoxification pathway begins with hydroxylation and dehydrogenation at positions C-1 and C-2 (**2** and **3**) followed by methylation of both oxygens to produce an unreactive dimethoxy compound (**4**) that is eliminated from the bacteria (Kim, 2007).

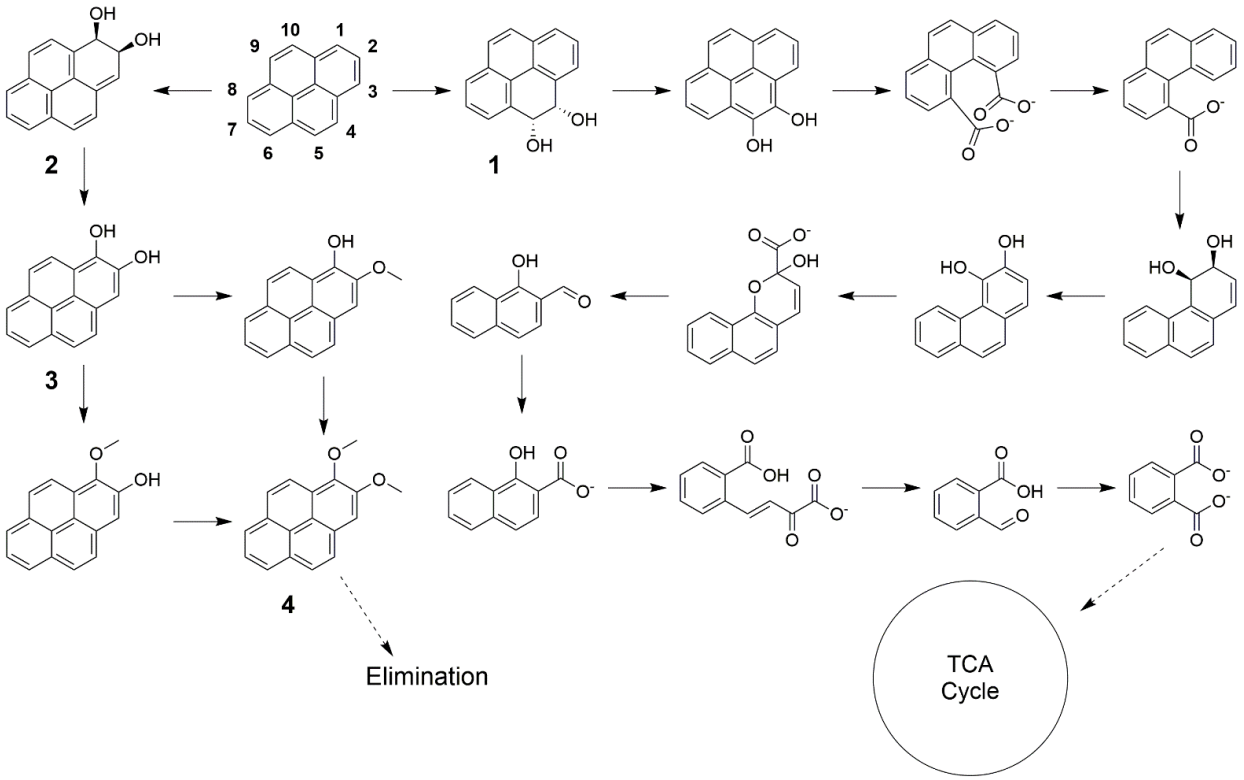

Scheme 1.1: Degradation pathway for pyrene by *M. vanbaalenii* PYR-1 (Adapted from ref. Kim, 2007)

c. Mycobacteria Physiological Responses

In addition to having the genetic capability to degrade various hydrocarbons, *Mycobacterium* spp. have other characteristics and physiological responses to PAHs that enhance their ability to degrade these PAHs. The low oxygen concentration at contamination sites is typically a limiting factor for PAH degradation because many enzymes involved in PAH degradation require oxygen as a substrate (Kim, 2010). Fritzsche showed that an isolated *Mycobacterium* sp. was capable of degrading pyrene while limiting cell growth in oxygen concentrations that are typically too low for PAH degradation by other aerobic bacteria (Fritzsche, 1994). HMW PAHs can be quite large and passive diffusion through the cell membrane may be difficult. *M. vanbaalenii* PYR-1 has 23 ORFs within regions A and B that are involved in

membrane transport and function to transport PAHs and necessary nutrients into the cell (Kim, 2008). HMW PAHs are highly recalcitrant because of their hydrophobicity and low bioavailability. Mycobacteria have cell walls with thick, hydrophobic cell envelopes rich in mycolic acids. When exposed to PAH contaminants, Mycobacteria can modify their cellular envelopes by increased production of mycolic acid with longer fatty chains to better adhere to and increase the bioavailability of hydrophobic PAHs. For example, when a *Mycobacterium* sp. is grown with solid anthracene as the sole carbon source it alters the composition of its cell surface which allows it to produce a biofilm on anthracene and increase anthracene bioavailability (Wick, 2002). Bogan et al. showed that after growth on soil supplemented with phenanthrene, *M. vanbaalenii* PYR-1 had a high membrane hydrophobicity (52%), significantly higher than that of LMW PAH-degrading bacteria (0-26%) (Table 1.5) (Bogan, 2003). These physiological adaptions to the presence of PAH contaminants and the local environment of contaminated soils make Mycobacteria well-suited to thrive within contaminated environments.

Isolate	Medium	Culture age (days)	Hydrophobicity (%)
Acidovorax temperans GTI-19	MSM/phenanthrene	1	3
Burkholderia sp. GTI-3	MSM/phenanthrene	6	15
Pseudomonas viridiflava GTI-5	MSM/phenanthrene	6	4
Sphingomonas SP. GTI-7	MSM/phenanthrene	2	15
Sphingomonas SP. GTI-8	MSM/phenanthrene	6	26
Sphingomonas SP. GTI-10	MSM/phenanthrene	6	0
Sphingomonas SP. GTI-11	MSM/phenanthrene	6	18
Sphingomonas subarctica GTI-12	MSM/phenanthrene	2	0
Mycobacterium austroafricanum GTI-23	YPS/phenanthrene	6	48
Mycobacterium austroafricanum ATCC 33464	YPS	6	41
Mycobacterium sp. PYR-1	YPS/phenanthrene	6	52

Table 1.5: Measured hydrophobicity after growth in mineral salts medium (MSM), or MSM with added yeast extract, peptone, and starch (YPS) supplemented with phenanthrene (Bogan, 2003).

d. *M. vanbaalenii* PYR-1 in Bioremediation of PAHs

M. vanbaalenii PYR-1 is specialized for the degradation of HMW PAHs through its physiological and genetic adaptations and is an ideal candidate for use in bioremediation efforts. In 2003, *M. vanbaalenii* PYR-1 was used in a two-phase partitioning bioreactor to degrade phenanthrene, pyrene, naphthalene, and anthracene contaminants. *M. vanbaalenii* PYR-1 completely degraded phenanthrene and pyrene within 4 days (168 mg/L/day and 38 mg/L/day) and degraded 75% of naphthalene and 95% of anthracene after 10 days (14.5mg/L/day and 40mg/L/day) (MacLeod, 2003). Although these results are promising, documentation of applications of *M. vanbaalenii* PYR-1 for bioremediation since 2003 has not been reported.

M. vanbaalenii PYR-1 HMW PAH degradation pathways are overlapping and complex. Many enzymes within these pathways have relaxed substrate specificities and may be functional in multiple pathways. For *M. vanbaalenii* PYR-1 to be used efficiently in bioremediation applications it is important that the expression of the enzymes assigned to the various transformations in the proposed pathways be confirmed and that enzymatic mechanisms and regulation of various pathways be well understood (Kim, 2008; Kweon, 2010). Proteomic and genomic analysis has elucidated genes that are involved in specific catabolic pathways under limited conditions, but systems biology experiments under various conditions will give insights into the regulation of gene expression and enzyme functions (Kweon, 2010). The roles of many of these genes are assigned based on homology with known enzymes. Biochemical evidence for enzyme functions and identification of intermediates is needed to confirm the annotated pathways (Kweon, 2010). The work presented in this dissertation provides some of the much needed biochemical evidence.

Chapter 2: Investigation of the Ring-Cleaving Dioxygenase and Hydratase-Aldolase Reactions in the *M. vanbaalenii* PYR-1 Naphthalene Catabolic Pathway

2.1 Introduction

Naphthalene is one of the most common pollutants found in petroleum-contaminated sites. After inhalation of naphthalene, cytochrome P450 enzymes process naphthalene into compounds that display pulmonary toxicity in mice and olfactory and respiratory toxicity in rats, but the evidence for naphthalene toxicity in humans is controversial (Hu, 2014; Abdo, 2001; Bailey, 2016; Li, 2017). Bacterial degradation is the predominant means for lowering naphthalene concentration in the environment. The series of reactions used to process one aromatic ring of the naphthalene system represents a major strategy that is repeated in other PAH catabolic pathways. Hence, elucidation of the bacterial naphthalene catabolic pathway is critical for elucidation of other, more complex PAH catabolic pathways. While much work has been done to elucidate the naphthalene catabolic pathways for various bacteria, little work has been done to elucidate the naphthalene catabolic pathway in *Mycobacterium vanbaalenii* PYR-1 (Seo, 2009; Kelley, 1990). Kelley et al. isolated metabolites after introducing a culture of *M. vanbaalenii* PYR-1 to naphthalene and proposed the abbreviated catabolic pathway shown in Scheme 2.1.

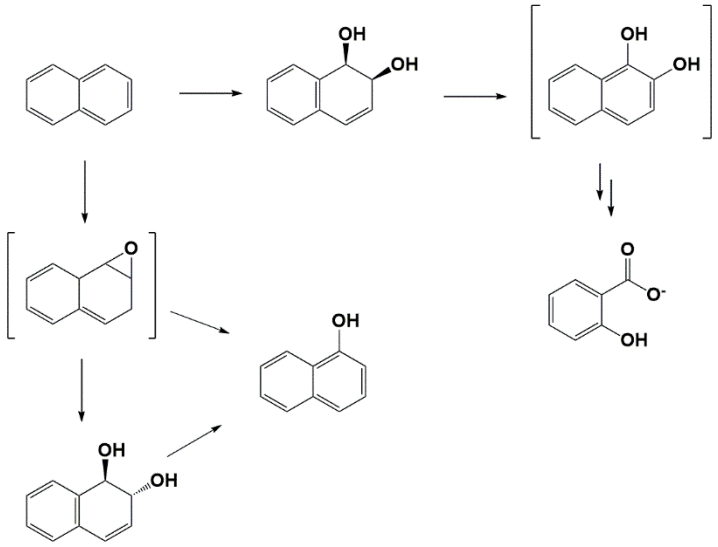

Scheme 2.1: Metabolites isolated after growth of *M. vanbaalenii* PYR-1 in the presence of naphthalene. Compounds in brackets were not isolated (adapted from Kelley, 1990).

The generally accepted naphthalene catabolic route that agrees with the isolated metabolites is shown in Scheme 2.2. This pathway was first characterized for plasmid NAH7 in *Pseudomonas putida* G7 (Schell, 1983). The pathway begins with oxidation of naphthalene (**5**) at C-1 and C-2 to produce **6**, followed by dehydrogenation to aromatize the ring (**7**). The ring is opened via a dioxygenase-catalyzed cleavage at the meta position (indicated on 7) and the product non-enzymatically cyclizes to **8**. Typically, a glutathione-dependent isomerase catalyzes the *cis* to *trans* isomerization of **8** to **9** before a hydratase-aldolase cleaves **9** to salicylaldehyde (**10**) and pyruvate. The aldehyde is oxidized to salicylic acid (**11**) and is further processed through the catechol catabolic pathway that feeds into the TCA cycle.

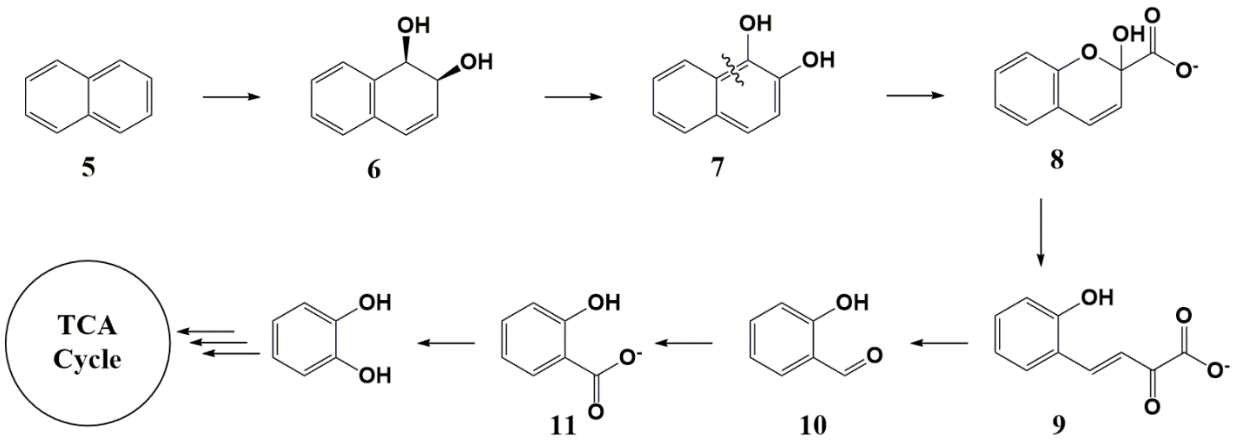

Scheme 2.2: Proposed naphthalene catabolic pathway by *M. vanbaalenii* PYR-1.

The catabolism of some HMW-PAHs produces an intermediate, 1-hydroxy-2-naphthoate (**12**), that is structurally similar to 1,2-dihydroxynaphthalene (**7**). For example, the upper catabolic pathway for pyrene ends in the production of **12** (Kim, 2007) (Scheme 2.3). The lower catabolic pathway begins with cleavage of **12** at the ortho position to produce **13** that is processed to 2-carboxybenzaldehyde. The pathway ends with the production of phthalate that can ultimately feed into the TCA cycle. Proteomic studies performed after growth of *M. vanbaalenii* PYR-1 in the presence of pyrene show that iron-dependent dioxygenases (designated PhdI and PhdF) and hydratase-aldolases (designated PhdJ and PhdG) are upregulated (Kim, 2007; Kweon, 2007). PhdF is annotated as a type I extradiol dioxygenase and is thought to catalyze the ring cleavage of **19** and **36**. PhdG catalyzes hydration of the ring-opened product of **24** followed by a retro-aldol fission to produce **26** in the upper catabolic pathway (Scheme 2.3). PhdI is annotated as an intradiol dioxygenase and is thought to be responsible for ortho-ring cleavage of **12** and PhdJ is responsible for hydration of **13** and subsequent retro-aldol fission in the lower catabolic pathway.

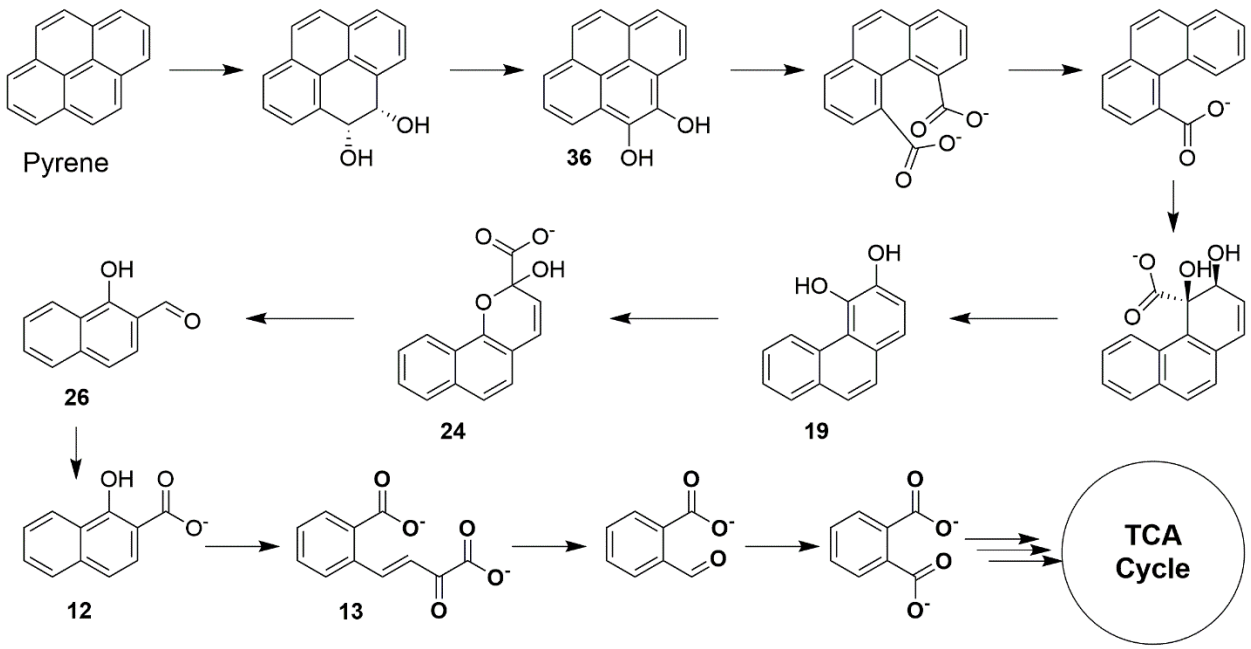

Scheme 2.3: The catabolism of pyrene by *M. vanbaalenii* PYR-1 (adapted from Kim, 2007).

Only the enzymes responsible for the ring-hydroxylating and dehydrogenation steps in the naphthalene catabolic pathway in *M. vanbaalenii* PYR-1 have been experimentally characterized. The gene products of several ring-hydroxylating oxygenase genes within the PAH catabolic regions (Figure 1.2) have been shown to hydroxylate naphthalene (to produce **6** in Scheme 2.2), although at slower rates than HMW PAHs (Kim, 2006; Kweon, 2014). Although there are several ring-cleaving dioxygenase and hydratase-aldolase genes within the catabolic regions of *M. vanbaalenii* PYR-1, no enzymes have been identified and assigned as those that catalyze ring-cleavage or hydratase-aldolase reactions within the naphthalene catabolic pathway. There is no gene within the PAH catabolic regions that has significant sequence similarity with an isomerase known to be active within naphthalene catabolic pathways (NahD of the NAH7 plasmid in *Pseudomonas putida* G7), and no annotated isomerase is upregulated in *M. vanbaalenii* PYR-1 in the presence of PAHs (Thompson, 2007; Kweon, 2007; Kim, 2007). It is predicted that the non-

enzymatic *cis* to *trans* isomerization of **8** to **9** is sufficient and no isomerase is required (Scheme 2.2).

Based on the structural similarities of **12** with **7** (CO_2^- vs OH) and **13** with **9** (CO_2^- vs OH), it is possible that the enzymes that cleave **12** and **13** can also cleave **7** and **9** (Scheme 2.4). PhdI has a modest sequence similarity (46%) with a cupin superfamily type III extradiol dioxygenase (PhdI from *Nocardioides* sp KP7) known to cleave **12** in the ortho position (between substituents) (Iwabuchi, 1998). PhdI from *Nocardioides* sp KP7 is unique in that it requires ferrous iron to cleave its substrate in the ortho position whereas other ortho ring-cleaving dioxygenases require ferric iron (Iwabuchi, 1998). It is possible that PhdI from *M. vanbaalenii* PYR-1 can catalyze cleavage of **12** at the ortho position and **7** at the meta position (adjacent to substituents) (Bugg, 2003; Iwabuchi, 1998). It is also possible that PhdI cleaves **7** in the ortho position and/or **12** in the meta position (Scheme 2.4). If PhdI cleaves **7** in the ortho position, a hydratase-aldolase would degrade the product **15** to 2-carboxybenzaldehyde (**16**) that is oxidized and processed through the phthalate catabolic pathway (Keum, 2006; Seo, 2006; Seo, 2007). If PhdI cleaves **12** at the meta position, a hydratase-aldolase would degrade the product **14** to salicylaldehyde that is further processed through the catechol catabolic pathway that feeds into the TCA cycle (Roy, 2014).

Although PhdF likely acts in the upper catabolic pathway for pyrene, PhdF is the gene product in *M. vanbaalenii* PYR-1 with the highest sequence similarity (35%) to a type I extradiol dioxygenase (NahC of the NAH7 plasmid *Pseudomonas putida* G7) known to ring-cleave **7** at the meta position and may be responsible for catalyzing this reaction. PhdJ is the gene product in *M. vanbaalenii* PYR-1 with the highest sequence similarity (45% and 56%, respectively) to hydratase-aldolases known to catalyze the hydration of **9** and subsequent retro-aldol cleavage (NahE of the

NAH7 plasmid in *Pseudomonas putida* G7) and the hydration of **13** and subsequent retro-aldol cleavage (PhdJ of *Nocardioides* sp. KP7) and is likely responsible for catalyzing both reactions. PhdG also has high sequence similarity to these hydratase-aldolases (36% and 34%, respectively) and may also be able to catalyze these reactions.

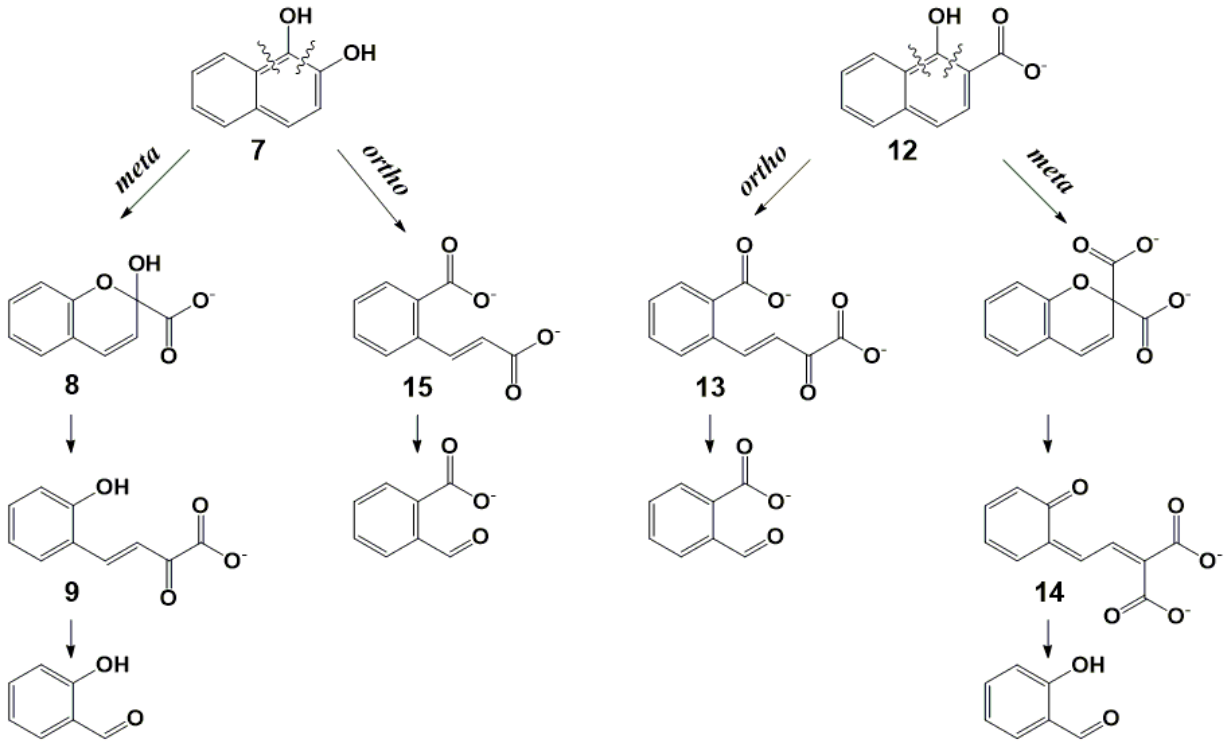

Scheme 2.4: Possible ring-cleavage reactions of 1,2-dihydroxynaphthalene (**7**) and 1-hydroxy-2-naphthoate (**12**) and subsequent hydratase-aldolase reactions.

One goal of this work is to determine which oxygenase, PhdI or PhdF, is responsible for the cleavage of **7** and/or **12** and at what position the cleavage occurs (Scheme 2.4). We also want to determine if an enzyme is required to catalyze the isomerization of the cleavage products and which hydratase-aldolase, PhdJ or PhdG, catalyzes cleavage of these products (**9** or **15** and **13** or **14**). Products of each reaction were isolated and identified and kinetic analysis was performed.

2.2 Experimental Procedures

Materials

Chemicals, biochemicals, buffers, and solvents were purchased from Sigma-Aldrich Chemical Co. (St. Louis, MO), Fisher Scientific Inc. (Pittsburgh, PA), Fluka Chemical Corp. (Milwaukee, WI), or EMD Millipore, Inc. (Billerica, MA). 1,2-Dihydroxynaphthalene, 1-hydroxy-2-naphthoic acid, salicylaldehyde, 2-carboxybenzaldehyde, and 2-hydroxybenzaldehyde were purchased from Sigma-Aldrich Chemical Co. The Gibson Assembly Cloning Kit was purchased from New England Biolabs, Inc (Ipswich, MA). The DEAE-Sepharose resin, the HiLoad 16/60 Superdex resin, and the Sephadex G-25 resin were obtained from GE Healthcare (Piscataway, NJ). The HisPur Ni-NTA resin was purchased from Sigma-Aldrich Chemical Co. The EconoColumn chromatography columns were obtained from BioRad (Hercules, CA). The Amicon stirred cell concentrators and ultrafiltration membranes (10000 Da cutoff) were purchased from EMD Millipore Inc.

Bacterial Strains, Plasmids and Enzymes

The pET vectors were obtained from Novagen (Madison, WI). *Escherichia coli* strain C41(DE3) and TEV protease were obtained from Sigma-Aldrich Chemical Co. *E. coli* ArcticExpress cells were obtained from Agilent Technologies (Santa Clara, CA). Isolated genomic DNA from *Mycobacterium vanbaalenii* PYR-1 was a gift from the laboratory of Dr. Carl Cerniglia (National Center for Toxicology Research, Food and Drug Administration, Jefferson, AR). PhdJ and PhdG were expressed and purified as described previously (LeVieux, 2016).

General Methods

Oligonucleotide primers were synthesized by Sigma-Aldrich Co. The PCR amplification of DNA was conducted in a GeneAmp 2700 thermocycler (Applied Biosystems, Carlsbad, CA). The GenElute gel extraction kit was purchased from Sigma-Aldrich Co. Enzymes and reagents used for molecular techniques were purchased from New England Biolabs, Inc. DNA sequencing was performed in the DNA Core Facility in the Institute for Cellular and Molecular Biology (ICMB) at the University of Texas at Austin. The QIAprep spin miniprep kit was purchased from Qiagen (Hilden, Germany). Sonication was performed using a W385 sonicator of Heat systems-ultrasonics, Inc. (Farmingdale, NY). Sodium dodecyl sulfate-polyacrylamide gel electrophoresis (SDS-PAGE) was carried out on a Bio-Rad Mini-Protean II gel electrophoresis apparatus. Protein concentrations were determined using the Bradford method (Bradford, 1976). Electrospray ionization mass spectrometry (ESI-MS) was carried out on an LCQ electrospray ion-trap mass spectrometer (Thermo, San Jose, CA) housed in the ICMB Protein and Metabolite Analysis Facility at the University of Texas. Steady-state kinetic assays were performed on an Agilent 8453 diode-array spectrophotometer. Nonlinear regression data analysis was performed using the program Grafit (Erithacus Software Ltd., Staines, U.K.). Nuclear magnetic resonance (NMR) spectra were recorded on a Varian UNITY+ 300 MHz (Palo Alto, CA). NMR signals were analyzed using the software program SpinWorks 3.1.6 (Copyright 2009 Kirk Marat, University of Manitoba).

Cloning of *M. vanbaalenii* PYR-1 genes 0468 (PhdI), 0469 (PhdJ), 0470 (PhdF) and 0472 (PhdG)

For PhdI and PhdF, amplification of the desired genes was achieved through two rounds of PCR. The first round used overhang PCR primers that annealed within 100 bp around the desired gene. The second round isolated the desired gene flanked with appropriate restriction sites. For PhdJ and PhdG, amplification of the desired genes was achieved through a single round of PCR. Primers used for PCR are shown in Table 2.1. The 100 µl amplification reaction contained the *M. vanbaaleni* PYR-1 genomic DNA as a template (15 ng), dNTPs (0.4 mM), MgCl (2 mM), primers (0.4 µM), 1x buffer, and Vent Polymerase (1 unit). The PCR amplification protocol consisted of a 5 min denaturation step at 94°C followed by 35 cycles of 94°C for 1 min, 55°C for 1 min, and 72°C for 3 min and ended with a 10 min elongation step at 72°C. The PCR reaction product size was confirmed on a 1% agarose gel and isolated using the GenElute gel extraction kit and elution into 60 µL of water. The PCR products were inserted into pET24 or pET32 between appropriate restriction sites (Table 2.1) using digestion and ligation procedures reported elsewhere (Deininger, 1990). For PhdG, a sequence encoding a C-terminal His-tag and TEV cleavage site was inserted using a Gibson Assembly cloning kit following the manufacturer's protocol. An aliquot of the individual ligation mixture (30 µL) of PhdJ and PhdG was transformed into *E. coli* Arctic Express cells using a calcium heat shock method (Deininger, 1990). An aliquot of the individual ligation mixture (30 µL) of PhdI and PhdF was transformed into *E. coli* C41(DE3) using a calcium heat shock method. Transformed cells were grown on agar plates containing the appropriate antibiotic (100 µg/mL ampicillin for pET32 and 50 µg/mL kanamycin for pET24) at 37 °C overnight. A

single colony was used for the generation of additional plasmid for sequencing and protein expression.

Gene	Overhang Fwd Primer	Overhang Reverse Primer	Fwd Primer	Reverse Primer	Restriction Enzymes		Vector
PhdI	CCCAAGAGGTCAGCTCAGTG	GGAGGGCGTAGGGATAATGC	TAGCCAGGATCCTCCACCGCC	GAATCGGAATTCTCAGCGGGC	BamHI	EcoRI	pET32
PhdJ	-	-	CGAGAGAGCATATGGTGCACGT	TCCTCAGGATCCGTGGTTCGAGAC	NdeI	BamHI	pET24a
PhdG	-	-	CACGGCTCGGATCCACAACACG	CCGGCGTGAGCTCCTATGACGAGG	BamHI	SacI	pET24a

Table 2.1: Primers used for cloning of PhdI, PhdF, PhdJ, and PhdG genes from *M. vanbaalenii* PYR-1.

Expression of Enzymes

PhdI and PhdF

LB media cultures (25 mL) containing ampicillin (100 µg/mL) were inoculated using a single colony and grown overnight at 37 °C. LB media cultures (1.6 L) were inoculated using an appropriate amount of the overnight culture to make OD_{600} = 0.05 A.U and grown at 37°C for 2.5 h. Protein expression was induced overnight (18 h) at 21 °C using a final isopropyl-β-D-thiogalactoside concentration of 0.1 mM. Cells were harvested by centrifugation (10,000 × g) with yields ranging from 3-5 g and stored at −80 °C.

Purification of Enzymes

PhdI and PhdF

Cells were suspended to a final concentration of 10 mg/mL in Buffer A (20 mM HEPES, 300 mM NaCl, pH 7) with 15 mM imidazole. Cells were disrupted by sonication and the resulting solution was centrifuged for 30 min at 17,700 × g and 4 °C. The supernatant was loaded onto a Ni-NTA column (1 × 10 cm, ~6 mL resin) pre-equilibrated with Buffer A + 15 mM imidazole. The column was washed with Buffer A + 70 mM imidazole and the desired protein was eluted with

Buffer A + 90 mM imidazole. Protein purity was confirmed by the observation of a single band on an SDS-PAGE gel stained with Coomassie blue. The eluant was concentrated to ~1 mg/mL and exchanged into 20 mM HEPES, 300 mM NaCl, 5% glycerol, pH7 (Buffer B) using an Amicon stirred cell equipped with an ultrafiltration membrane (10,000 Da cutoff).

Activation of PhdF

To activate PhdF, ascorbate (4 mM final), Iron(II) chloride (2 mM final) and acetone (5% final) were added to aliquots (~500 ul) of protein (1 mg/mL final concentration) purified as described above and the resulting mixture was incubated on ice for 30 min. The sample was centrifuged for 5 min at 20,800 × g and exchanged into Buffer B using a PD-10 column. Activity decreases within 8 h of activation so protein is activated and assayed on the same day.

Product Identification

*Reaction of PhdI with 1,2-Dihydroxynaphthalene (**7**)*

PhdI was purified as described above. Aliquots of PhdI (1 – 10 µL, 6 – 60 nM final) and 1,2-dihydroxynaphthalene in ethanol (1 µM – 1 mM final) were added to Buffer A (1 mL) and the reactions monitored using UV spectroscopy. No change in absorbance other than that caused by non-enzymatic oxidation was observed.

*Reaction of PhdI with 1-Hydroxy-2-Naphthoate (**12**)*

PhdI-expressing *E. coli* cells (1.2 g), prepared as described above, were suspended in 40 mL of 20 mM HEPES at pH 7.0, lysed by sonication and the resulting solution was centrifuged

for 30 min at 17,700 × g and 4 °C. The supernatant was diluted to 150 mL using 20 mM HEPES at pH 7.0 and 1-hydroxy-2-naphthoate (25 mg in 1.5 mL ethanol) was added dropwise to the supernatant, which was stirring on ice. Aliquots (1 mL) of the solution were removed every 5 min, centrifuged at 20,800 × g for 2 min, and the clarified supernatant was monitored by UV spectroscopy until the reaction was complete (30 min) as determined by no further increase in absorbance at 294 nm. The reaction was centrifuged at 10,000 × g and 4 °C for 20 min. The pH of the clarified supernatant was adjusted to 8.0 using drops of 10 M potassium hydroxide. Proteins were removed using an Amicon stirred cell concentrator equipped with an ultrafiltration membrane (10,000 Da cutoff). The protein-free flow-through was concentrated in vacuo to 1.5 mL and loaded onto a Sephadex G-25 column. The column was washed with water and the eluate monitored using UV spectroscopy (294 nm). The product-containing fractions (~10 mL) were combined and dried in vacuo. The product was resuspended in ~0.6 mL of $CDCl_3$, placed in an NMR tube, and a ^1H NMR spectrum was obtained. The ^1H NMR spectrum matched that of pure *trans-o*-carboxybenzylidenepyruvate (**13**, Scheme 2.4).

*Reaction of PhdF with 1,2-Dihydroxynaphthalene (**7**) and 1-Hydroxy-2-Naphthoate (**12**)*

PhdF was purified and activated as described above. Aliquots of PhdF (20 nM – 1 µM final) and 1,2-dihydroxynaphthalene in ethanol (1 µM – 1mM final) or 1-hydroxy-2-naphthoate in ethanol (2 – 80 µM final) were added to 1 mL of 20 mM HEPES at pH 7.0 and the reaction monitored using UV spectroscopy. No change in absorbance other than that caused by non-enzymatic oxidation was observed for either compound.

*Reactions of PhdJ and PhdG with trans-o-Hydroxybenzylidenepyruvate (HBP, **9**)*

Aliquots of PhdJ (210 nM final) or PhdG (230 nM final) prepared as described above were added to 1 mL of 20 mM HEPES at pH 7.0. An aliquot of HBP in ethanol (30 µM final) was added to initiate the reaction. The reaction was monitored by following an increase in absorbance at 255 nm until completion as determined by no increase in absorbance. The resulting spectrum of the products was compared to the spectrum of an aliquot of pyruvate (dissolved in ethanol) in 1 mL of 20 mM HEPES at pH 7.0 (20 µM final) and an aliquot of salicylaldehyde (dissolved in ethanol) in 1 mL of 20 mM HEPES at pH 7.0 (40 µM final).

*Reactions of PhdJ and PhdG with trans-o-Carboxybenzylidenepyruvate (CBP, **13**)*

Aliquots of PhdJ (20 nM final) or PhdG (320 nM final) prepared as described above were added to 1 mL of 20 mM HEPES at pH 7.0. An aliquot of CBP in ethanol (30 µM final) was added to initiate the reaction. The reaction was monitored by following the decrease in absorbance at 300 nm until completion as determined by no further decrease in absorbance. The resulting spectrum of the products was compared to the spectrum of an aliquot of pyruvate (dissolved in ethanol) in 1 mL of 20 mM HEPES at pH 7.0 (20 µM final) and an aliquot of 2-carboxybenzaldehyde (dissolved in ethanol) in 1 mL of 20 mM HEPES at pH 7.0 (40 µM final).

Steady-State Kinetic Analysis

*PhdI with 1-Hydroxy-2-Naphthoate (**12**)*

An aliquot of pure PhdI (2 µL) prepared as described above was added to 1 mL of 20 mM HEPES at pH 7.0 to give a final concentration of 19 nM. Assays were initiated by the addition of aliquots of a stock solution of 1-hydroxy-2-naphthoate in ethanol (34 mM). The final substrate concentration ranged from 3 – 270 µM. The reaction was monitored by following an increase in absorbance at 300 nm ($\varepsilon = 8637\ M^{-1}\ cm^{-1}$). Initial rates were determined from the first 30 s of the reaction, plotted versus substrate concentration, and fit to the Michaelis-Menten equation to calculate the steady-state parameters k_{cat} and K_M using Grafit (Johnson, 2011).

*PhdJ and PhdG with trans-o-Hydroxybenzylidenepyruvate (**9**) and trans-o-Carboxybenzylidenepyruvate (**13**)*

Aliquots of PhdJ or PhdG were added to 20 mM HEPES at pH 7.0 to final enzyme concentrations of 21 nM and 210 nM for PhdJ and 320 nM and 230 nM for PhdG. The assays were initiated by the addition of aliquots of a stock solution of HBP (19 mM in ethanol) or CBP (3 mM and 5.2 mM in ethanol). Final concentrations are summarized in Table 2.2. The reactions with HBP were monitored by following an increase in absorbance at 255 nm ($\varepsilon = 7{,}896\ M^{-1}\ cm^{-1}$). The reactions with CBP were monitored by following a decrease in absorbance at 300 nm ($\varepsilon = 8{,}637\ M^{-1}\ cm^{-1}$). Initial rates were determined from the first 60 s of the reaction, plotted versus substrate concentration, and fit to the substrate inhibition or Michaelis-Menten equation to calculate the steady-state parameters k_{cat}, $K_{M,}$ and K_i using Grafit (Johnson, 2011; Haldane, 1930).

Enzyme	Susbstrate	[Substrate] (μM)	[Enzyme] (μM)
PhdJ	HBP	0.4 - 132	0.21
	CBP	2.6 - 156	0.021
PhdG	HBP	1 - 65	0.23
	CBP	6.6 - 175	0.32

Table 2.2: Enzyme and substrate concentrations for hydratase-aldolase kinetic assays.

Coupled Assays using PhdI and PhdJ or PhdG

A coupled assay was used to follow the reactions of PhdJ and PhdG with the ring-opened product generated from 1-hydroxy-2-naphthoate using PhdI. The reactions were initiated by adding 100 μL of PhdI supernatant prepared as described above and various concentrations of 1-hydroxy-2-naphthoate in ethanol (0.6 to 40 μM for PhdJ and 4 to 114 μM for PhdG) to 1 ml of 20 mM HEPES at pH 7.0. The reactions were monitored by following the increase in absorbance of the product at 300 nm until completion as determined by no further change in absorbance (< 5 min). Upon completion, aliquots of PhdJ (75 nM final) or PhdG (240 nM final) were added and the decrease in absorbance at 300 nm (ε = 8,637 M^{-1} cm^{-1}) was followed. Initial rates were determined from the first 60 s of the reaction, plotted versus substrate concentration, and fit to the substrate inhibition or Michaelis-Menten equation to calculate the steady-state parameters k_{cat}, $K_{M,}$ and K_i using Grafit (Johnson, 2011; Haldane, 2003).

2.3 Results

Product Identification

*Reactions of PhdI with 1,2-Dihydroxynaphthalene (**7**) and 1-Hydroxy-2-Naphthoate (**12**)*

No reaction was observed when PhdI was incubated with 1,2-dihydroxynaphthalene. To determine the ring-opening position of 1-hydroxy-2-naphthoate (**12**) by PhdI, the two were mixed and the reaction was allowed to reach completion. The absorbance spectrum for the reaction is shown in Figure 2.1. The decrease at 250 nm corresponds to the decrease in concentration of **12** and the increase at 301 nm corresponds to the increase in the concentration of the product. The product of the reaction was isolated and identified using ^{1}H NMR spectroscopy. The product was determined to be CBP (**13**) and the proposed ortho-cleavage reaction shown in Scheme 2.3 was confirmed.

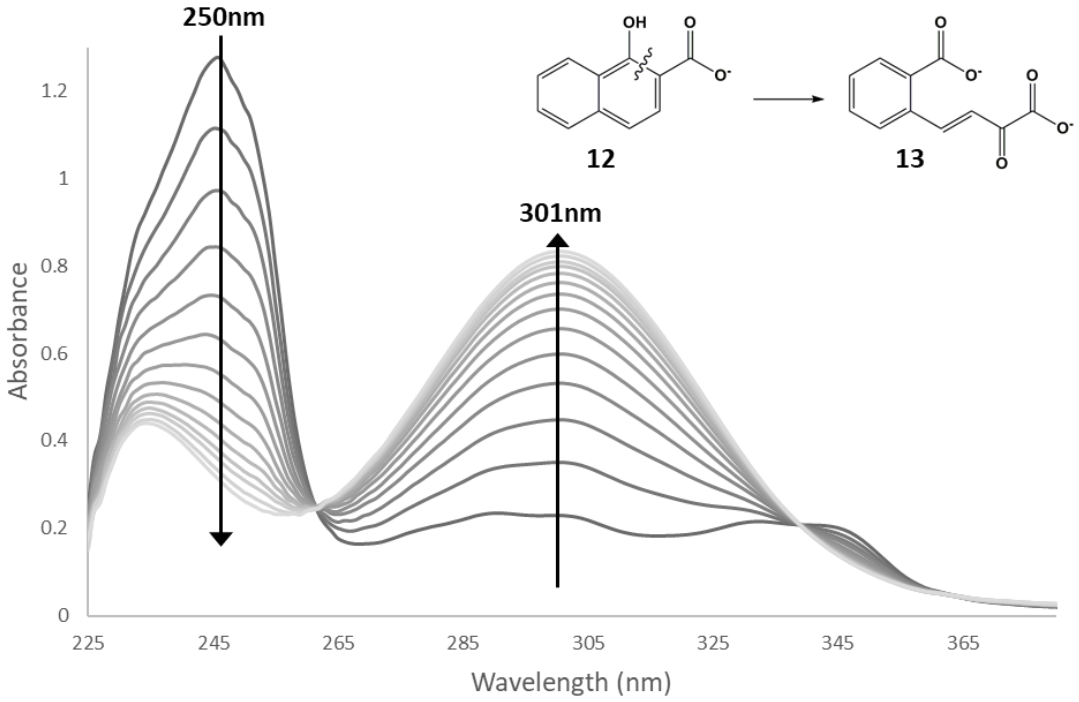

Figure 2.1: Absorbance spectra following the reaction of PhdI and 1-hydroxy-2-naphthoate (**12**).

*Reactions of PhdF with 1,2-Dihydroxynaphthalene (**7**) and 1-Hydroxy-2-Naphthoate (**12**)*

No reaction was observed when PhdF was incubated with 1,2-dihydroxynaphthalene (**7**) or with 1-hydroxy-2-naphthoate (**12**).

*Reactions of PhdJ and PhdG with trans-o-Hydroxybenzylidenepyruvate (**9**) and trans-o-Carboxybenzylidenepyruvate (**13**)*

To identify the products of the reactions of PhdJ and PhdG with **9** and **13**, the enzymes and substrates were mixed, and the reactions were allowed to reach completion. The absorbance spectra for the reactions of PhdG with **9** and PhdJ and **13** are shown in Figure 2.2. For the reaction using HBP, the decrease in absorbance at 293 nm corresponds to the decrease in concentration of HBP and the increase in absorbance at 255 nm corresponds to the increase in concentration of the product (**10**). For the reaction using CBP, the decrease in absorbance at 300 nm corresponds to a decrease in the concentration of CBP. The absorbance spectra for the reaction of PhdJ with HBP and PhdG with CBP match those shown. Absorbance spectra for pyruvate, salicylaldehyde and 2-carboxybenzaldehyde, the proposed reaction products, were obtained and compared to the absorbance spectra for the actual reaction products (Figure 2.3). The product spectra matched the proposed product spectra for each reaction therefore confirming the proposed reactions.

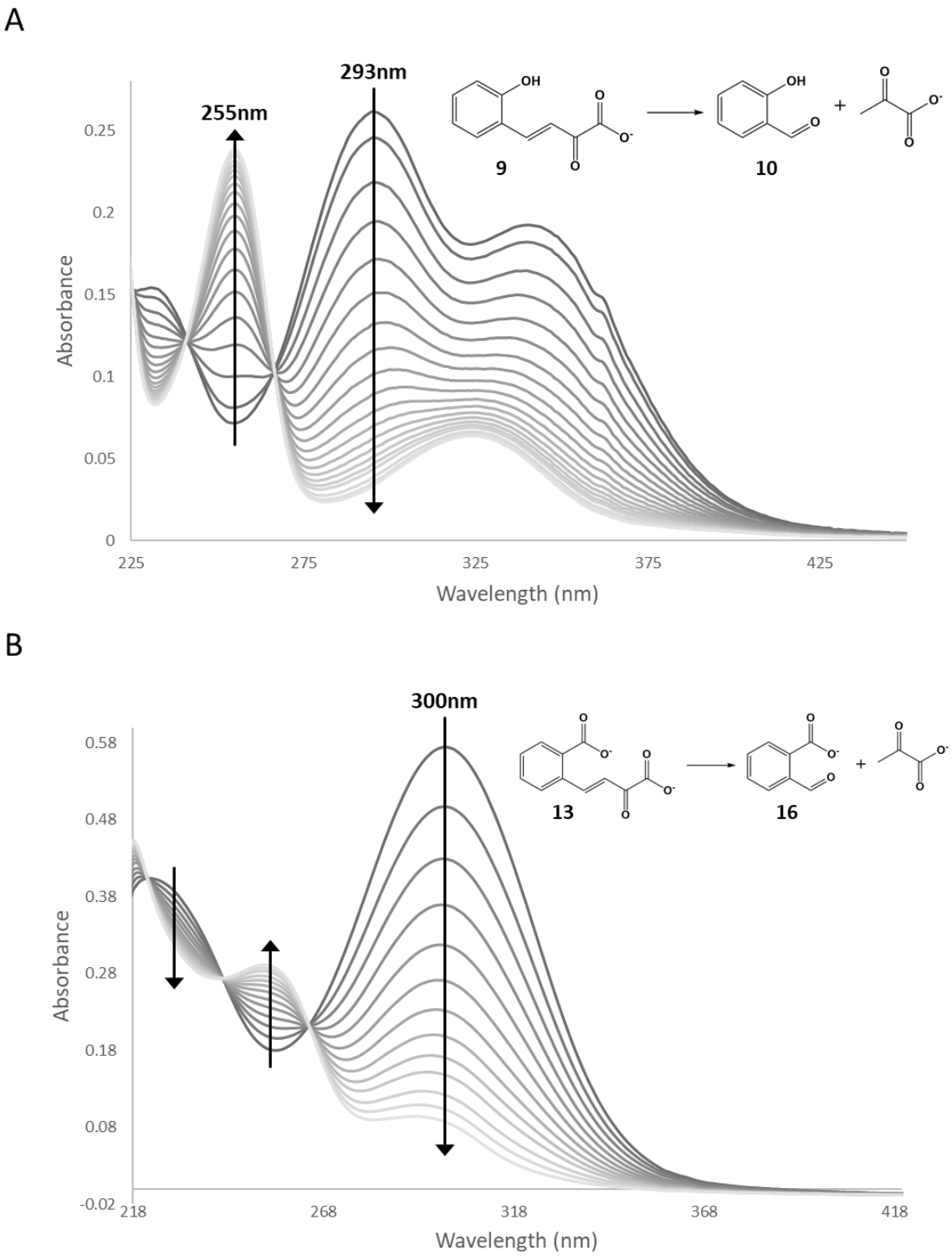

Figure 2.2: Absorbance spectra for the reaction of A) PhdG and HBP (**9**) and B) PhdJ and CBP (**13**).

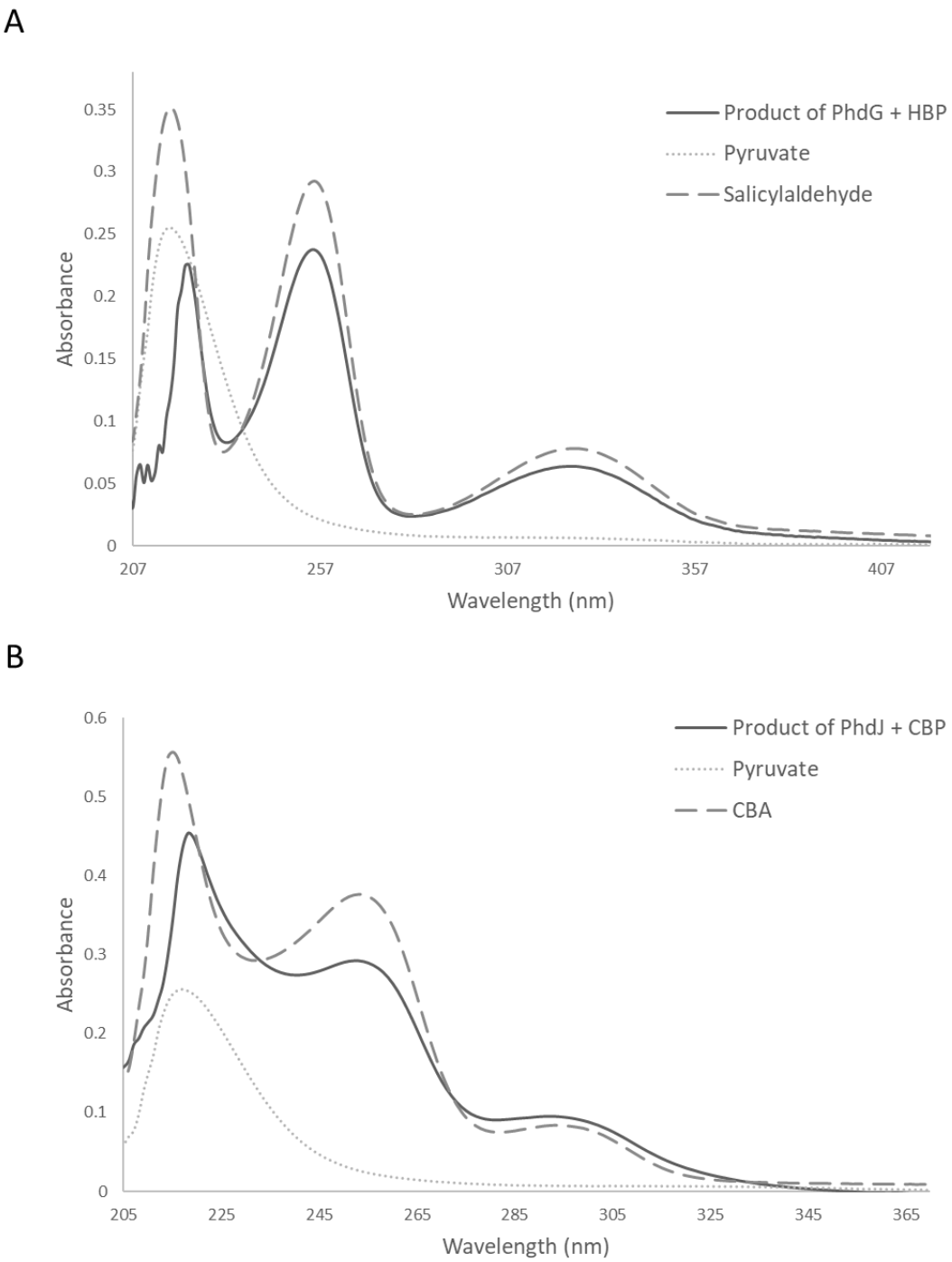

Figure 2.3: Absorbance spectrum of (A) the product of the reaction of PhdG and HBP (solid line), pyruvate (dotted line), and salicylaldehyde (dashed line) and B) the product of the reaction of PhdJ and CBP (solid line), pyruvate (dotted line), and 2-carboxybenzaldehyde (dashed line).

Steady-State Kinetic Analysis

*PhdI with 1-Hydroxy-2-Naphthoate (**12**)*

Kinetic parameters were determined for the reaction of PhdI and 1-hydroxy-2-naphthoate (**12**). A graph of k_{obs} vs 1-hydroxy-2-naphthoate concentration is given in Figure 2.4. The data are fit to the Michaelis-Menten equation (Johnson, 2011). The kinetic parameters are given in Table 2.3. The k_{cat}/K_M for this reaction is 3.1 x 10^5 $M^{-1}s^{-1}$.

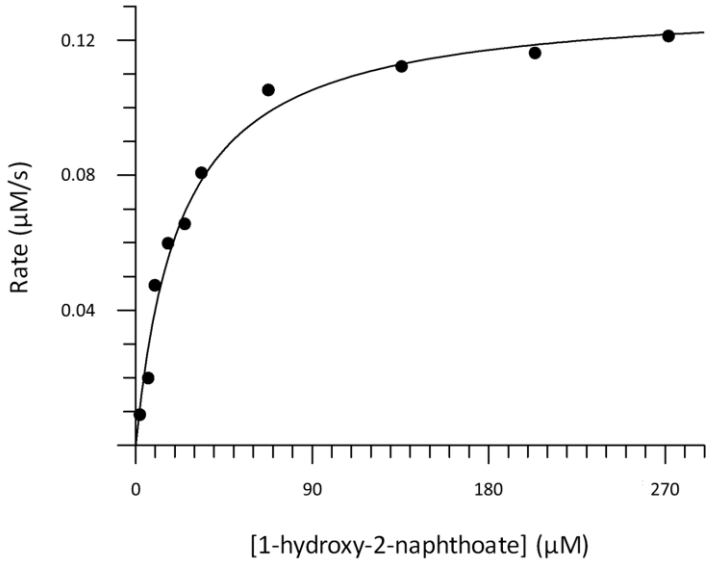

Figure 2.4: Plot of k_{obs} vs 1-hydroxy-2-naphthoate concentration for the reaction with PhdI. Data are fit to the Michaelis-Menten equation (Johnson, 2011).

Enzyme	Substrate	k_{cat} (s^{-1})	K_M (μM)	k_{cat}/K_M ($M^{-1}s^{-1}$)
PhdI	1-hydroxy-2-naphthoate	7.0 ± 0.2	23 ± 2	(3.1 ±0.3)E+05

Table 2.3: Kinetic parameters for the reaction of PhdI and 1-hydroxy-2-naphthoate (**12**).

*PhdJ and PhdG with trans-o-Hydroxybenzylidenepyruvate (**9**) and trans-o-Carboxybenzylidenepyruvate (**13**)*

The kinetic parameters were determined for the reactions of PhdJ and PhdG with HBP (**9**) and CBP (**13**). Plots of k_{obs} vs substrate concentration for each reaction are given in Figure 2.5. Data for the reaction of PhdG with HBP displays substrate inhibition and is fit to the substrate inhibition equation (Haldane, 1930). All other reactions appear to obey classic Michaelis-Menten kinetics and the data are fit using the Michaelis-Menten equation (Johnson, 2011). The kinetic parameters are given in Table 2.4. The k_{cat}/K_M values for the reaction of PhdJ and PhdG with HBP are identical (1.8×10^4 $M^{-1}s^{-1}$). The k_{cat}/K_M value for the reaction of PhdJ with CBP is 14-fold higher than that of PhdG with CBP.

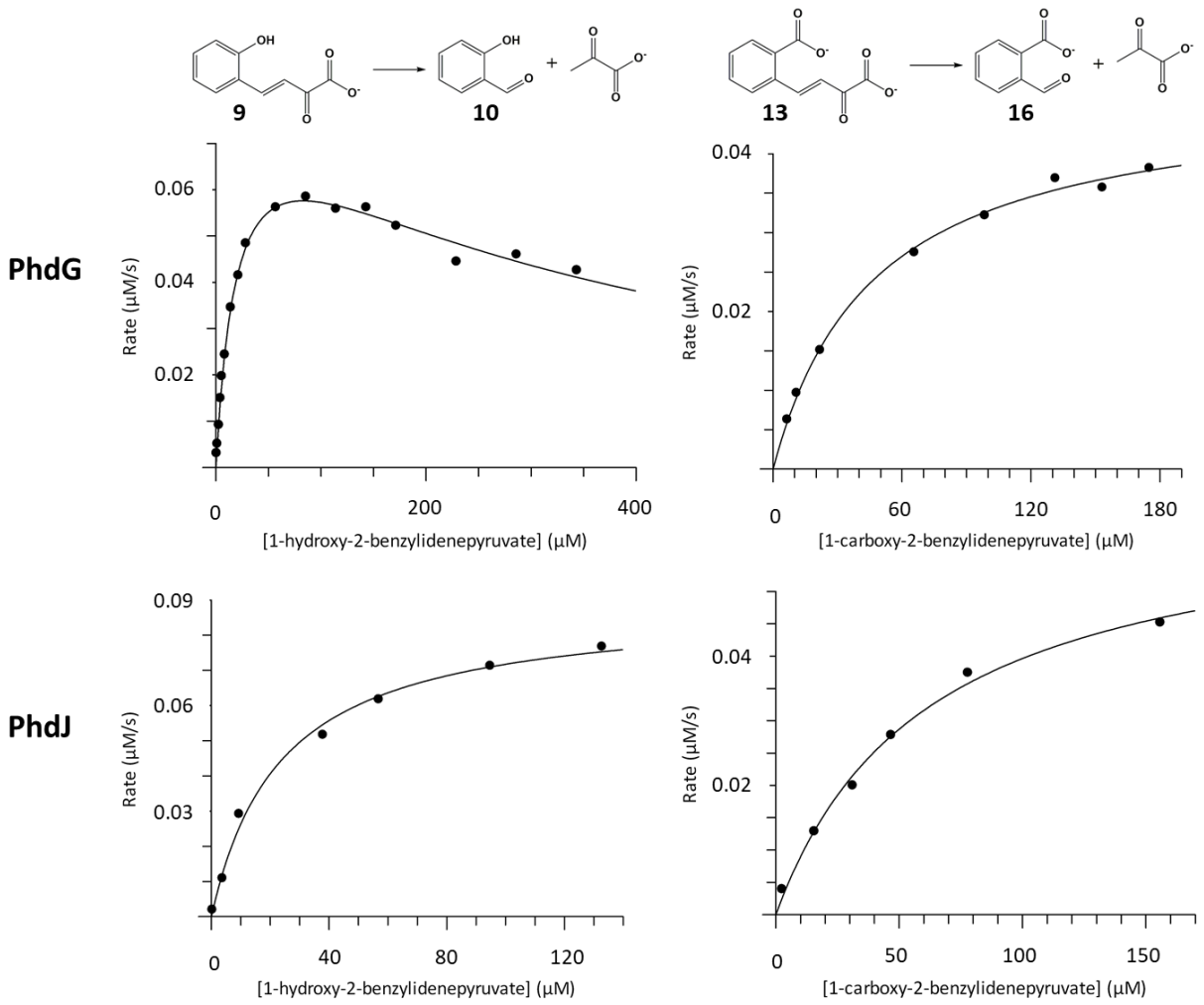

Figure 2.5: Plots of k_{obs} vs substrate concentration for each hydratase-aldolase reaction. The data for the reaction of PhdG with HBP are fit to the substrate inhibition equation (Haldane, 1930). All other data are fit to the Michaelis-Menten equation (Johnson, 2011).

Enzyme	Substrate	k_{cat} (s^{-1})	K_M (μM)	k_{cat}/K_M ($M^{-1}s^{-1}$)	K_i (μM)
PhdJ	*trans-o*-hydroxybenzylidenepyruvate	0.42 ± 0.01	24 ± 2	(1.8 ± 0.2) E+04	—
	trans-o-carboxybenzylidenepyruvate	3.0 ± 0.2	60 ± 8	(5.0 ± 0.9) E+04	—
PhdG	*trans-o*-hydroxybenzylidenepyruvate	0.37 ± 0.02	21 ± 2	(1.8 ± 0.3) E+04	330 ± 50
	trans-o-carboxybenzylidenepyruvate	0.148 ± 0.004	47 ± 4	(3.2 ± 0.4) E+03	—

Table 2.4: Steady-state kinetic parameters for PhdJ- and PhdG-catalyzed reactions.

Coupled Assays using PhdI and PhdJ or PhdG

Coupled assays were used to determine whether PhdG and PhdJ could directly process the product of the reaction of PhdI and 1-hydroxy-2-naphthoate (**12** to **13**). The absorbance spectra of the substrate 1-hydroxy-2-naphthoate (**12**), the product of the reaction of PhdI and 1-hydroxy-2-naphthoate (**13**), and the product after addition of PhdJ (**16**) are shown in Figure 2.6. The absorbance spectra for the reaction using PhdG matches that shown in Figure 2.6. Kinetic analysis was performed for these reactions and graphs of k_{obs} vs substrate concentration are shown in Figure 2.7. The data are fit to the Michaelis-Menten equation (Johnson, 2011). Kinetic parameters are given in Table 2.5. The k_{cat}/K_M value for the reaction with PhdJ is 2-fold higher than that with PhdG.

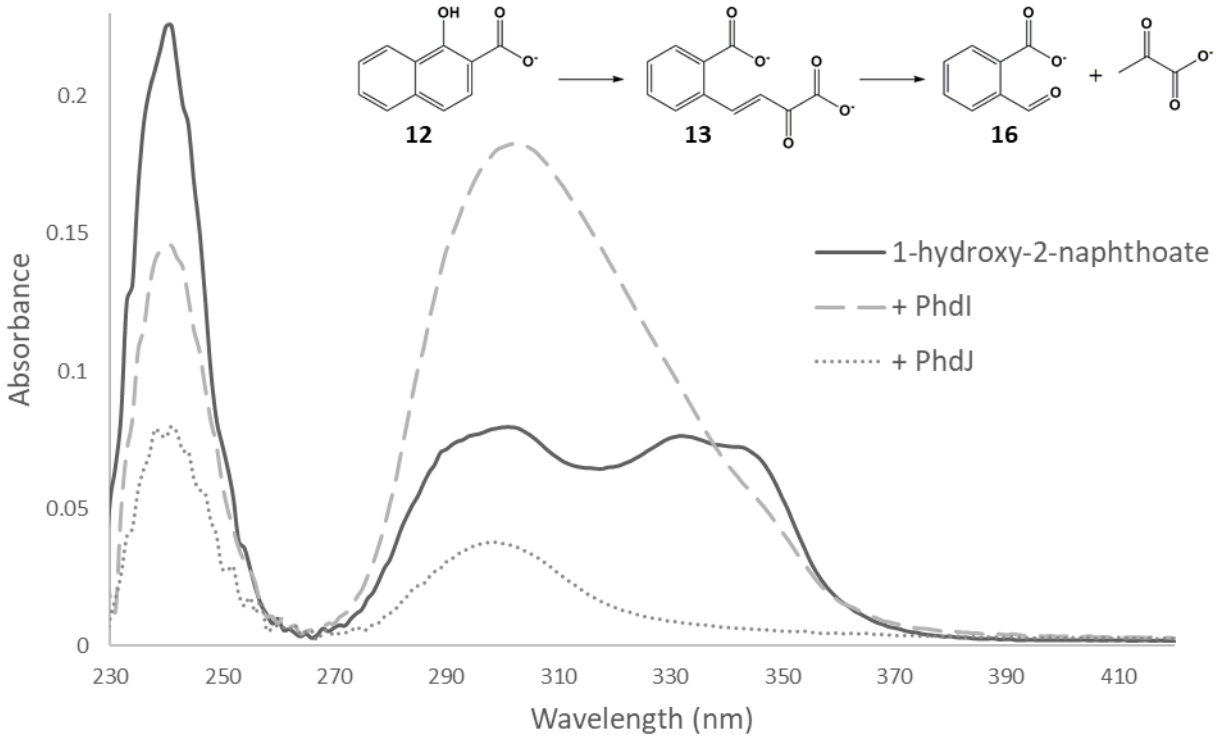

Figure 2.6: Absorbance spectrum of 1-hydroxy-2-naphthoate (solid line), after the addition of PhdI (dashed line), and after the addition of PhdJ.

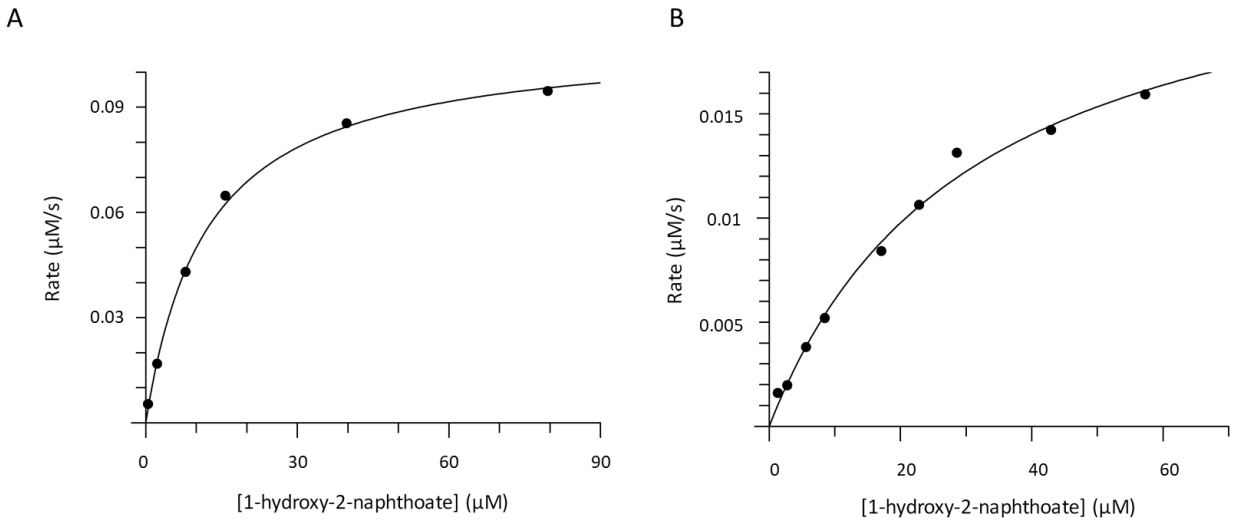

Figure 2.7: Plots of k_{obs} vs 1-hydroxy-2-naphthoate concentration for the coupled assay using PhdI and A) PhdJ or B) PhdG. The data are fit to the Michaelis-Menten equation (Johnson, 2011).

Enzyme	Substrate	k_{cat} (s^{-1})	K_M (µM)	k_{cat}/K_M ($M^{-1}s^{-1}$)	K_i (µM)
PhdJ	1-hydroxy-2-naphthoate	1.47 ± 0.04	12 ± 1	(1.2 ±0.1)E+04	—
PhdG	1-hydroxy-2-naphthoate	0.103 ± 0.007	31 ± 5	(3.5 ± 0.7)E+03	—

Table 2.5: Kinetics parameters for the coupled assays with PhdI, 1-hydroxy-2-naphthoate, and PhdJ or PhdG.

2.4 Discussion

PhdI, a dioxygenase encoded by a gene within the PAH catabolic region, has a modest sequence similarity (46%) with a known 1-hydroxy-2-naphthoate dioxygenase from *Nocardioides* sp. KP7 and has been annotated as such (Kim, 2008; Iwabuchi, 1998). 1-Hydroxy-2-naphthoate (**12** in Scheme 2.3) is an intermediate that has been identified within the lower catabolic pathway of pyrene by *M. vanbaalenii* PYR-1. Other isolated metabolites for this lower pathway include **13**, 2-carboxybenzaldehyde, and phthalate which suggests that **12** is cleaved by a dioxygenase at the ortho position (Scheme 2.3). 1-Hydroxy-2-naphthoate dioxygenases typically cleave at the ortho position and requires ferrous iron (Iwabuchi, 1998). PhdI was purified and assayed for activity with **12** and cleavage of **12** at the ortho position was confirmed by product identification. Kinetic parameters were determined for this reaction and PhdI has a high k_{cat}/K_M value of 3.1 x 10^5 $M^{-1}s^{-1}$ with **12**. These data support the annotation of PhdI as a 1-hydroxy-2-naphthoate dioxygenase (Scheme 2.5).

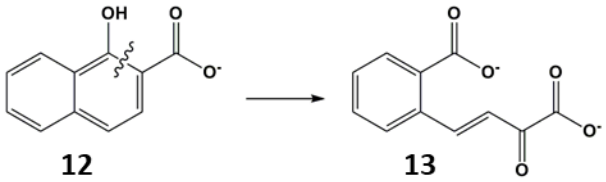

Scheme 2.5: Ring-opening of 1-hydroxy-2-naphthoate by PhdI.

Due to the similarity of **12** and 1,2-dihydroxynaphthalene (**7** in Scheme 2.2), PhdI might be the dioxygenase responsible for ring-opening of **7** in the naphthalene catabolic pathway of *M. vanbaalenii* PYR-1. 1,2-Dihydroxynaphthalene-1,2-diol (**6**, Scheme 2.2) and 2-hydroxybenzoate (**11**) were the only metabolites identified after growth of *M. vanbaalenii* PYR-1 in the presence of

naphthalene, suggesting that **7** is cleaved at the meta position. However, PhdI did not show ring-opening activity when incubated with **7**. PhdF is a dioxygenase putatively assigned to all ring-cleavage reactions within the upper catabolic pathways for phenanthrene, pyrene, and fluoranthene by *M. vanbaalenii* PYR-1 (Kweon, 2007; Kim, 2007; Stingley, 2004). The location of the gene encoding PhdF (gene 0470) within the PAH catabolic region suggests that PhdF is a suitable alternative candidate for ring-opening of **7**. PhdF was purified and assayed for ring-opening activity with **7** and no activity was observed. We have not identified a dioxygenase that is capable of cleaving **7**, but there are six other annotated type I extradiol dioxygenases genes within the genome of *M. vanbaalenii* PYR-1 and three of these (genes 0545, 0591, and 4413) are also within the catabolic regions (Kim, 2008). It is possible that one of these dioxygenases is responsible for cleavage of **7**. These dioxygenases will be the targets of future studies.

The next step in the catabolism of **12** is the hydration of *trans*-carboxybenzylidenepyruvate (**13** in Scheme 2.3) followed by a retro-aldol cleavage by a hydratase-aldolase. PhdJ is proposed to be the hydratase-aldolase that is active in the lower catabolic pathways of HMW PAHs, while PhdG has been proposed to function in the upper catabolic pathways (Kweon, 2007; Kim, 2007; Stingley, 2004). PhdJ and PhdG were assayed for hydratase-aldolase activity with **13** using a coupled assay and **13** alone. Both hydratase-aldolases converted **13** to 2-carboxybenzaldehyde, and the catalytic efficiencies for the coupled assays are consistent with those found using substrate alone. PhdJ has a k_{cat}/K_M that is 14-fold higher than that of PhdG and is likely the hydratase-aldolase responsible for this reaction *in vivo*.

The product of meta-cleavage of **7** by a dioxygenase is 2-hydroxychromene-2-carboxylate (**8**, Scheme 2.2). Some bacteria utilize a glutathione-dependent isomerase to convert **8** to *trans*-hydroxybenzylidenepyruvate (**9)** before processing by a hydratase-aldolase (Thompson, 2007). There is not a gene encoding a product with significant sequence similarity to a similar isomerase (NahD of the NAH7 plasmid in *Pseudomonas putida* G7) within the genome of *M. vanbaalenii* PYR-1 (Thompson, 2007). Moreover, mycobacteria do not produce glutathione (Anderberg, 1998). There are several genes annotated as mycothiol-dependent isomerases within the genome of *M. vanbaalenii* PYR-1. Mycothiol-dependent isomerases utilize a thiol similarly to glutathione-dependent isomerases and may be responsible for the isomerization of **8** to **9** in *M. vanbaalenii* PYR-1. It is also possible that the dioxygenase that cleaves **7** may function as an isomerase. We did not observe ring-opening of **7** by either of the dioxygenases (phdI or PhdF) purified in these experiments. PhdJ and PhdG were assayed for activity with **9** and both enzymes processed **9** to salicylaldehyde. The k_{cat}/K_M values for this reaction were comparable for PhdJ and PhdG. Hence, either PhdJ or PhdG could be responsible for cleavage of **9**, but the activities of the enzymes have not been confirmed *in vivo*. The non-enzymatic isomerization of **8** to **9** could be sufficient for the reaction to proceed, PhdJ and PhdG could have an inherent isomerase activity, or the dioxygenase that cleaves **7** could also catalyze the isomerization of **8** to **9**. These possibilities will be investigated in future work.

Chapter 3: Investigation of the Ring-Cleaving Dioxygenase and Hydratase-Aldolase Reactions in the *M. vanbaalenii* PYR-1 Phenanthrene Catabolic Pathway

3.1 Introduction

Phenanthrene is a polycyclic aromatic hydrocarbon (PAH) composed of three aromatic rings that displays various toxicities including disruption of nutritional and photosynthesis functions in maize, oxidative stress induction in guppies, and visual and cardiac developmental defects in zebrafish (Dupuy, 2015; Machado, 2014; Huang, 2013; Zhang, 2013). Phenanthrene is a model substrate for elucidation of various PAH catabolic pathways because its structure is similar to those of some carcinogenic HMW PAHs. Phenanthrene contains a bay-region (C-3 and C-4) and a K-region (C-9 and C-10) that are potential sites for epoxide formation by cytochrome p450 enzymes (Scheme 3.1). Epoxide formation at these regions gives HMW PAHs carcinogenic properties (Seo, 2009). Elucidating the phenanthrene catabolic pathway is also important because many of the catabolic pathways for the more toxic HMW PAHs feed into the phenanthrene pathway (Kweon, 2011).

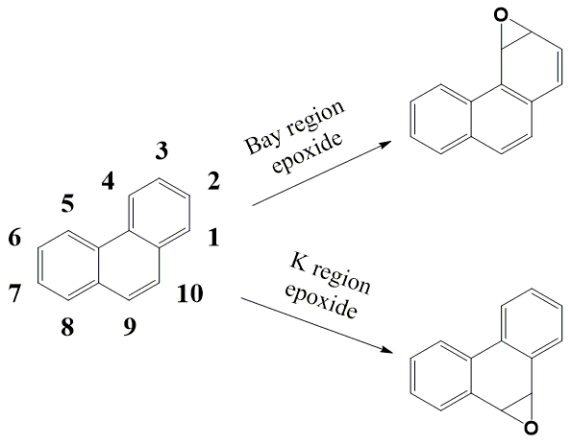

Scheme 3.1: Epoxide formation at the Bay and K regions of phenanthrene.

The phenanthrene catabolic pathway has been most extensively studied in *Mycobacterium vanbaalenii* PYR-1 using metabolomic, proteomic, and genomic experiments (Moody, 2001; Stingley, 2004; Kim, 2005; Kim, 2008; Kweon, 2011). Phenanthrene catabolism by *M. vanbaalenii* PYR-1 involves the multiple routes shown in Scheme 3.2 (Stingley, 2004; Bayly, 1966; Kweon, 2011). Degradation of phenanthrene begins with dioxygenation at the K-region to form **18**, the bay-region to form **19** or the non-K and non-bay region (C-1 and C-2) to form **20** (Scheme 3.2). Oxygenation at the non-K and non-bay region is thought to result in the methylated dead-end product **21** while **18** continues in the degradation pathway through ortho-ring cleavage to **22** and **19** continues through ortho- or meta-ring cleavage (**23** and **24** respectively) (Kim, 2005). The meta-cleavage product **24** undergoes *cis* to *trans* isomerization (**25**), but it is unclear whether this isomerization is enzyme-catalyzed (a similar step in the naphthalene catabolic pathway is catalyzed by NAhD). Both the ortho- and meta-cleavage products are cleaved by a hydratase-aldolase and the products (**27** and **26**, respectively) undergo another round of processing. These pathways result in the production of phthalate or salicylate that can be further degraded into TCA cycle intermediates to be used by the cell for energy production. Gene products have not been assigned to all possible transformations in the pathway.

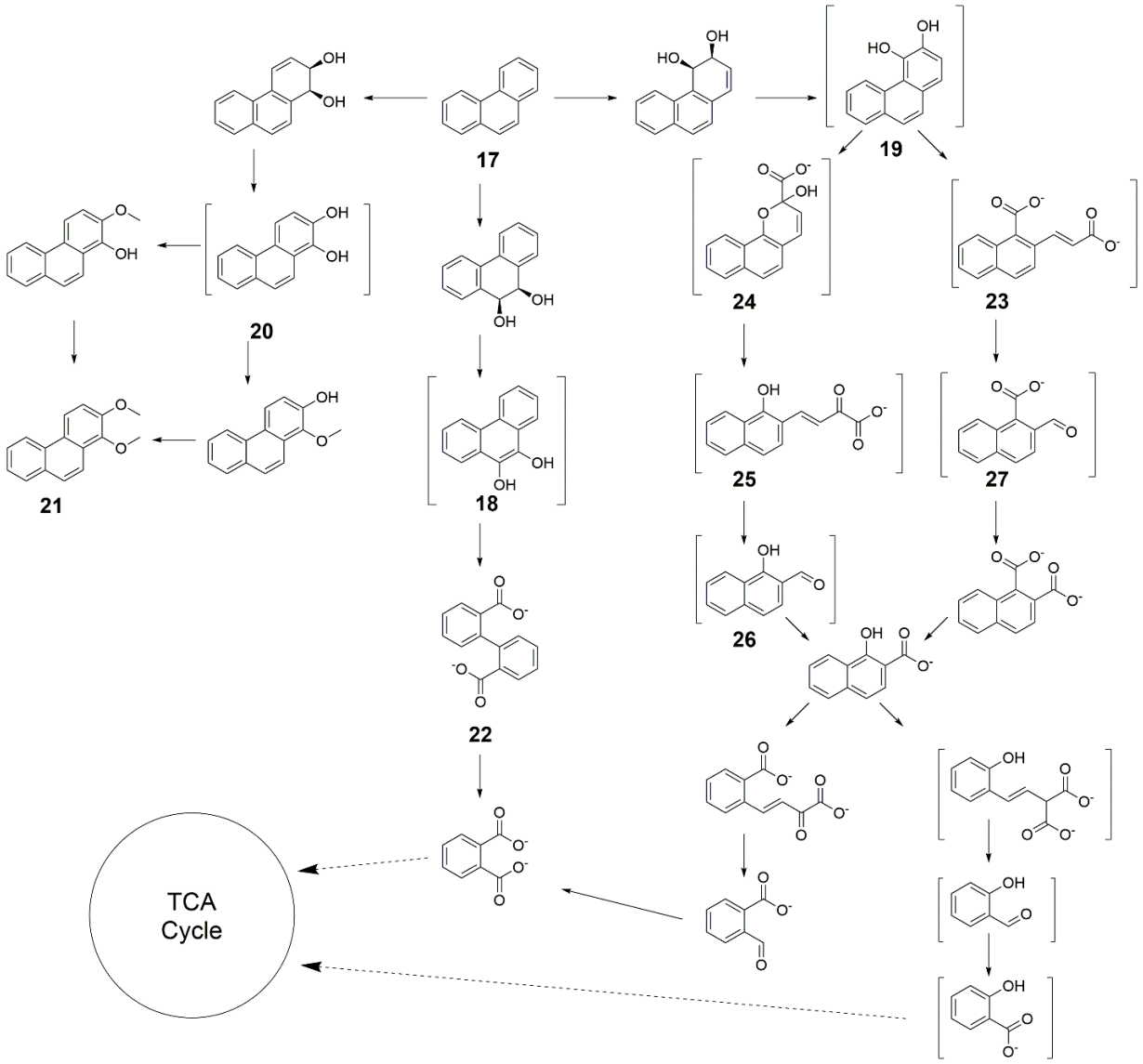

Scheme 3.2: Proposed phenanthrene catabolism by *M. vanbaalenii* PYR-1. Brackets indicate compounds that have not been isolated (Stingley, 2004; Moody, 2001; Kim, 2005).

The *M. vanbaalenii* PYR-1 gene 0470 encodes the iron-dependent type I extradiol dioxygenase PhdF that is upregulated in the presence of pyrene whose catabolic pathway ultimately intersects with phenanthrene's through production of 3,4-dihydroxyphenanthrene (**19**) (Scheme 2.3) (Kim, 2007; Stingley, 2004). Stingley et al also showed that PhdF is likely involved in phenanthrene catabolism through the degradation route beginning with oxidation at positions C-3 and C-4 to produce **19** that is cleaved in the meta position to afford **24** (Stingley, 2004) (Scheme 3.3). Although *M. vanbaalenii* Pyr-1 can utilize the degradation route beginning with **19**, the route beginning with 9,10-dihydroxyphenanthrene (**18**) is the preferred route for degradation of phenanthrene (Moody, 2001). This route involves the intradiol cleavage of **18** to produce **22**. Cleavage at the intra- and extra-diol positions requires dioxygenases with different active-site residues and iron cofactors with different oxidation states, so it is highly unlikely that PhdF is responsible for the proposed meta-cleavage of **19** and the ortho-cleavage of **18** (Vaillancourt, 2006). A previous study using *Arthrobacter* sp. P1-1 showed that **19** can also be cleaved in the ortho position and that **20** can be cleaved in both the ortho and meta positions rather than methylated and eliminated from the cell (Scheme 3.3) (Seo, 2006). It is possible that PhdF cleaves all three phenanthrene catechol compounds (**18**, **19**, and **20**) in either the ortho or the meta positions (Scheme 3.3) or is not responsible for cleavage of all three compounds.

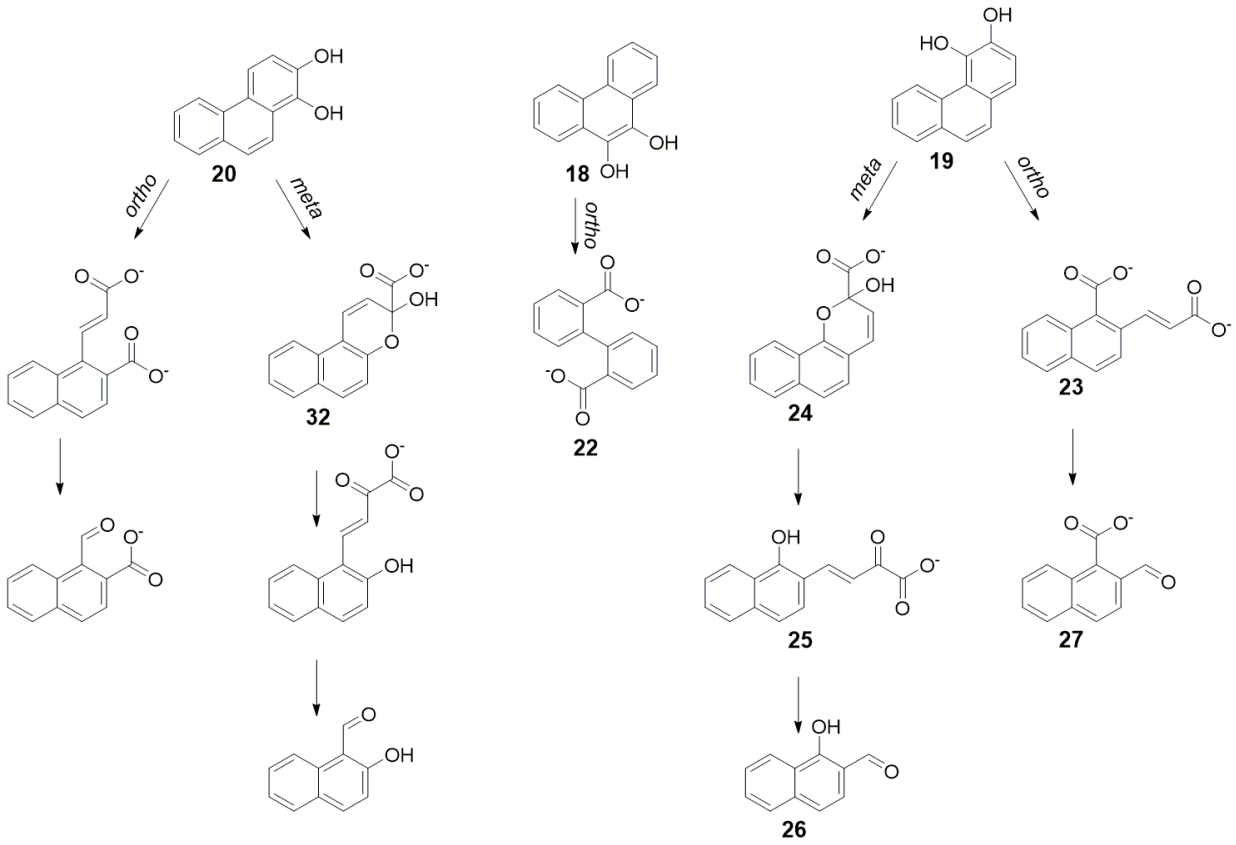

Scheme 3.3: Possible ring-cleavage reactions of phenanthrene catechol compounds (**18**, **19**, **20**) and subsequent isomerization and/or hydrolysis.

The *M. vanbaalenii* PYR-1 gene 0469 encodes the hydratase-aldolase PhdG that is also upregulated in the presence of pyrene. This, along with a study by Stingley et al, implicates PhdG in the phenanthrene degradation pathway involving **19**. The activity of a hydratase-aldolase is not required for the phenanthrene degradation pathway involving **18**. If *M. vanbaalenii* PYR-1 utilizes the pathway involving **20** for energy production, the product of ring-cleavage of **20** would be structurally similar to the product of ring-cleavage of **19** (Scheme 3.3) and it is likely that PhdG would be able to process both compounds.

A BLAST search reveals three *M. vanbaalenii* PYR-1 gene products with high sequence similarity to that of the type I extradiol dioxygenase 0470: 5306 with 39%, 4413 with 38%, and 2891 with 38%. To date, none of these genes has been implicated in PAH catabolism, but all three are annotated as ring-cleaving dioxygenases and the 4413 gene is located within a catabolic gene cluster. All four ring-cleaving dioxygenases were cloned, expressed, purified, and assayed with the three proposed phenanthrene catechols (**18**, **19**, and **20** in Scheme 3.3). The reaction products were purified and identified. The catechol compounds that did not act as substrates were also tested as inhibitors. The hydratase-aldolase PhdG was assayed for activity with the enzyme-catalyzed ring-opened catechols and the products were purified and identified.

3.2 Experimental Procedures

Materials

Chemicals, biochemicals, buffers, and solvents were purchased from Sigma-Aldrich Chemical Co. (St. Louis, MO), Fisher Scientific Inc. (Pittsburgh, PA), Fluka Chemical Corp. (Milwaukee, WI), or EMD Millipore, Inc. (Billerica, MA). 2,3-Dihydroxybiphenyl (99%) was purchased from Wako Chemicals Inc. (Richmond, VA). 3-Methylcatechol, 9,10-phenanthrenequinone, 2,3-dimethoxybenzaldehyde, 3,4-dimethoxybenzaldehyde, and 3,4-dimethoxybenzoic acid were purchased from Sigma-Aldrich Chemical Co. The synthetic procedures for 1,2-dihydroxyphenanthrene (**20**), 2,3-dihydroxyphenanthrene, 3,4-dihydroxyphenanthrene (**19**), and 9,10-dihydroxypheananthrene (**18**) are reported in the supplemental material (Section 3.5). The DEAE-Sepharose resin and the prepacked PD-10 Sephadex G-25 columns were obtained from GE Healthcare (Piscataway, NJ). The HisPur Ni-

NTA resin was purchased from Sigma-Aldrich Chemical Co. The EconoColumn® chromatography columns were obtained from BioRad (Hercules, CA). The Amicon stirred cell concentrators, ultrafiltration membranes (10,000 Da cutoff), and Amicon Ultra centrifuge concentrators (3000 Da cutoff) were purchased from EMD Millipore Inc.

Bacterial Strains, Plasmids and Enzymes

The pET vectors were obtained from Novagen (Madison, WI). *Escherichia coli* strain C41(DE3) was obtained from Sigma-Aldrich Chemical Co. Isolated genomic DNA from *Mycobacterium vanbaalenii* PYR-1 and *Mycobacterium vanbaalenii* PYR-1 gene 4413 in pET17b were obtained from the laboratory of Dr. Carl Cerniglia (National Center for Toxicology Research, U.S. Food and Drug Administration, Jefferson, AR).

General Methods

Oligonucleotide primers were synthesized by Sigma-Aldrich Co. The PCR amplification of DNA sequences was conducted in a GeneAmp 2700 thermocycler (Applied Biosystems, Carlsbad, CA). The GenElute gel extraction was purchased from Sigma-Aldrich Co. Enzymes and reagents used for in these procedures were purchased from New England Biolabs, Inc (Ipswich, MA). DNA sequencing was performed in the DNA Core Facility in the Institute for Cellular and Molecular Biology (ICMB) at the University of Texas at Austin. The QIAprep spin miniprep kit was purchased from Qiagen (Hilden, Germany). Sonication was performed using a W385 sonicator from Heat systems-ultrasonics, Inc. (Farmingdale, NY). Sodium dodecyl sulfate-polyacrylamide gel electrophoresis (SDS-PAGE) was carried out on a Bio-Rad Mini-Protean II

gel electrophoresis apparatus. Protein concentrations were determined using the Bradford method (Bradford, 1976). Electrospray ionization mass spectrometry (ESI-MS) was carried out on an LCQ electrospray ion-trap mass spectrometer (Thermo, San Jose, CA) housed in the ICMB Protein and Metabolite Analysis Facility at the University of Texas. Steady-state kinetic assays were performed on an Agilent 8453 diode-array spectrophotometer (Agilent Technologies, Santa Clara, CA). Nonlinear regression data analysis was performed using the program Grafit (Erithacus Software Ltd., Staines, U.K.). Nuclear magnetic resonance (NMR) spectra were recorded on a Varian UNITY+ 300 MHz spectrometer (Palo Alto, CA) or a Bruker AVANCE III 500 MHz spectrometer (Billerica, MA). NMR signals were analyzed using the software program SpinWorks 3.1.6 (Copyright 2009 Kirk Marat, University of Manitoba).

Cloning of *M. vanbaalenii* PYR-1 genes 2891 and 5306

Amplification of the desired genes was achieved through two rounds of PCR. The first round used overhang PCR primers that annealed within 100 bp around the desired gene. The second round isolated the desired gene flanked with appropriate restriction sites. The primers used for PCR are shown in Table 3.1. The 100 µL amplification reaction contained the *M. vanbaalenii* PYR-1 genomic DNA as a template (15 ng), dNTPs (0.4 mM), MgCl (2 mM), primers (0.4 µM), 1× buffer, and Vent Polymerase (1 unit). The PCR amplification protocol consisted of a 5 min denaturation step at 94°C followed by 35 cycles of 94°C for 1 min, 55°C for 1 min, and 72°C for 3 min and ended with a 10 min elongation step at 72°C. The PCR reaction product size was confirmed using a 1% agarose gel and isolated using a GenElute gel extraction kit and elution into 60 µL of water. The second round of PCR was set up and run identically to round one except 5 µL

of round one PCR product was used as template DNA and the primers containing restriction sites were used. The product was purified as described above. The PCR products were inserted into pET44 or pET32 between appropriate restriction sites (Table 3.1) using digestion and ligation procedures reported elsewhere (Deininger, 1990). An aliquot of the ligation mixture (30 µL) was transformed into *E. coli* C41(DE3) using a calcium heat shock method (Deininger, 1990). Transformed cells were grown on agar plates containing ampicillin (100 µg/mL) at 37 °C overnight. A single colony was used for the generation of additional plasmid for sequencing and protein expression.

Gene	Overhang Primers Fwd	Overhang Primers Rev	Round 2 Primers Fwd	Round 2 Primers Rev	Restriction Enzymes		Vector
PhdF	TGGGCCGCACTC CAGCAGCGCTAT	TTAGGAACCGGA TCGCCATTTCAC	GGACAGCAC**GAA** **TTC**TTGGTGAA	GCCGTCGAG**AAG** **CTT**TCATGTTG	EcoRI	HindIII	pET32
2891	TGGTCCCAGTGC GTGATCT	CGATGATCTGAC GGGGTCG	GTCGGGCAG**GAG** **CTC**AGTCTGATC	TGTCGGTGC**AAG** **CTT**TCACGGACG	SacI	HindIII	pET44
5306	GAACTGCCCCAGC ACATTCC	TTTCCTCGGAGG GGGATAGTT	ATAGTTC**GGATC** **C**ACGATCAAG	GAGGACA**AAGCT** **T**CTAGGATTT	BamHI	HindIII	pET32
4413	—	—	—	—	NdeI	XhoI	pET17

Table 3.1: Primers and restriction enzymes used for PCR amplification of *M. vanbaalenii* PYR-1 dioxygenase genes.

Expression of 0470 (PhdF), 2891, 4413, and 5306

LB cultures (25 mL) containing ampicillin (100 µg/mL) were inoculated using a single colony and grown overnight at 37 °C. LB cultures (4 × 400 mL) were then inoculated using an appropriate amount of the overnight culture to make OD_{600} = 0.05 AU and grown at 37°C for 2.5 h. Protein expression was induced overnight (18 h) at 21 °C using a final isopropyl-β-D-thiogalactoside concentration of 0.1 mM. Cells were harvested by centrifugation (10,000 × g) with yields ranging from 3-5 g and stored at −80 °C.

Purification of Enzymes

0470, 2891, and 5306

Cells were suspended to a final concentration of 10 mg/mL in Buffer A (20 mM HEPES, 300 mM NaCl, pH 7) with 15 mM imidazole. Cells were disrupted by sonication and the resulting solution was centrifuged for 30 min at 17,700 × g and 4 °C. The supernatant was loaded onto a Ni-NTA column (1 × 10 cm, ~6 mL resin) pre-equilibrated with Buffer A + 15 mM imidazole. The column was washed with Buffer A + 70 mM imidazole and the desired protein was eluted with Buffer A + 90 mM imidazole. Protein purity was confirmed by SDS-PAGE by the presence of a single band at the correct molecular mass after staining using Coomassie Blue. The eluant was concentrated to ~1 mg/mL and exchanged into 20 mM HEPES, 300 mM NaCl, 5% glycerol, pH7 (Buffer B) using an Amicon stirred cell concentrator (10,000 MW cutoff).

4413

Cells were suspended in Buffer A to a concentration of 10 mg/mL, lysed by sonication and the resulting solution was centrifuged for 30 min at 17,700 × g and 4 °C. The clarified supernatant was loaded onto a DEAE-Sepharose column (1 × 10 cm, ~8 mL resin) pre-equilibrated with Buffer A. The column was washed with 20 mL of Buffer A followed by a linear salt gradient (0–0.5 M NaCl, 200 mL total). Pure protein typically elutes at 0.3 M NaCl as determined by activity assays and SDS-PAGE. Protein purity was confirmed by SDS-PAGE by the presence of a single band after staining using Coomassie Blue. The protein-containing fractions were combined and concentrated to ~1 mg/mL and exchanged into Buffer B using an Amicon stirred cell concentrator (10,000 MW cutoff).

Activation of 0470 (PhdF), 2891, 4413, and 5306

To activate the enzymes, ascorbate (4 mM final concentration), Iron(II) chloride (2 mM final concentration) and acetone (5% final concentration) were added to aliquots (~500 uL) of protein purified as described above and the resulting mixture was incubated on ice for 30 min. The sample was centrifuged for 5 min at 20,800 × g and exchanged into Buffer B using a PD-10 column. Activity decreases within 8 h of activation so protein is activated and assayed on the same day.

Steady-State Kinetic Analysis Using Dioxygenases

For kinetic analysis, enzymes were kept on ice to slow deactivation. Aliquots of enzyme were added to 1 mL 20 mM HEPES at pH 7.0 to final enzyme concentrations ranging from 20 nM to 1 µM for PhdF, 100 nM to 300 nM for 2891, 70 nM to 1 µM for 4413, and 41 nM to 1.3 µM for 5306 as determined by the Bradford method (Bradford, 1976). The reaction was initiated by the addition of 1-20 µL of substrate in ethanol from stock solutions of 3-methylcatechol (20 – 175 mM), 2,3-dihydroxybiphenyl (1 – 4.5 mM), 3,4-dihydroxyphenanthrene (0.7 – 6 mM), and 1,2-dihydroxyphenanthrene (2 mM). Final substrate concentrations are summarized in Table 3.2. UV spectroscopy was used to monitor the reactions as follows: for 3-methylcatechol, monitor the increase in absorbance at 388 nm (ε = 13,800 M^{-1} cm^{-1}); for 2,3-dihydroxybiphenyl, monitor the increase in absorbance at 434 nm (ε = 21,700 M^{-1} cm^{-1}); for 3,4-dihydroxyphenanthrene, monitor the decrease in absorbance at 245 nm (ε = 25,800 M^{-1} cm^{-1}); and for 1,2-dihydroxyphenanthrene, monitor the decrease in absorbance at 263 nm (ε = 32,800 M^{-1} cm^{-1}). Initial rates were determined from the first 15 s of the reaction, plotted versus substrate concentration, and fit to the Michaelis-

Menten or substrate-inhibition equations to calculate the steady-state parameters k_{cat}, K_M, and K_i using Grafit (Johnson, 2011, Haldane, 1930). PhdF, 2891, 4413, and 5306 showed no enzymatic activity when incubated with 2,3-DHP.

Enzyme	Substrate	[Substrate] (μM)	[Enzyme] (ηM)
PhdF	3-methylcatechol	6-580	80
	2,3-dihydroxybiphenyl	35	510
	1,2-dihydroxyphenanthrene	—	—
	3,4-dihydroxyphenanthrene	1-9	10
2891	3-methylcatechol	3-1600	220
	2,3-dihydroxybiphenyl	2-440	8
	1,2-dihydroxyphenanthrene	5-35	310
	3,4-dihydroxyphenanthrene	1-40	40
4413	3-methylcatechol	80-6200	30
	2,3-dihydroxybiphenyl	14-1700	30
	1,2-dihydroxyphenanthrene	—	—
	3,4-dihydroxyphenanthrene	5-330	20
5306	3-methylcatechol	64-7200	120
	2,3-dihydroxybiphenyl	5-360	60
	1,2-dihydroxyphenanthrene	7-43	1030
	3,4-dihydroxyphenanthrene	0.3-40	5

Table 3.2: Enzyme and substrate concentration used in steady-state kinetic assays.

Identification of Dioxygenase Reaction Products

2,3-Dihydroxybiphenyl, 3,4-Dihydroxyphenanthrene, and 1,2-Dihydroxyphenanthrene

PhdF was used to generate the ring-opened products of 2,3-dihydroxybiphenyl (2,3-DHB) and 3,4-dihydroxyphenanthrene (3,4-DHP) (**30** and **25** respectively, Scheme 3.4). The enzyme 2891 was used to generate the 1,2-dihydroxyphenanthrene (1,2-DHP) cleavage product (**32** in Scheme 3.4). PhdF was also used to generate the 3-methylcatechol ring-opened product (**28**) in order to validate and optimize the product purification methodology. The products were identified by UV spectroscopy, derivatization, and NMR spectroscopy.

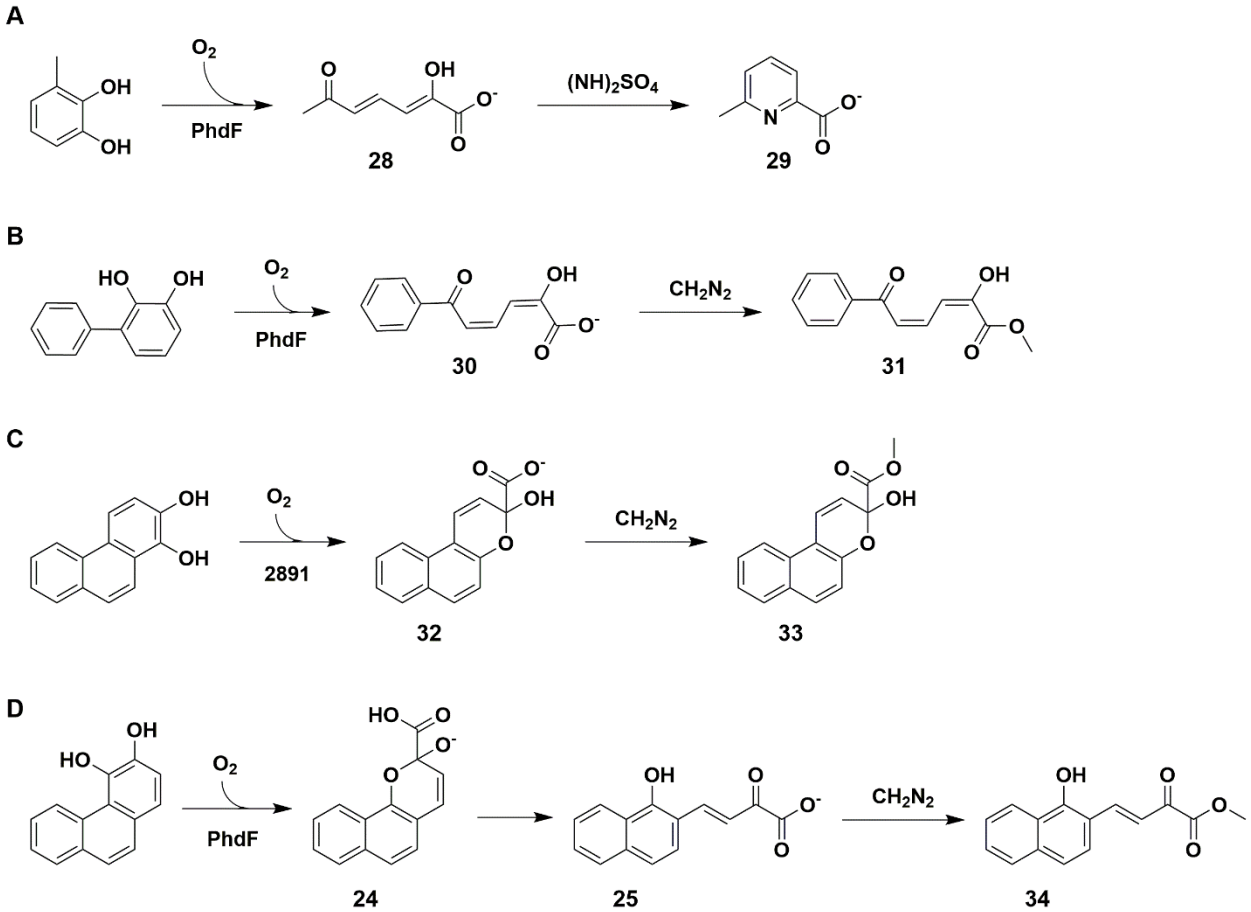

Scheme 3.4: Reaction products were generated and isolated as described in the text and converted to the indicated stable compounds for analysis.

After expression of the enzymes as described above, the cells were centrifuged at 17,700 × g for 30 min. The cell pellet was washed 3 times by resuspension in Buffer A (OD_{600} = 0.5 for 10 µL suspension in 1 mL buffer) and then centrifuged (17,700 × g for 30 min). The pellet was then resuspended in Buffer A to an OD_{600} of 0.5 for 10 µL PhdF in 1 mL of buffer and an OD_{600} of 0.5 for 40 µL of 2891 in 1 mL buffer. The final volume was 100 mL for the 2,3-DHB reaction, 300 mL for the 3,4-DHP reaction, and 600 mL for the 1,2-DHP reaction. Stock substrates were prepared in ethanol immediately before use at concentrations of 50 mg/mL. An aliquot of the stock substrate (2 mL) was added to the cell suspension, which was stirring on ice, over the course of 5 min to final concentrations of 1 mg/mL for 2,3-DHB, 0.33 mg/mL for 3,4-DHP, and 0.17 mg/mL for 1,2-DHP. Every 5 min, aliquots (500 µL) were removed, centrifuged at 20,800 × g for 2 min, and the cell free supernatant monitored by UV spectroscopy until the reaction was complete (~30 min) as determined by no further change in absorbance. The reactions were monitored as follows: for 2,3-dihydroxybiphenyl, monitor the increase in absorbance at 434 nm; for 3,4-dihydroxyphenanthrene, monitor the decrease in absorbance at 245 nm; and for 1,2-dihydroxyphenanthrene, monitor the decrease in absorbance at 263 nm. The reaction was centrifuged at 17,700 x g for 20 min and the cell-free supernatant acidified to a pH of 2.25 using drops of 10 M HCl. The acidic solutions were extracted using 2.5 volumes of ether and the collected ether layers were dried over anhydrous magnesium sulfate. The unstable reaction products were methylated using diazomethane generated using a Diazald kit following the manufacturer's instructions (Scheme 3.4). The methylated products were purified on a silica column using 2:1 hexane:ethyl acetate for **31** and 4:1 hexanes:ethyl acetate for **33** and **35** (Scheme 3.4). The product-containing fractions, as determined by TLC, were combined and evaporated to

dryness. The products were analyzed using ESI-MS. The masses were consistent with the calculated masses (255.24 Da for **31** and 256.28 Da for **33** and **34**). The methylated products were resuspended in ~0.6 mL of $CDCl_3$ and placed in an NMR tube. ^1H NMR and/or ^{13}C NMR spectrums were obtained for each product. **31**: ^1H NMR ($CDCl_3$, 300 MHz) δ 3.9 (3H, s), 6.4 (1H, dd, J = 0.6 Hz, 11.7 Hz), 6.5 (1H, s), 7.1 (1H, dd, J = 0.6 Hz, 15.3 Hz), 7.5 (3H, m), 7.9 (1H, dd, J = 11.7 Hz, 15.3 Hz), 7.9 (2H, m); ^{13}C NMR ($CDCl_3$, 75 MHz) δ 53.5, 109.4, 127.2, 128.45, 128.6, 132.8, 137.0, 138.0, 144.7, 165.1, 190.5. **34**: ^1H NMR ($CDCl_3$, 300 MHz) δ 3.9 (3H, s), 6.4 (1H, dd, J = 0.7 Hz, 11.7 Hz), 7.1 (1H, dd, J = 0.6 Hz, 15.3 Hz), 7.5 (2H, m), 7.58 (1H, m), 7.87 (1H, dd, J + 11.7 Hz, 15.3 Hz), 7.97 (2H, m); ^{13}C NMR ($CDCl_3$, 75 MHz) δ 169.8, 145.8, 134.9, 127.8, 127.6, 127.0, 126.0, 124.7, 124.5, 122.0, 121.8, 117.7, 113.6, 94.0, 54.1. **33**: ^1H NMR ($CDCl_3$, 300 MHz) δ 3.97 (3H, s), 4.47 (1H, s), 6.03 (1H, d, J = 10.0 Hz), 7.2 (1H, d, J = 8.9 Hz), 7.43 (1H, m), 7.55 (1H, m), 7.61 (1H, d, J = 9.7 Hz), 7.8 (2H, m), 8.08 (1H, dd, J = 8.7 Hz, 0.6 Hz); ^{13}C NMR ($CDCl_3$, 75 MHz) δ 169.7, 148.5, 130.6, 129.9, 129.9, 128.8, 127.3, 124.5, 122.9, 121.4, 118.0, 117.7, 112.1, 93.5, 54.1.

3-Methylcatechol

PhdF was used to generate the ring-opened product for 3-methylcatechol (3-MC) (**28** in Scheme 3.4). Protein was expressed as described above and cells were resuspended in Buffer A at a concentration of 1 mg / 30 mL. The cells were disrupted via sonication and the resulting solution was centrifuged for 30 min at 17,700 × g and 4C. The clarified supernatant was mixed with 3-MC and the product was converted to the picolonic acid derivative (**29**) for isolation and purification. Briefly, 80 tubes containing 2 mL Buffer A, 100 µL of clarified supernatant, and 40 µL of 22

mg/mL 3-MC in ethanol were incubated at room temperature for ~20 min. Ammonium sulfate (2 mL of 4 mM stock solution) was added to each tube and the tubes were combined and extracted with methanol. The extract was mixed with silica, concentrated in vacuo, washed with 10% methanol in chloroform, and the product was recovered using 9:3:1 chloroform:methanol:acetic acid. The solution was evaporated to dryness and the product resuspended in ~0.6 mL of $CDCl_3$ and placed in an NMR tube. A ^{13}C NMR spectrum was obtained and matched that of authentic **29**. **29**: ^{1}H NMR (D_2O, 300 MHz) δ 2.4 (3H, s), 7.2 (1H, d, J = 8.1 Hz), 7.5 (1H, d, J = 7.8 Hz), 7.7 (1H, t).

Inhibition of PhdF

The inhibition of PhdF by 1,2-dihydroxyphenanthrene (1,2-DHP), 2,3-dihydroxyphenanthrene (2,3-DHP), and 9,10-dihydroxyphenanthrene (9,10-DHP) was determined as follows. The enzyme (1 mg/mL) was incubated with an excess of compound dissolved in ethanol (10 mM final concentration) in Buffer B (1 mL) for 30 min at 22 °C. In a separate control experiment, the same quantity of PhdF was incubated without inhibitor under otherwise identical conditions. The reaction was exchanged into Buffer B using an Amicon Ultra-0.5 mL centrifugal filter to remove unbound compounds. The washed enzymes were assayed for residual activity. Samples treated with 1,2-DHP, 2,3-DHP, or 9,10-DHP had no activity while the control sample retained full activity. The four samples were exchanged into 20 mM ammonium carbonate using Amicon Ultra-0.5 mL centrifugal filters and analyzed using ESI-MS.

PhdG Activity and Product Identification

The gene 0469 was cloned and the protein PhdG was expressed and purified as described in Chapter 2. Activity of PhdG with **25** (Scheme 3.3) was analyzed by mixing PhdF (0.30 µM final concentration) and PhdG (0.9 µM final concentration) in 1 mL of 20 mM HEPES buffer at pH 7. The reaction was initiated with the addition of 3,4-DHP in ethanol (40 µM final concentration) and monitored using UV spectroscopy until the absorbance at 392 nm no longer increased. The product, **26**, was extracted with 3 volumes of ethyl acetate and purified using a silica gel column with elution by ethyl acetate. The collected fractions were evaporated to dryness and the residue analyzed by ESI-MS. Activity of PhdG with **32** (Scheme 3.3) was analyzed by mixing 2891 (1 µM final concentration) and PhdG (0.9 µM final concentration) in 1 mL 20 mM HEPES buffer at pH 7. The reaction was initiated by the addition of 1,2-DHP dissolved in ethanol (40 µM final concentration) and monitored by UV spectroscopy. PhdG showed no activity when incubated with **32**.

Steady-State Kinetic Analysis Using PhdG

A coupled assay was used to determine kinetic parameters for PhdG with **25**. An aliquot of PhdF, prepared as described above, was added to Buffer A (1 mL) to give a final concentration of 1 µM. Aliquots (0.2 – 20 µL) of 3,4-dihydroxyphenanthrene in ethanol (1 mM stock) were added and the reaction was monitored using UV spectroscopy until completion as determined by no further decrease at 245 nm. This process generates **25**. An aliquot (3 µL, 0.6 µM final) of PhdG prepared as described in Chapter 2 was added to the solution and the increase in absorbance at 392 nm (ε = 3,768 M^{-1} cm^{-1}) was used to monitor the reaction. Initial rates were determined from the

first 15 s of the reaction, plotted versus substrate concentration, and fit to the substrate inhibition equation to calculate the steady-state parameters k_{cat}, $K_{M,}$ and K_i using Grafit (Haldane, 1930).

3.3 Results

Steady-State Kinetic Analysis Using Dioxygenases

The k_{obs} vs substrate concentration was plotted for the reactions of all four dioxygenase enzymes with 3-methylcatechol (3-MC), 2,3-dihydroxybiphenyl (2,3-DHB), 1,2-dihydroxyphenanthrene (1,2-DHP), and 3,4-dihdroxyphenanthrene (3,4-DHP). The plots are shown in Table 3.3. The reactions using 2891 and 2,3-dihydroxybiphenyl and 3,4-dihydroxyphenanthrene and 4413 and 3,4-dihydroxyphenanthrene display substrate inhibition and the data are fit using the substrate inhibition equation (Haldane, 1930). All other reactions appear to obey classic Michaelis-Menten kinetics and the data are fit using the Michaelis-Menten equation (Johnson, 2011). It is possible that some of the reactions assumed to follow classic Michaelis-Menten kinetics may display substrate inhibition if it were possible to assay using higher substrate concentrations, specifically the reactions of 2891 with 3-methylcatechol and 1,2-dihydroxyphenanthrene. Higher substrate concentrations are precluded by absorbance values outside of the acceptable range (>1 AU).

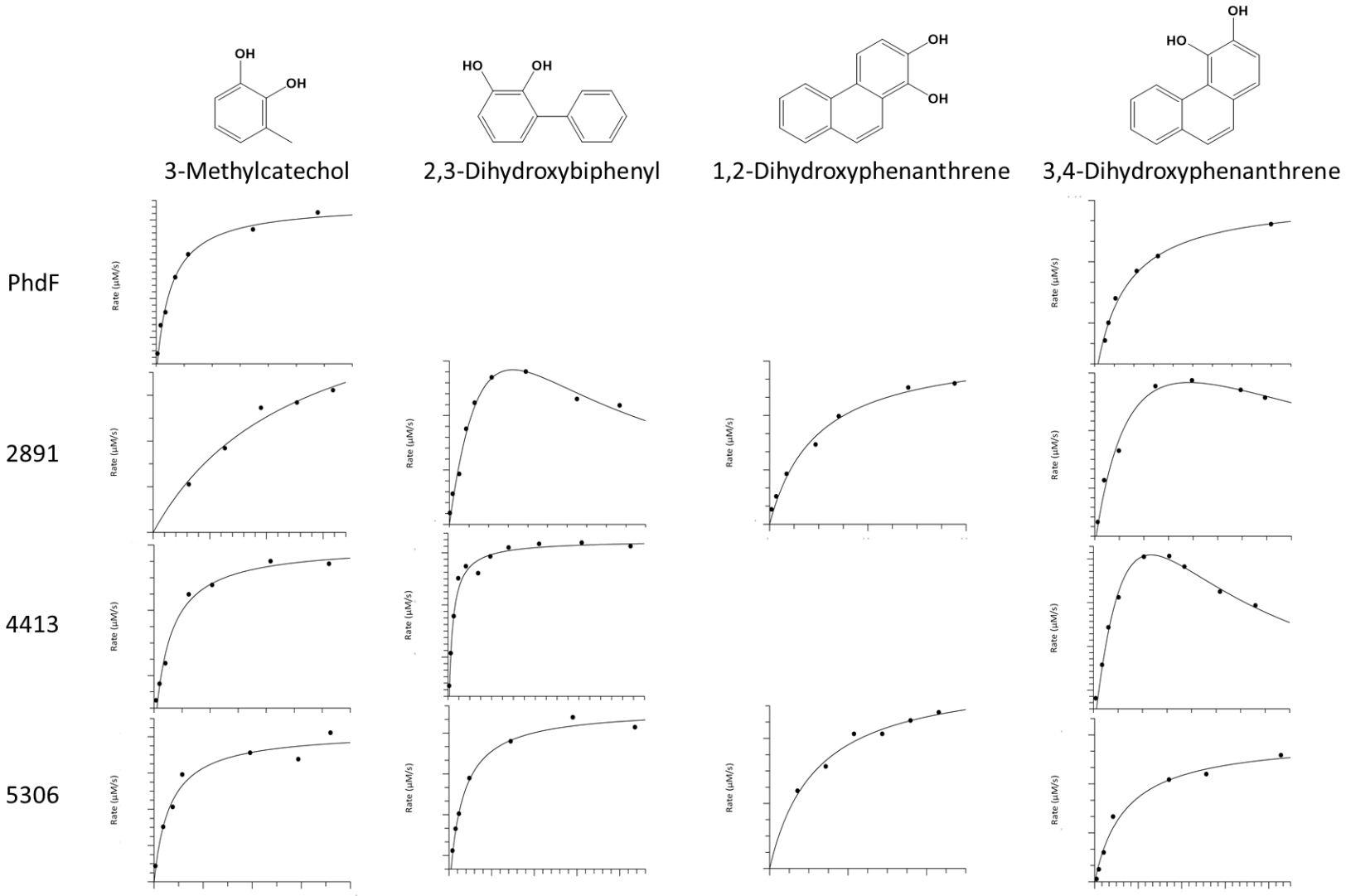

Table 3.3: Plots of kobs vs substrate concentration for dioxygenase reactions. The data for 2891 with 2,3-dihydroxybiphenyl and 3,4-dihydroxyphenanthrene and 4413 with 3,4-dihydroxyphenanthrene are fit using the substrate inhibition equation (Haldane, 1930). All other data are fit using the classic Michaelis-Menten equation (Johnson, 2011).

When 2,3-dihydroxyphenanthrene (2,3-DHP) or 9,10-dihydroxyphenanthrene (9,10-DHP) was incubated with each enzyme for >30 min no spectral changes other than non-enzymatic oxidation were observed suggesting that these compounds might not be substrates for any of the four enzymes. It should be noted that the rate of non-enzymatic oxidation of 9,10-dihydroxyphenanthrene to quinone is faster than the non-enzymatic oxidation of the other phenanthrene compounds and makes 9,10-dihydroxyphenanthrene difficult to assay. When 1,2-dihydroxyphenanthrene was incubated with PhdF or 4413 for >30 min no spectral changes other than non-enzymatic oxidation were observed suggesting that 1,2-dihydroxyphenanthrene might not be a substrate for PhdF or 4413. 1,2-Dihydroxyphenanthrene was processed by 2891 and 5306 and the absorbance spectrum for the reaction with 2891 is shown in Figure 3.1B. 3,4-Dihydroxyphenanthrene was processed by all four enzymes and the absorbance spectrum for the reaction of 3,4-dihydroxyphenanthrene and PhdF is shown in Figure 3.1A. Product identification is discussed later.

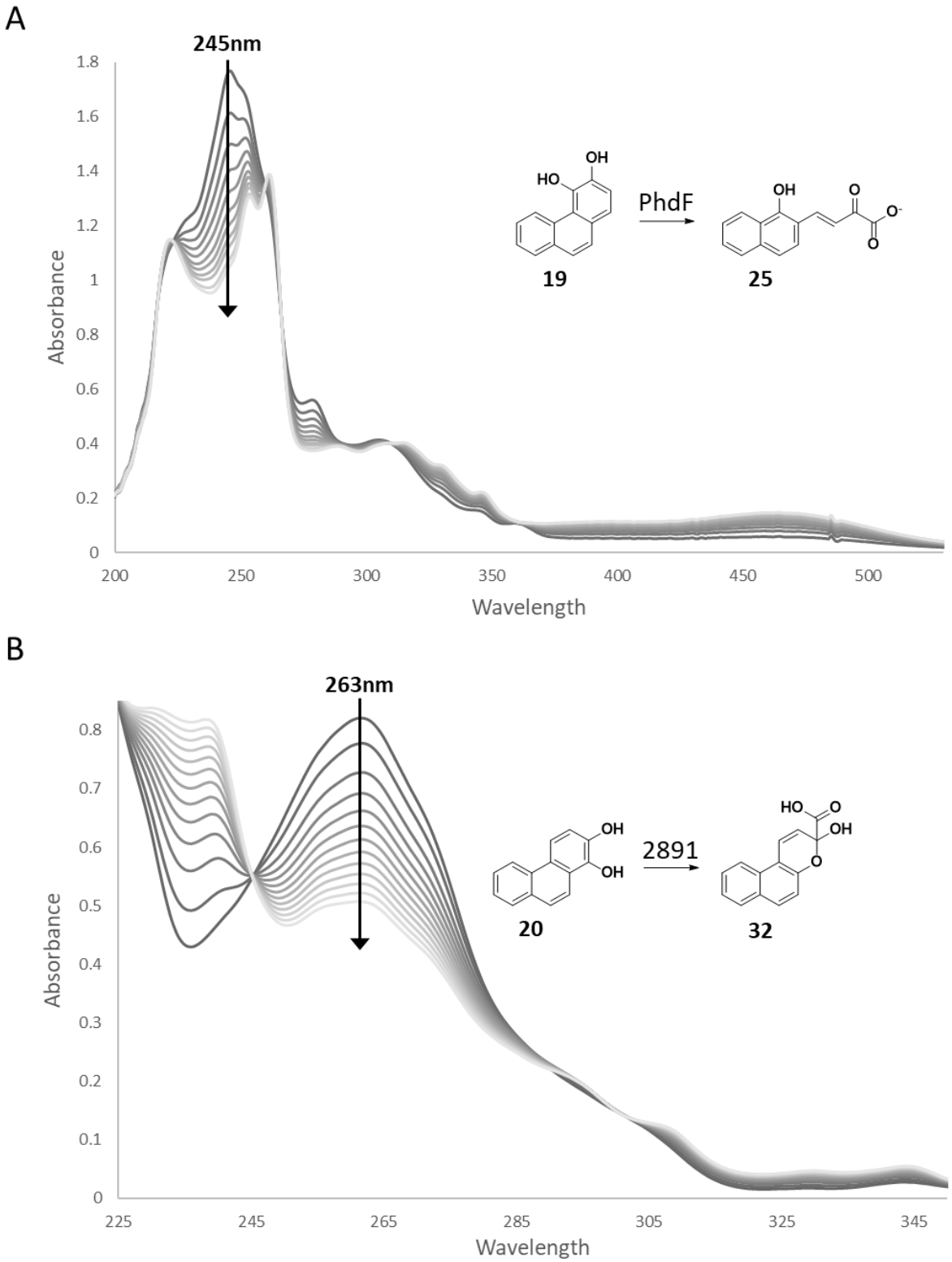

Figure 3.1: Absorbance spectra for A) the reaction of PhdF and 3,4-dihydroxyphenanthrene and B) the reaction of 2891 and 1,2-dihydroxyphenanthrene.

1,2-Dihydroxyphenanthrene and 3,4-dihydroxyphenanthrene undergo non-enzymatic oxidation to a quinone species accompanied by a spectral shift identical to that of the enzymatic ring-cleavage reactions. The rate of the non-enzymatic oxidation to quinone for these two substrates was determined for all substrate concentrations assayed. If the non-enzymatic oxidation rate is less than 10% of the enzymatic reaction rate, then the non-enzymatic rate is considered insignificant and ignored. If the non-enzymatic oxidation rate is higher than 10% of the enzymatic reaction rate, then the difference between the enzymatic reaction rate and the non-enzymatic oxidation rate is used for analysis.

For all four enzymes, the highest k_{cat}/K_M was measured using 3,4-dihydroxyphenanthrene as the substrate. Extradiol dioxygenases are typically efficient enzymes with k_{cat}/K_M values ranging up to $1x10^6$ $M^{-1}s^{-1}$.[71] The k_{cat}/K_M for the enzymes studied here show comparable efficiencies only with 3,4-dihydroxyphenanthrene as the substrate. Kinetic parameters are summarized in Table 3.4.

Enzyme	Substrate	k_{cat} (s^{-1})	K_M (μM)	k_{cat}/K_M ($M^{-1}s^{-1}$)	K_i (μM)
PhdF	3-methylcatechol	0.32 ± 0.01	50 ± 6	6.5E+03 ± 0.9E+03	NA
	2,3-dihydroxybiphenyl	0.168 ± 0.002	<10.8	>1.5e+04	NA
	1,2-dihydroxyphenanthrene	NA	NA	NA	NA
	3,4-dihydroxyphenanthrene	9.3 ± 0.9	1.7 ± 0.5	6.0E+06 ± 2.0E+06	NA
2891	3-methylcatechol	0.52 ± 0.07	1300 ± 300	5.0+E02 ± 1.0+E02	NA
	2,3-dihydroxybiphenyl	60 ± 20	180 ± 80	5E+05 ±3E+05	150 ± 70
	1,2-dihydroxyphenanthrene	0.32 ± 0.01	10 ± 1	3.4E+04 ± 0.6E+04	NA
	3,4-dihydroxyphenanthrene	9 ± 2	10 ± 4	1.2E+06 ± 0.7E+06	40 ± 20
4413	3-methylcatechol	19.2 ± 0.7	510 ± 80	3.9E+04 ± 0.7E+04	NA
	2,3-dihydroxybiphenyl	1.09 ± 0.02	28 ± 2	4.0E+04 ± 0.4E+04	NA
	1,2-dihydroxyphenanthrene	NA	NA	NA	NA
	3,4-dihydroxyphenanthrene	640 ± 80	150 ± 20	5.0E+06 ± 1.0E+06	90 ± 10
5306	3-methylcatechol	0.135 ± 0.007	700 ± 100	2.2E+02 ± 0.6E+02	NA
	2,3-dihydroxybiphenyl	2.2 ± 0.7	15 ± 1	1.5E+05 ± 0.2E+05	NA
	1,2-dihydroxyphenanthrene	0.058 ± 0.003	12 ± 2	5.0E+03 ± 1.0E+03	NA
	3,4-dihydroxyphenanthrene	8.9 ± 0.6	4.2 ± 0.9	2.3E+06 ± 0.6E+06	NA

Table 3.4: Steady-state kinetic parameters for dioxygenases kinetic assays.

Identification of Dioxygenase Reaction Products

To determine whether cleavage by the dioxygenases occurs at the ortho or meta position the products of each reaction were purified and identified. 3-Methylcatechol, 2,3-dihydroxybiphenyl, and 3,4-dihydroxyphenanthrene were treated with whole cell suspensions of PhdF, and 1,2-dihydroxyphenanthrene was treated with whole cell suspensions of 2891. The reaction product **28** was converted to picolinic acid and the reaction products **30**, **32**, and **25** were converted to stable, methylated compounds (Scheme 3.4) that were purified and identified using ESI-MS and ^{1}H and/or ^{13}C NMR spectroscopy. All dioxygenases assayed cleaved substrates at the meta position. Ring-opening of 3,4-dihydrxoyphenanthrene (**19**) results in a product in the *trans*

form (**25**) while ring-opening of 1,2-dihydroxyphenanthrene (**20**) results in a product in the *cis* form (**32**).

Inactivation of PhdF and Mass Spec Analysis

In view of the observation that the reaction of PhdF and 3,4-dihydroxyphenanthrene has a high k_{cat}/K_M, but PhdF does not process 1,2-DHP, 2,3-DHP, or 9,10-DHP, all of which are structural isomers of 3,4-DHP, we examined the ability of 1,2-DHP, 2,3-DHP, and 9,10-DHP to function as inhibitors of PhdF. After aerobic incubation of PhdF with excess of either 1,2-DHP, 2,3-DHP, or 9,10-DHP at 22 °C for 30 min, all enzyme activity was lost. Removing the inhibitor does not restore PhdF activity. In the absence of the inhibitors, the same protocol does not result in a reduction of PhdF activity. To determine whether 1,2-DHP. 2,3-DHP, or 9,10-DHP had covalently modified the enzyme, mass spec analysis was performed on samples of inhibited PhdF and compared to the active PhdF control. Analysis did not show a mass difference between the inhibited and control samples, suggesting that the inhibitors do not covalently modify PhdF.

Identification of PhdG Reaction Products

PhdG converts **25** to **26** but does not process **35** (Scheme 3.5). The UV spectrum corresponding to the reaction of PhdG, PhdF and 3,4-dihydroxyphenanthrene (**19**) is shown in Figure 3.2. The product **26** was isolated and the mass was determined. The mass (172.05 Da) is consistent with the predicted mass (172.18 Da).

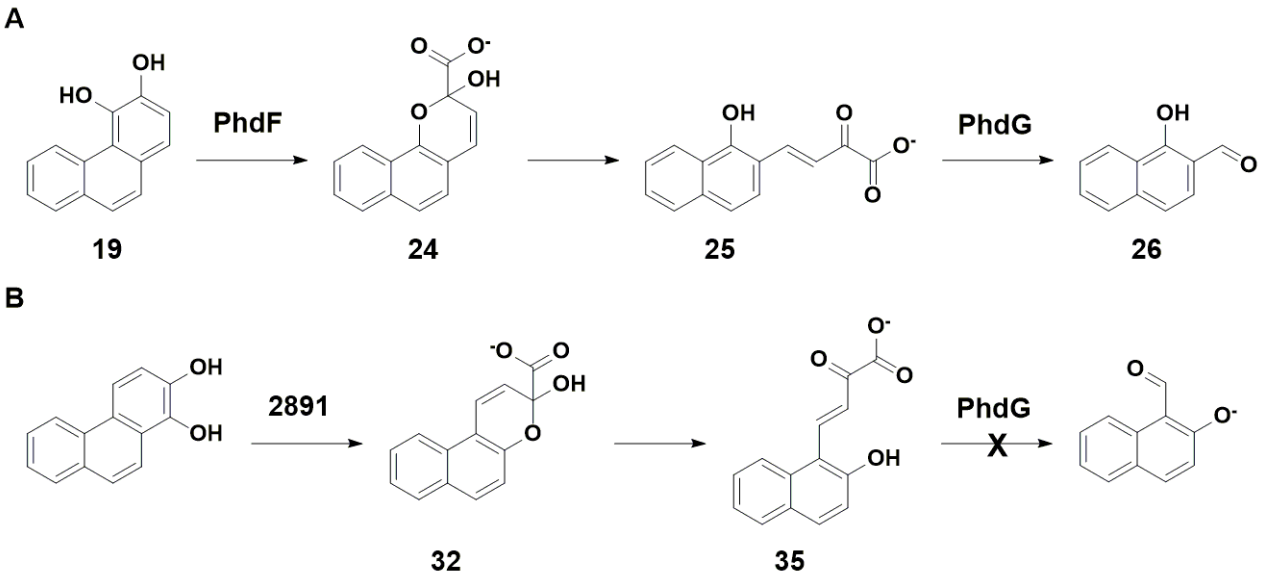

Scheme 3.5: Proposed reaction of PhdG with A) the reaction product of PhdF and 3,4-dihydroxyphenanthrene and B) the reaction product of 2891 and 1,2-dihydroxyphenanthrene. PhdG does not process the reaction product of 2891 and 1,2-dihydroxyphenanthrene.

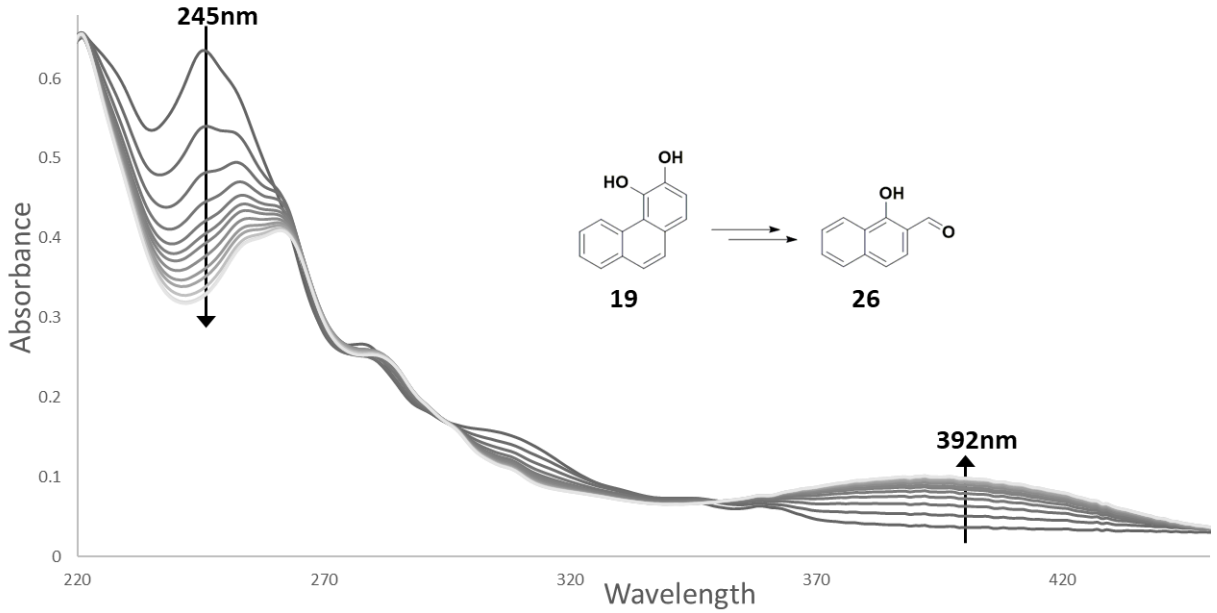

Figure 3.2: Absorbance spectrum of the reaction of PhdF, PhdG and 3,4-dihydroxyphenanthrene.

Steady-State Kinetic Analysis Using PhdG

A coupled assay with PhdF, 3,4-dihydroxyphenanthrene (**19**), and PhdG was used to determine the kinetic parameters for PhdG with **25**. The absorbance spectrum of the reaction is shown in Figure 3.3. A plot of k_{obs} vs 3,4-dihydroxyphenanthrene concentration is shown in Figure 3.4. The reaction displayed substrate inhibition and the data were fit to the substrate inhibition equation (Haldane, 1930). The kinetic parameters are given in Table 3.5.

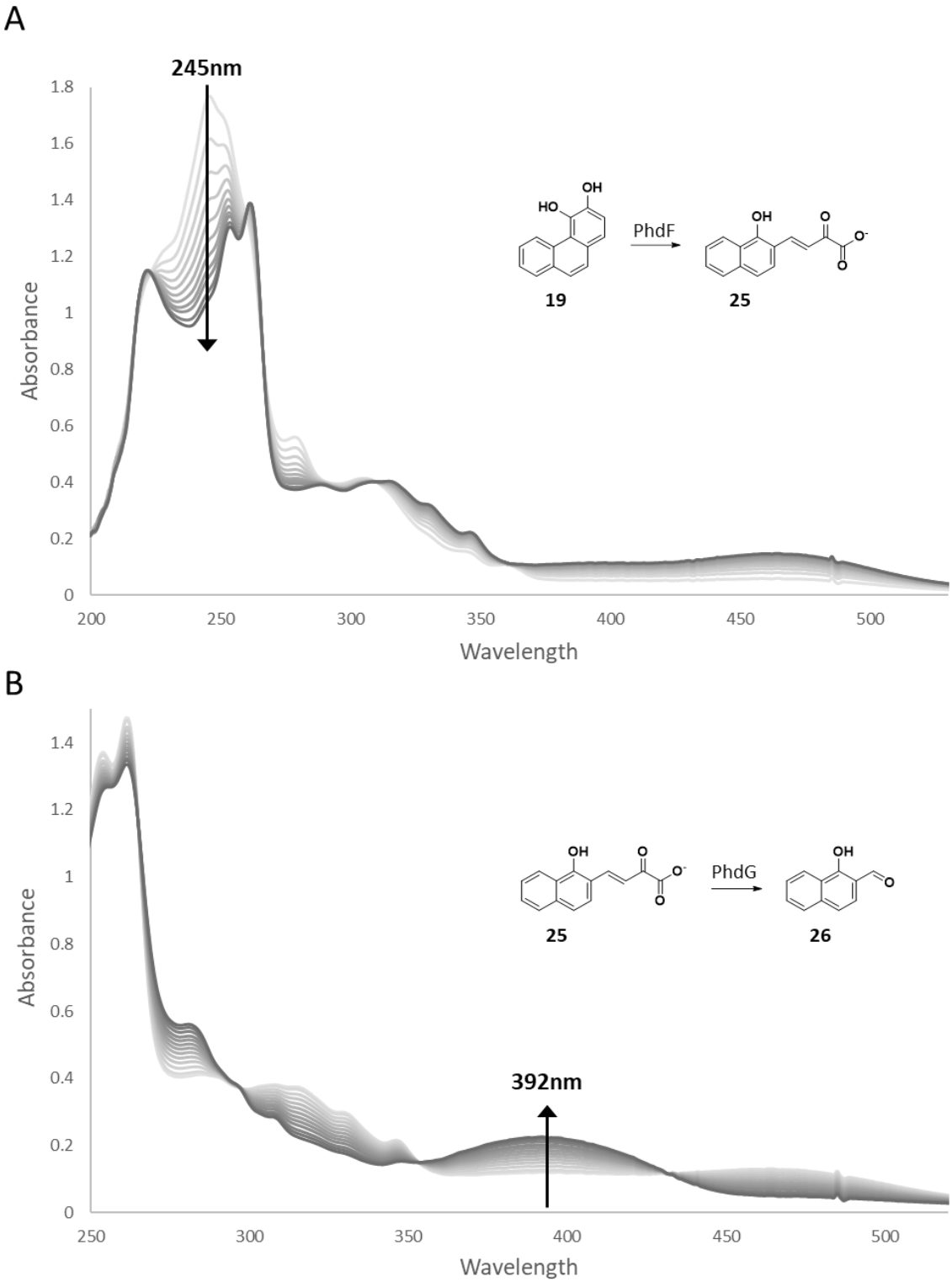

Figure 3.3: Absorbance spectrum of A) the reaction of PhdF and 3,4-dihydroxyphenanthrene (**19**) until completion and B) the addition of PhdG to the reaction described in A.

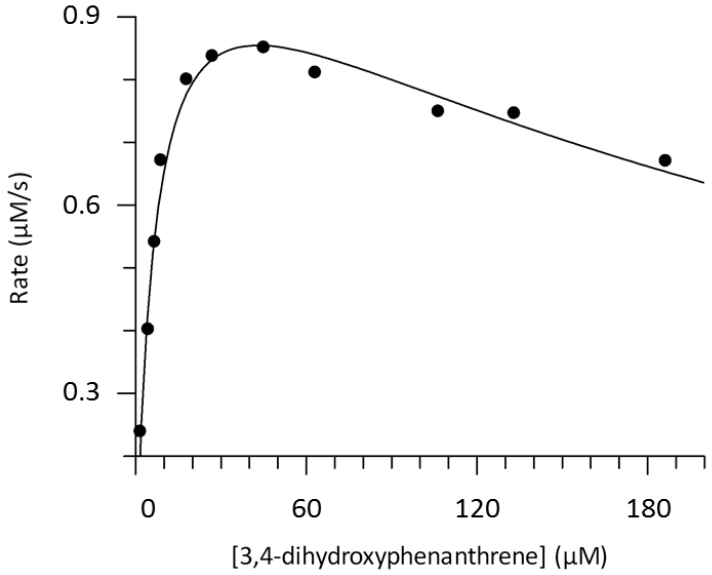

Figure 3.4: Plot of k_{obs} vs 3,4-dihydroxyphenanthrene (**19**) concentration for the reaction of PhdG and **25**. The data is fit to the substrate inhibition equation (Haldane, 1930).

	k_{cat} (s^{-1})	K_M (μM)	k_{cat}/K_M ($M^{-1}s^{-1}$)	K_i (μM)
PhdG	1.93 ± 0.09	6.8 ± 0.8	2.9E+05 ± 0.5E+05	270 ± 40

Table 3.5: Kinetic parameters for the reaction of PhdG and **25**.

3.4 Discussion

Our overall goal in this chapter is to provide biochemical evidence for proposed reactions in the phenanthrene catabolic pathway of *M. vanbaalenii* PYR-1. Specifically, we wanted to identify the ring-opening dioxygenase and hydratase-aldolase enzymes that act in this pathway and determine whether an isomerase is required.

PhdF has been previously annotated as a type I extradiol dioxygenase that catalyzes the ring-opening of 3,4-dihydroxyphenanthrene (**19**) in the meta position (Scheme 3.2) during catabolism of phenanthrene and pyrene by *M. vanbaalenii* PYR-1 (Stingley, 2004; Kim, 2007). Catabolism of phenanthrene by *M. vanbaalenii* PYR-1 also produces 9,10-dihydroxyphenanthrene (**18**), which is ring-opened in the ortho position and 1,2-dihydroxyphenanthrene (**20**), which is methylated and eliminated from the cell (Scheme 3.2) (Stingley, 2004; Kweon, 2011). Studies using other bacteria show that 3,4-dihydroxyphenanthrene can also be ring-opened in the ortho position and that 1,2-dihydroxyphenanthrene can be ring-opened at the ortho or meta position instead of being methylated and eliminated from the cell (Seo, 2006). We examined the activity of PhdF with 3,4-dihydroxyphenanthrene, 9,10-dihdyroxyphenanthrene, and 1,2-dihydroxyphenanthrene. In our hands, PhdF did not ring-open 9,10-dihydroxyphenanthrene or 1,2-dihydroxyphenanthrene but did ring-open 3,4-dihydroxyphenanthrene with a k_{cat}/K_M of 4 x 10^6 $M^{-1}s^{-1}$. The product of the reaction of PhdF with 3,4-dihydroxyphenanthrene was identified as **25** (Scheme 3.2) which confirms the proposed ring-opening activity of PhdF in the meta position in this pathway (Scheme 3.6). It is likely that PhdF is active in the catabolic pathway of phenanthrene that begins with oxidation at the C-3 and C-4 positions.

The inhibition of extradiol ring-cleaving dioxygenases has been well-studied (Vaillancourt, 2006). Inhibition can be achieved through covalent modification of active site residues, but the more accepted mechanism of inhibition is oxidation of the active site iron (Vaillancourt, 2006). After a substrate or inhibitor enters the active site a solvent molecule bound to the iron is displaced allowing oxygen to enter the active site. A superoxide is formed that can oxidize the ferrous iron to ferric iron (Cho, 2010). Extradiol ring-cleaving dioxygenases require ferrous iron for activity (Vaillancourt, 2006). We tested 9,10-dihydroxyphenanthrene and 1,2-dihydroxyphenanthrene for their ability to inhibit PhdF. Our results indicate that both compounds irreversibly inactivate PhdF in a non-covalent manner. Further tests, including substrate protection studies and/or determination of the presence of and ionization state of the active-site iron in the presence of the inhibitor, will be carried out in future work in order to determine the mechanism of inactivation. The dead-end pathway utilized by *M. vanbaalenii* PYR-1 after production of 1,2-dihydroxyphenanthrene could be a means of preventing inactivation of PhdF by 1,2-dihydroxyphenanthrene.

To identify a dioxygenase that potentially functions in the catabolic pathways of 1,2-dihydroxphenanthrene (**20** Scheme 3.2) and 9,10-dihydroxphenanthrene (**18**) we assayed three other putative type I extradiol dioxygenases in the *M. vanbaalenii* PYR-1 genome with moderate sequence similarity to PhdF (38-39%). These putative dioxygenases are products of the genes 2891, 4413, and 5306. All three gene products ring-opened 3,4-dihydroxyphenanthrene through cleavage at the meta position (**19**, Scheme 3.2), and the gene products of 2891 and 4413 display substrate inhibition with this compound. Mechanism-based substrate inhibition is well-documented for extradiol dioxygenases (Vaillancourt, 2006). None of the three dioxygenases ring-

opened 9,10-dihydroxyphenanthrene, but the products of 2891 and 5306 ring-opened 1,2-dhydroxyphenanthrene through cleavage at the meta position. These three genes are not upregulated during the catabolism of pyrene, a process that generates 3,4-dihydroxyphenanthrene as an intermediate, so it seems unlikely that any of these dioxygenases are responsible for cleavage of 3,4-dihydroxyphenanthrene during phenanthrene catabolism by *M. vanbaalenii* PYR-1. Although no intermediates that would be produced in the catabolism of 1,2-dihydroxyphenanthrene via an energy-producing pathway have been isolated, if such a pathway is utilized by *M. vanbaalenii* PYR-1 (possibly under conditions differing from those used in previous studies) the gene products of either 2891 or 5306 may be active within this pathway. A dioxygenase has not been identified that is capable of cleavage of 9,10-dihydroxyphenanthrene. The gene encoding protocatechuate-3,4-dioxygenase is the only annotated intradiol dioxygenase gene within the *M. vanbaalenii* PYR-1 genome and the gene product is responsible for ortho-cleavage of protocatechuate. It is possible that this enzyme is responsible for cleavage of both protocatechuate and 9,10-dihydroxyphenanthrene. This will be the subject of a future study.

In addition to these questions, we are interested in determining whether an isomerase is required to isomerize the ring-opened products before they are further processed by a hydratase-aldolase. There is not a gene within the PAH catabolic gene clusters that has significant sequence similarity with a glutathione-dependent isomerase (NahD in *Pseudomonas putida* G7) known to be active within the naphthalene catabolic pathway (Kim, 2008). Also, mycobacteria are inhibited by the presence of glutathione and do not utilize this compound (Anderberg, 1998). PhdG, a hydratase-aldolase proposed within the phenanthrene catabolic pathway of *M. vanbaalenii* PYR-

1, was assayed for activity with the product of the reaction of PhdF and 3,4-dihydroxyphenanthrene directly (Scheme 3.5A). PhdG cleaves this product (**25**) without the need for an isomerase and the product of this reaction was identified as **26** (Scheme 3.6). This suggests that either the non-enzymatic isomerization of **24** to **25** is sufficient or that the dioxygenase can catalyze the isomerization and no isomerase is required. PhdG was also assayed for activity with the product of the reaction of 2891 and 1,2-dihydroxyphenanthrene (Scheme 3.5B). PhdG did not process the ring-cleaved product. If the non-enzymatic isomerization of **24** to **25** is sufficient then it is unlikely that an isomerase would be required for the transformation of **32** to **35**. If the isomerization of **32** to **35** occurs non-enzymatically it is possible that **35** either cannot enter the active-site of PhdG or it binds the active-site of PhdG in a non-productive fashion. If the ring-cleaving dioxygenase is responsible for the isomerization of **24** to **25** then it is possible that the dioxygenase cannot catalyze the isomerization of **32** to **35** and that **32** is not a substrate for PhdG. Further studies such as inhibition assays and/or crystal structure determination of PhdG with **25** and isomerase activity assays of the dioxygenases with the ring-opened products **24** and **32** can clarify this issue.

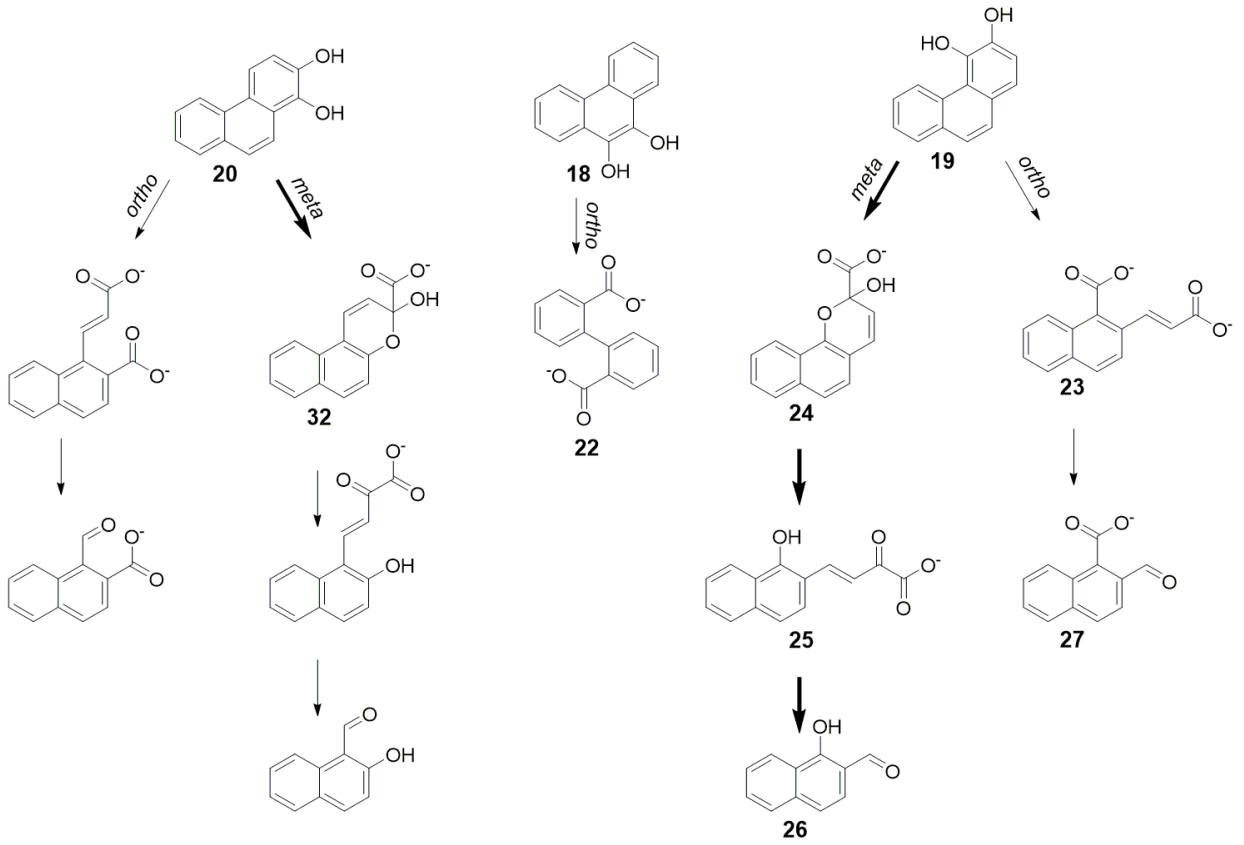

Scheme 3.6: Reactions analyzed in this experiment. Bold arrows indicate confirmed reactions.

Overall, the work in this chapter addressed questions about the reactions and enzyme functions in the phenanthrene catabolic pathway of *M. vanbaalenii* PYR-1. The major findings are 1) the identification of PhdF as the ring-cleaving dioxygenase; 2) the identification of PhdG as the hydratase-aldolase; and 3) the absence of an isomerase within the phenanthrene catabolic route beginning with 3,4-dihydroxyphenanthrene. The work also showed that the ring-cleaving dioxygenase reaction within the catabolic pathway beginning with 9,10-dihydroxyphenanthrene must be catalyzed by an enzyme other than PhdF. Dioxygenases capable of cleaving 1,2-dihydroxyphenanthrene were identified, but the genes encoding these dioxygenases are not upregulated in the presence of PAHs and the hydratase-aldolase that is upregulated in the presence

of PAHs does not cleave the dioxygenase product. The results here support but do not confirm the claim that the production of 1,2-dihydroxyphenanthrene does not result in an energy-producing pathway.

3.5 Supplemental

*3,4-Dihydroxyphenanthrene Synthesis (**19**)*

5,6-Dimethoxyisobenzofuran-1(3H)-one was synthesized from 3,4-dimethoxybenzoate following a published procedure (von Kleist, 2016) (step i). Benzylic bromination and hydrolysis converts 5,6-dimethoxyisobenzofuran-1(3H)-one to a mixture of 2-formyl-4,4-dimethoxybenzoic acid and 3-hydroxy-5,6-dimethoxyisobenzofuran-1(3H)-one (Nandakumar, 2013) (step ii). A Haworth methylation was used to synthesize methyl 2-formyl-4,5-dimethoxybenzoate (step iii). A Wittig reaction using the reagent benzyltriphenylphosphonium bromide and potassium tert-butoxide was used to synthesize methyl-4,5-dimethoxy-2-styrylbenzoate (step iv). Photocyclization using iodine and radiation synthesized methyl 3,4-dimethoxyphenanthrene-1-carboxylate (Pampin, 2003) (step v). Ester hydrolysis using NaOH followed by acidification produced 3,4-dimethoxyphenanthrene-1-carboxylic acid (step vi). Decarboxylation using copper in quinoline produced 3,4-dimethoxyphenanthrene (step vii). ^{1}H and ^{13}C NMR spectroscopy were used to confirm the identity of this compound. This stable compound was stored at -20 C°. When needed, small amounts of 3,4-dimethoxyphenanthrene were hydrolyzed under argon to 3,4-dihydroxyphenanthrene using boron tribromide (step viii). 3,4-Dimethoxyphenanthrene: ^{1}H NMR ($CDCl_3$, 300 MHz) δ 4.0 (s, 1H), 4.1 (s, 1H), 7.4 (d, 1H J = 8.7 Hz), 7.6 (m, 5H), 7.9 (dd, 1H, J =

1.8 Hz, 7.7 Hz), 9.7 (dd, 1H J = 0.9 Hz, 8.2 Hz); ^{13}C NMR ($CDCl_3$, 75 MHz) δ 56.5, 59.7, 113.0, 124.6, 124.8, 125.5, 126.48, 120.51, 126.9, 127.9, 128.26, 128.33, 129.6, 133.0, 147.1, 151.5

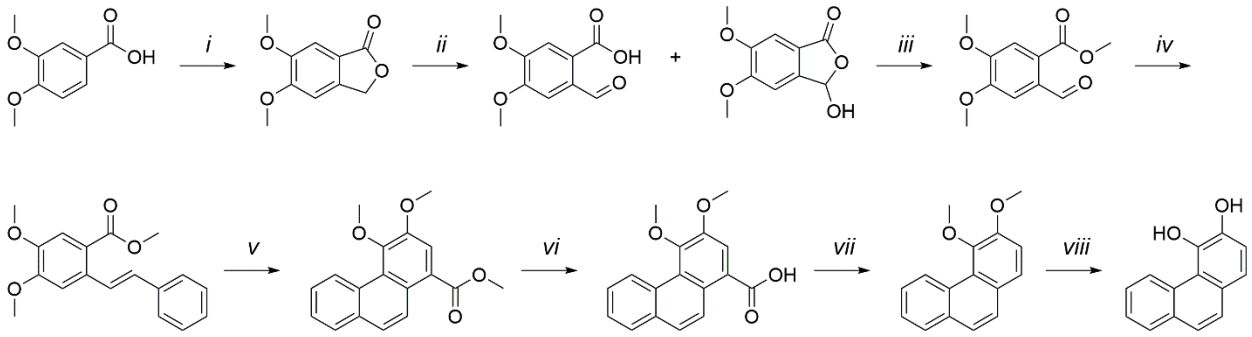

Scheme 3.7: Synthesis of 3,4-dihydroxyphenanthrene.

*1,2-Dihydroxyphenanthrene (**20**) and 2,3-Dihydroxyphenanthrene Synthesis*

Synthesis of 1,2-dihydroxyphenanthrene and 2,3-dihydroxyphenanthrene began with 2,3-dimethoxybenzaldehyde and 3,4-dimethoxybenzaldehyde, respectively, and followed steps iv-viii described above for the synthesis of 3,4-dihydroxyphenanthrene. 1,2-Dimethoxyphenanthrene: ^{1}H NMR ($CDCl_3$, 400 MHz) δ 4.02 (s, 3H), 4.04 (s, 3H), 7.37 (d, 1H, J = 9.1 Hz), 7.54 (m, 1H), 7.62 (m, 1H), 7.74 (d, 1H, J = 9.1 Hz). 7.86 (dd, 1H, J = 1.4 Hz, 7.8 Hz), 8.09 (dd, 1H, J = 0.5 Hz, 9.1 Hz), 8.42 (d, 1H, J = 9.0 Hz), 8.59 (dd, 1H, J = 0.5 Hz, 8.2 Hz); ^{13}C NMR ($CDCl_3$, 75 MHz) δ 56.4, 61.3, 113.4, 118.9, 120.2, 122.3, 125.4, 125.9, 126.7, 127.36, 127.41, 128.6, 130.3, 131.0, 143.8, 149.8. 2,3-Dimethoxyphenanthrene: ^{1}H NMR ($CDCl_3$, 500 MHz) δ 4.08 (s, 3H), 4.16 (s, 3H), 7.28 (s, 1H), 7.57 (m, 1H), 7.65 (m, 1H), 7.69 (m, 1H), 7.91 (d, 1H, J = 7.9 Hz), 8.05 (s, 1H), 8.57 (d, 1H, J = 8.3 Hz); ^{13}C NMR ($CDCl_3$, 125 MHz) δ 55.9, 56.0, 103.3, 108.3, 122.1, 124.9, 125.3, 125.6, 126.0, 126.2, 127.2, 128.7, 129.8, 131.4, 149.33, 149.35.

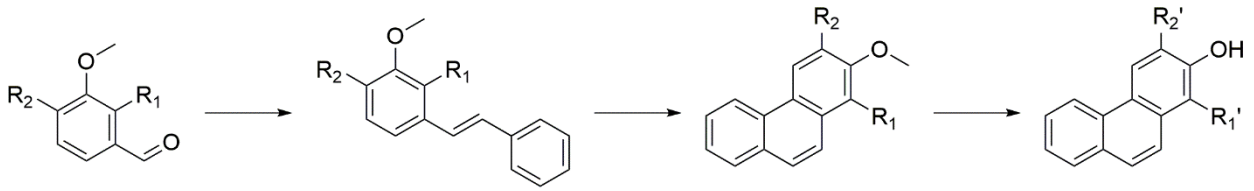

	R_1	R_2	R_1'	R_2'
1,2-DHP	OMe	H	OH	H
2,3-DHP	H	OMe	H	OH

Scheme 3.8: Synthesis of 1,2-dihydroxyphenanthrene and 2,3-dihydroxyphenanthrene.

*9,10-Dihydroxyphenanthrene (**18**) Synthesis*

9,10-Phenanthrene quinone was converted to phenanthrene-9,10-diyl diacetate by following a published procedure (Langvik, 2015). ^{1}H and ^{13}C NMR spectroscopy were used to confirm the identity of this compound. This stable compound was stored at -20 C°. When needed, small amounts of phenanthrene-9,10-diyl diacetate were hydrolyzed under argon to 9,10-dihydroxyphenanthrene using acetyl chloride and ethanol. Phenanthrene-9,10-diyl diacetate: ^{1}H NMR ($CDCl_3$, 300M Hz) δ 2.5 (s, 6H), 7.7 (m, 4H), 7.9 (m, 2H), 8.7 (d, 2H, J = 8.5 Hz); ^{13}C NMR ($CDCl_3$, 75 MHz) δ 20.5, 122.0, 123.0, 126.5, 127.1, 127.3, 129.7, 135.8, 168.2

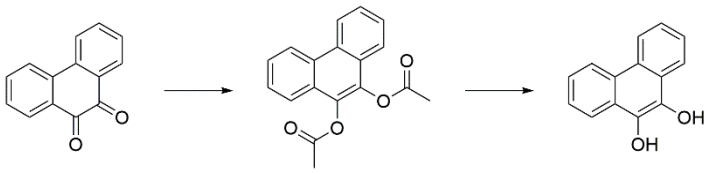

Scheme 3.9: Synthesis of 9,10-dihydroxyphenanthrene.

Chapter 4: Investigation of the Ring-Cleaving Dioxygenase and Hydratase-Aldolase Reactions in the *M. vanbaalenii* PYR-1 Pyrene and Fluoranthene Catabolic Pathways

4.1 Introduction

Pyrene is a high molecular weight (HMW) PAH with a four-ring aromatic structure (Scheme 4.1) that causes various toxicities such as oxidative stress in the liver of goldfish, abnormal cardiac development in zebrafish, abnormal behavior and neural development in pufferfish larvae, and hepatotoxicity in mice (Sun, 2008; Zhang, 2012; Sugahara, 2014; Zhang, 2015). While pyrene does not act as a carcinogen, the structure of pyrene is similar to some HMW PAHs that display carcinogenic properties, such as benzo[a]pyrene, indeno[1,2,3-cd]pyrene, and 1-nitropyrene, and elucidation of the catabolic pathway for pyrene might give insights into the catabolic pathways for these carcinogenic HMW PAHs. Flouranthene is another HMW PAH composed of naphthalene and benzene fused with a five-membered ring (Scheme 4.2). Toxicities caused by exposure to fluoranthene include genotoxicity by DNA strand breakage and adduct formation in rats, behavioral toxicity as demonstrated by suppressed motor activity in rats, reduced weight and growth rate in moth larvae, and inhibition of germination and growth of wheat (Vaca, 1992; Saunders, 2003; Mrdakovic, 2015; Tomar, 2015;).

Mycobacterium vanbaalenii PYR-1 can completely degrade pyrene and fluoranthene to carbon dioxide and water but cannot use either as the sole carbon source (Heitkamp, 1988). Metabolomic, proteomic, and genomic analysis elucidated catabolic pathways for both pyrene and fluoranthene in *M. vanbaalenii* PYR-1 (Kim, 2007; Kweon, 2007). The isolation and identification of 13 and 28 metabolic intermediates during growth of *M. vanbaalenii* PYR-1 in the presence of

pyrene and fluoranthene, respectively, allowed the formulation of potential catabolic routes for each (Scheme 4.1 and 4.2) (Heitkamp, 1988; Kim, 2005; Kweon, 2007). Proteins that are upregulated in the presence of either compound were identified using one-dimensional gel electrophoresis coupled with liquid-chromatography-mass spectrometry and comparison with a control. The genes encoding the upregulated proteins were determined using genomic analysis (Table 4.1). Many of the genes that are upregulated in the presence of pyrene are in the aromatic catabolic gene regions (Figure 4.1) and are not expressed in the control sample showing that the genes for aromatic catabolism are tightly regulated (Kim, 2007). Analysis of the genomic context of the upregulated genes and comparison of upregulated gene products to enzymes with known functions were used to tentatively annotate enzymes in the proposed catabolic pathways for pyrene (Scheme 4.1) and fluoranthene (Scheme 4.2).

Category	Function	No. of proteins upregulated by at least two-fold	
		Pyrene	Fluoranthene
Information storage and processing	Translation	3	6
	Transcription	10	5
	DNA replication	5	6
Cellular processes	Cell wall or membrane biogenesis	5	3
	Translation modification	2	3
	Intracellular trafficking	1	0
	Inorganic ion transport and metabolism	5	1
	Signal transduction	5	4
Metabolism	Energy production	11	11
	Carbohydrate metabolism	9	9
	Aromatic compound degradation	25	10
	Amino acid metabolism	13	10
	Nucleotide metabolism	2	4
	Coenzyme metabolism	7	6
	Lipid metabolism	15	14
	Secondary metabolites	2	3
Other categories	General function only	7	13
	Function unknown	5	6
	Uncategorized	10	3

Table 4.1: Proteins upregulated in *M. vanbaalenii* PYR-1 in the presence of pyrene or fluoranthene (Adapted from Kweon, 2007; Kim, 2007).

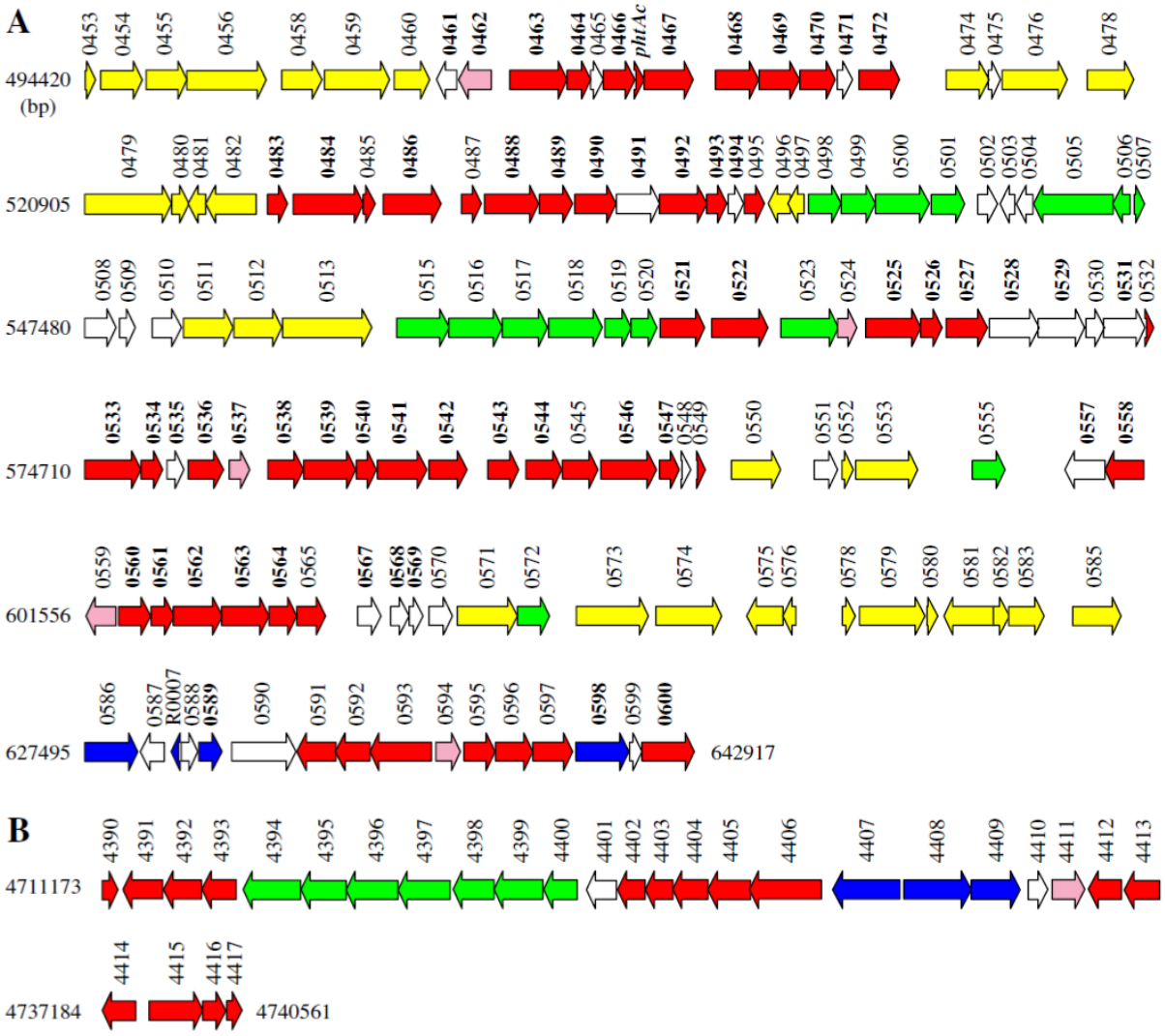

Figure 4.1: PAH catabolic gene regions in *M. vanbaalenii* PYR-1. Arrows indicate the direction of transcription. Numbers indicate the gene location. Bold numbers indicate genes expressed in the presence of pyrene or fluoranthene. Arrows are colored as follows: red: PAH catabolism, pink: transcriptional regulation, yellow: DNA mobilization, green: membrane transport system, blue: function outside of PAH degradation, white: no predicted function (Kim, 2008).

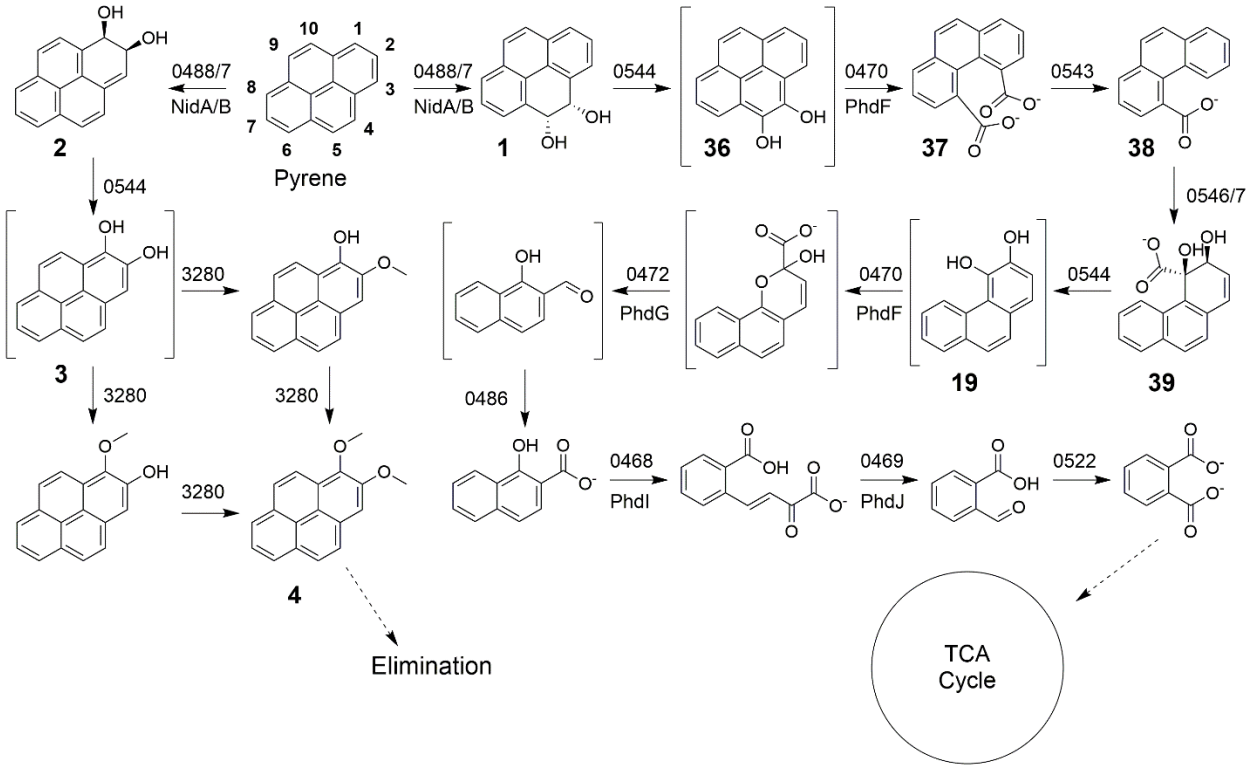

Scheme 4.1: Pyrene catabolism by *M. vanbaalenii* PYR-1. Brackets indicate compounds that were not isolated. The numbers above each arrow represent the gene location for the enzyme proposed to catalyze that reaction. Enzymes discussed in this chapter are written below the arrows. (Adapted from Kim, 2007)

Pyrene degradation begins with oxygenation at C-1 and C-2 (**2**) or C-4 and C-5 (**1**) followed by dehydrogenation to aromatize the ring (**3** and **36**, respectively) (Scheme 4.1). 1,2-Dihydroxypyrene (**3**) enters a peripheral detoxification pathway that methylates both oxygens to form **4**, which can be eliminated from the bacteria. 4,5-Dihydroxypyrene (**36**) is cleaved at the intradiol position by a ring-cleaving dioxygenase to produce **37** that is decarboxylated to yield **38**. Two hydroxyl groups are added (**39**), a carboxylate group is removed, and dehydrogenation results in aromatization. The resulting compound, 3,4-dihydroxyphenanthrene (**19**), is further degraded by the route described in Chapter 3 (Scheme 3.2). The enzymes proposed for every reaction in the degradation of pyrene to phthalate are upregulated in the presence of pyrene compared to a control (Kim, 2007). Analysis of the PAH metabolic gene clusters suggests *M. vanbaalenni* PYR-1 degrades phthalate through the ß-ketoadipate pathway (Stingley, 2004; Kim, 2008). The genes required for ß-ketoadipate catabolism are all found within the catabolic gene clusters except for ß-ketoadipyl CoA thiolase, which is found outside of the gene clusters.

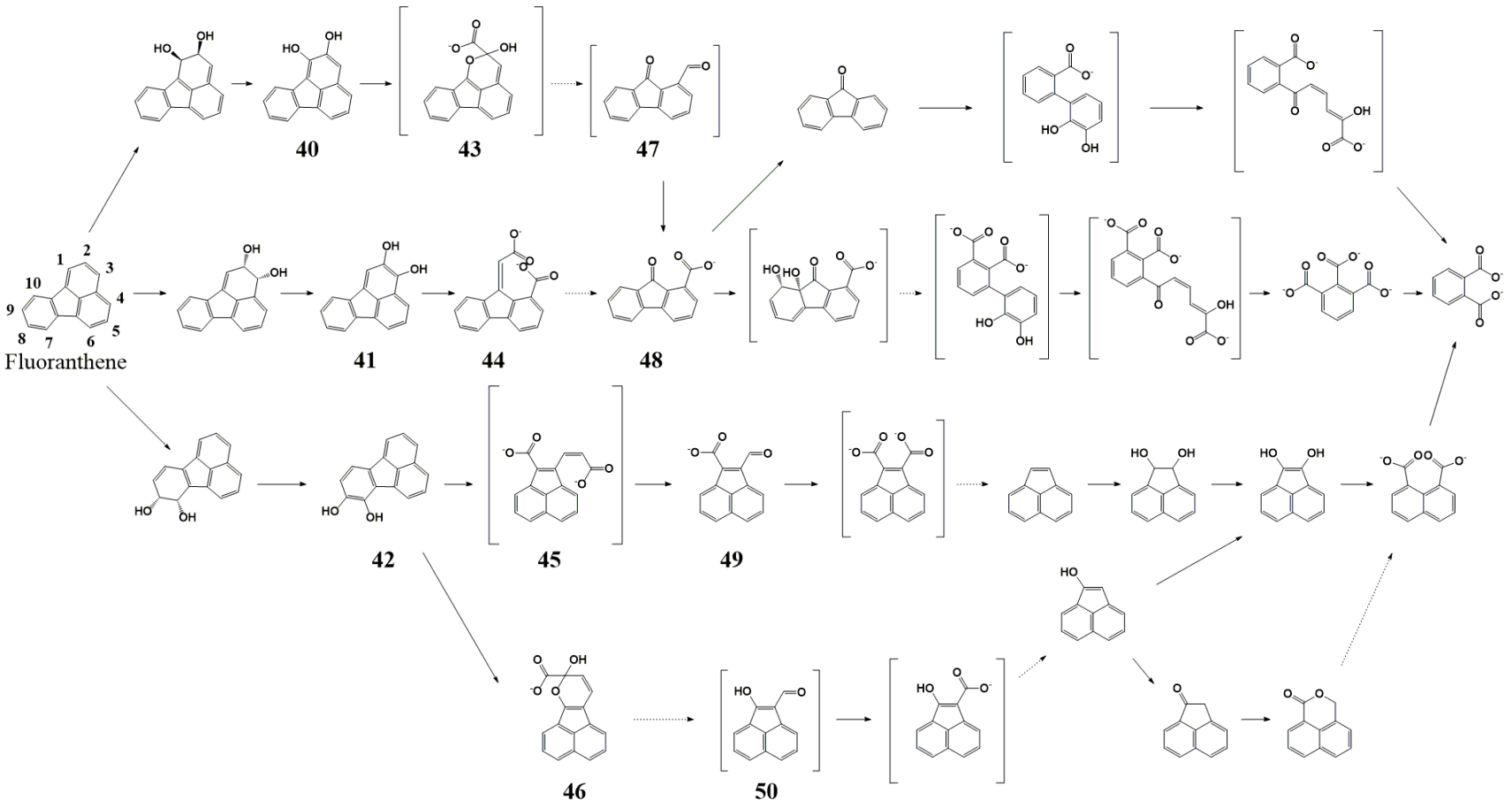

Scheme 4.2: Fluoranthene catabolism by M. vanbaalenii PYR-1. Dashed arrows represent multiple steps. Brackets indicate compounds that were not isolated. Non-energy producing routes are not shown. (Adapted from Kweon, 2007)

Degradation of fluoranthene begins with hydroxylation at positions C-1 and C-2, C-2 and C-3, or C-7 and C-8 followed by dehydrogenation to produce the dihydroxylated aromatic compounds **40**, **41**, and **42**, respectively (Scheme 4.2). The resulting dihydroxyfluoranthenes can be methylated and removed from the cell (not shown) or cleaved by a ring-cleaving dioxygenase at either the intradiol (**41** to **44** or **42** to **45**) or the extradiol position (**40** to **43** or **42** to **46**). A hydratase-aldolase is proposed to catalyze a hydration reaction followed by retro-aldol fission of the cleavage products converting **43** to **47**, **44** to **48**, **45** to **49**, and **46** to **50**. Further processing is shown in Scheme 4.2. The pathways ultimately converge to the common intermediate phthalate and proceed through the ß-ketoadipate catabolic pathway.

The fluoranthene catabolic pathway by *M. vanbaalenii* PYR-1 is not as well understood as other PAH catabolic pathways because the intermediate compounds are more complex and could be processed through several different reactions. Moreover, many of the proposed intermediates are structural isomers that could not be unequivocally identified. For example, a compound matching the molecular weight of the isomers **40**, **41**, and **42** was isolated, but the individual isomers were not separated and therefore their identity could not unequivocally established (Kweon, 2007). Similarly, a compound matching the molecular weight of a monohydroxylated fluoranthene was identified, but the location of the hydroxyl group was not determined and no intermediates in a catabolic pathway for this compound were identified (Kweon, 2007). Enzymes have not been annotated for all the transformation in the fluoranthene catabolic pathway because some of the proposed enzymes are expressed, but not upregulated when *M. vanbaalenii* PYR-1 is grown in the presence of fluoranthene. For example, the degradation pathway for 2,3-

dihydroxyfluoranthene (**41**) is shown in Scheme 4.3. The enzymes putatively assigned to each reaction are given above the reaction arrows and those that are upregulated in the presence of fluoranthene are shown in bold. Of the 16 enzymes required to convert **41** to TCA cycle intermediates, only three are upregulated in *M. vanbaalenii* PYR-1 in the presence of fluoranthene (Kweon, 2007). Assaying pure enzymes with their proposed intermediates and identifying the reaction products would be a major step in confirming the proposed reactions and correctly annotating the enzymes.

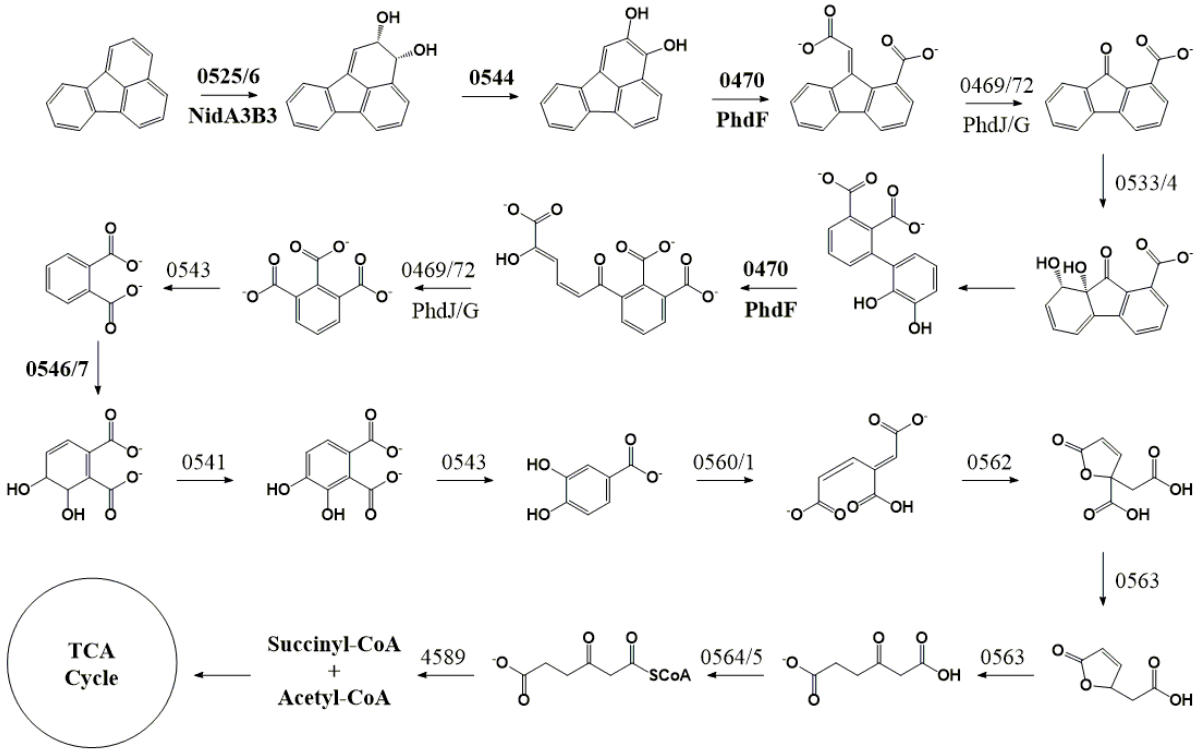

Scheme 4.3: Catabolism of 2,3-dihydroxyfluoranthene by *M. vanbaalenii* PYR-1. The numbers above each arrow represent the gene location for the enzyme proposed to catalyze that reaction. The numbers in bold are upregulated in the presence of fluoranthene. Enzymes discussed in this chapter are written below the arrows. (Adapted from Kweon, 2007)

There are several published studies identifying the ring-hydroxylating oxygenase (RHO) systems responsible for the initial step in the catabolism of HMW PAHs catabolized by *M. vanbaalenii* PYR-1. Specifically, the NidA, NidA3, and PdoA systems have been assigned to the initial oxidation step for pyrene, fluoranthene, and phenanthrene, respectively, although the substrate specificities for each are not stringent and all three systems can process all three compounds (Kim 2006; Kweon, 2010, Kweon, 2014). While there has been much attention directed towards identifying the enzyme responsible for catalysis of the initial dioxygenase reaction, little information is available regarding the ring-cleaving and hydratase-aldolase reactions. We are interested in identifying the enzymes that catalyze these reactions in both the pyrene and fluoranthene catabolic pathways. The cupin superfamily ring-cleaving dioxygenase PhdI, the type I extradiol dioxygenase PhdF, and the hydratase-aldolases PhdJ and PhdG are upregulated in *M. vanbaalenii* PYR-1 when grown in the presence of pyrene. In the presence of fluoranthene these four enzymes are constitutively expressed but only PhdF is upregulated. We are also interested in determining the cleavage sites for the ring-cleaving reactions. Previous studies have shown that **3** can be cleaved at the meta position rather than methylated and removed from the cell and that **36** can be cleaved at the meta position as well as the ortho position (Scheme 4.4) (Walter, 1991).

In this chapter, we assayed PhdF and three other annotated type I extradiol dioxygenases (products of genes 0545, 2891, and 4413) for activity with the dihydroxypyrenes **3** and **36**, and the dihydroxyfluoranthenes **41**, and **42** (Scheme 4.4). Their reactions with **40** could not be examined because **40** is not yet available. We assayed PhdG for activity with the products of any successful

ring-opening reactions. If the extradiol dioxygenases PhdF, 0545, 2891 or 4413 did not catalyze the expected reactions then PhdI, the other ring-cleaving dioxygenase upregulated in the presence of pyrene, was assayed for activity with the same compounds. If PhdG did not process the ring-cleavage products then PhdJ, the other hydratase-aldolase upregulated in the presence of pyrene, was assayed for activity with these compounds. The results are reported herein.

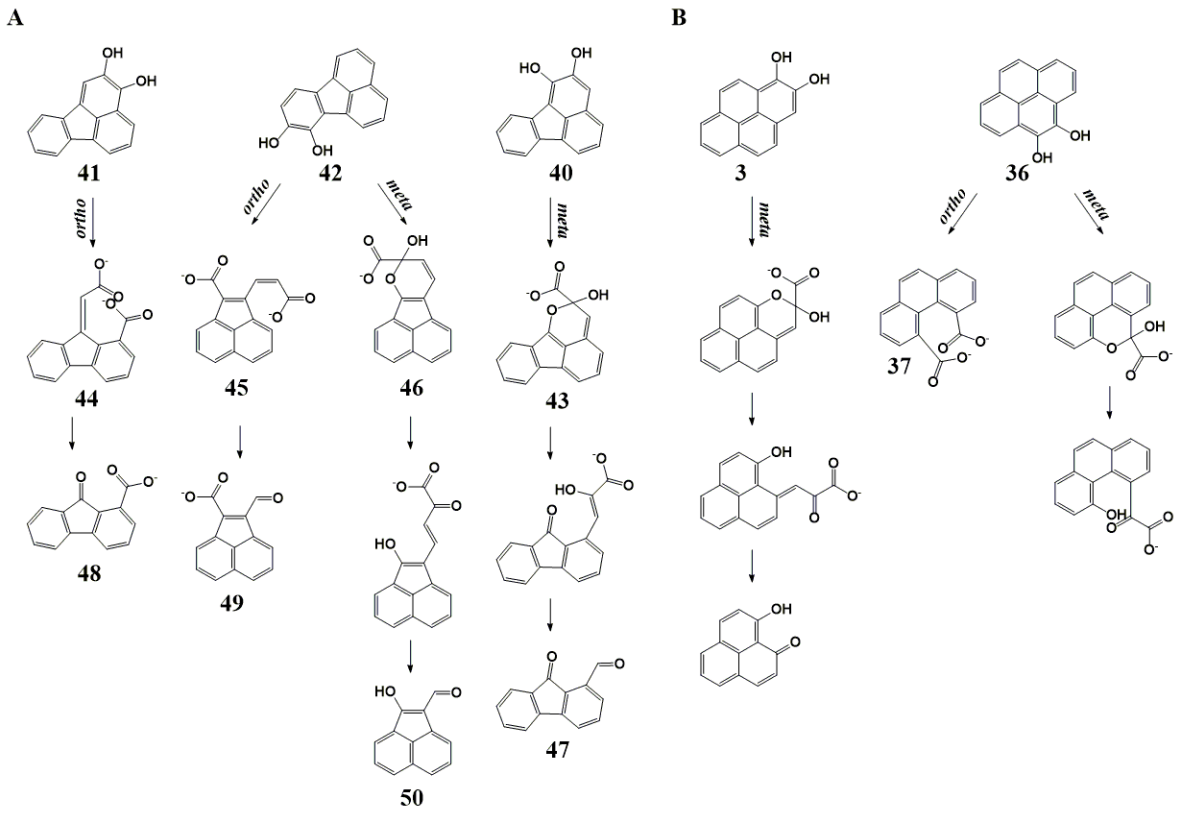

Scheme 4.4: Possible ring-cleavage and subsequent hydratase-aldolase reactions for A) fluoranthene catabolic intermediates and B) pyrene catabolic intermediates.

4.2 Experimental Procedures

Materials

Chemicals, biochemicals, buffers, and solvents were purchased from Sigma-Aldrich Chemical Co. (St. Louis, MO), Fisher Scientific Inc. (Pittsburgh, PA), Fluka Chemical Corp. (Milwaukee, WI), or EMD Millipore, Inc. (Billerica, MA). 1-Hydroxypyrene, pyrene-4,5-dione, fluoranthene, 1-hydroxynaphthalene, and 4-bromo-2-methoxy-1-methylbenzene were purchased from Sigma-Aldrich Chemical Co. The synthetic procedures for 1,2-dihydroxypyrene, 4,5-dihydroxypyrene, 1,2-dihydroxyfluoranthene, 2,3-dihydroxyfluoranthene, and 7,8-dihydroxyfluoranthene are reported in the supplemental material (Section 4.5). The Sephadex G-100 resin was obtained from GE Healthcare (Piscataway, NJ). The EconoColumn® chromatography columns were obtained from BioRad (Hercules, CA).

General Methods

Protein concentrations were determined using the Bradford method (Bradford, 1976). Electrospray ionization mass spectrometry (ESI-MS) was carried out on an LCQ electrospray ion-trap mass spectrometer (Thermo, San Jose, CA) housed in the ICMB Protein and Metabolite Analysis Facility at the University of Texas. Steady-state kinetic assays were performed on an Agilent 8453 diode-array spectrophotometer (Agilent Technologies, Santa Clara, CA). Nonlinear regression data analysis was performed using the program Grafit (Erithacus Software Ltd., Staines, U.K.). Nuclear magnetic resonance (NMR) spectra were recorded on a Varian UNITY+ 300 MHz (Palo Alto, CA) or a Bruker AVANCE III 500 MHz spectrometer (Billerica, MA). NMR signals

were analyzed using the software program SpinWorks 3.1.6 (Copyright 2009 Kirk Marat, University of Manitoba).

Enzymes

The purified dioxygenases PhdI and PhdF and the hydratase-aldolases PhdJ and PhdG were prepared as described in Chapter 2. The purified dioxygenases designated 2891, 4413, and 5306 were prepared as described in Chapter 3.

Activity Assays

*Reactions of Dioxygenases with 1,2-Dihydroxypyrene (**3**) and 4,5-Dihydroxypyrene (**36**)*

Aliquots of the purified dioxygenase enzymes PhdI, PhdF, and those designated 2891, 4413, or 5306 (1 – 15 µL, 5 – 100 nM final) and 1,2-dihydroxypyrene or 4,5-dihydroxypyrene in ethanol (1 µM – 1 mM final) were added to 20 mM HEPES buffer at pH 7.0 (1 mL) and the reactions monitored using UV spectroscopy. No change in absorbance other than that caused by non-enzymatic oxidation was observed using any dioxygenase.

*Reactions of Dioxygenases with 1,2-Dihydroxyfluoranthene (**40**), 2,3-Dihydroxyfluoranthene (**41**), and 7,8-Dihydroxyfluoranthene (**42**)*

Aliquots of the purified dioxygenase enzyme PhdI, PhdF, and those designated 2891, 4413, or 5306 (1 – 15 µL, 5 – 100 nM final) and 1,2-dihydroxyfluoranthene 2,3-dihydroxyfluoranthene or 7,8-dihydroxyfluoranthene in ethanol (1 µM – 1 mM final) were added to 20 mM HEPES buffer at pH 7.0 (1 mL) and the reactions monitored using UV spectroscopy. No change in absorbance

other than that caused by non-enzymatic oxidation was observed using any dioxygenase with 2,3-dihydroxyfluoranthene. No change in absorbance other than that caused by non-enzymatic oxidation was observed using PhdI, 2891 or 5306 with 7,8-dihydroxyfluoranthene. Reactions using PhdF or 4413 with 7,8-dihydroxyfluoranthene showed spectral shifts consistent with enzymatic activity.

*Reactions of a Hydratase-Aldolase with **46***

A coupled assay was used to follow the reaction of PhdG with the ring-opened product generated from 7,8-dihydroxyfluoranthene using PhdF. The reactions were initiated by adding 100 µl of PhdF supernatant prepared as described in Chapter 2 and various concentrations of 7,8-dihydroxyfluoranthene (1 µM – 1 mM final) in ethanol to 1 ml of 20 mM HEPES buffer at pH 7.0. The reactions were monitored by following the increase in absorbance of the product at 488 nm until completion as determined by no further change in absorbance. Upon completion, aliquots of PhdG (0.1 - 1 µM final) prepared as described in Chapter 2 were added. No change in absorbance was observed.

Product Identification

*Reaction of PhdF with 7,8-Dihydroxyfluoranthene (**42**)*

PhdF was used to generate the ring-opened product of 7,8-dihydroxyfluoranthene (7,8-DHF) and the product was identified by UV spectroscopy, derivatization, and NMR spectroscopy. After expression of PhdF as described in Chapter 2, the cells were centrifuged at 17,700 × g for 30 min. The cell pellet was washed 3 times by resuspension in 5 mM sodium phosphate at pH 7.0

(OD_{600} = 0.5 for 10 µL suspension in 1 mL buffer) and then centrifuged (17,700 × g for 30 min). The pellet was then resuspended in 5 mM sodium phosphate at pH 7.0 (OD_{600} = 0.5 for 10 µL PhdF in 1 mL of buffer) to a final volume of 10 mL. A solution of 7,8-DHF in ethanol (67 mg/mL stock concentration) was added to the cell suspension, which was stirring on ice, over the course of 5 min. Aliquots (500 uL) were removed every 5 min, centrifuged at 20,800 × g for 2 min, and the cell free supernatant monitored by UV spectroscopy until the reaction was complete (~30 min), as determined by no further change in absorbance at 488 nm. The reaction was centrifuged at 17,700 x g for 20 min and the pH of the cell-free solution adjusted to 8.0 using drops of 1M NaOH. The solution was washed using 2.5 volumes of ethyl acetate. The aqueous layer was collected and concentrated to 600 µL and loaded onto a Sephadex G-100 column. The column was washed with water and the eluate monitored using UV spectroscopy (488 nm). The product-containing fractions (~6 mL) were combined and evaporated to dryness. The product was analyzed using ESI-MS. The product was resuspended in ~0.6 mL of $CDCl_3$ and placed in an NMR tube. A ^1H NMR spectrum of the crude product is consistent with the structure of **46**. Once more compound is available, ^1H NMR and ^{13}C NMR spectroscopic analysis will be used to identify the product(s).

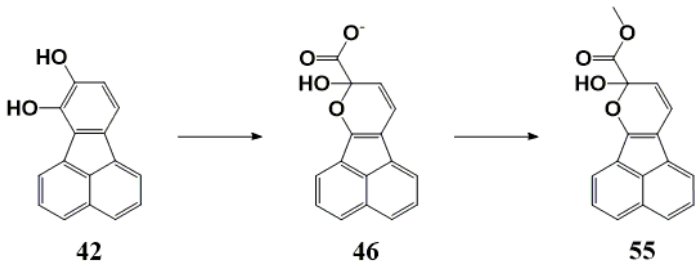

42 46 55

Scheme 4.5: Compound **46** was generated as described in the text. It is anticipated that **46** can be converted to **55** for characterization.

Steady-State Kinetic Analysis

*Reactions with 7,8-Dihydroxyfluoranthene (**42**)*

An aliquot of PhdF (15 µL) prepared as described in Chapter 2 or 4413 (6 µL), prepared as described in Chapter 3, was added to 1 mL of 20 mM HEPES at pH 7.0 to give a final concentration of 200 nM for PhdF and 140 nM for 4413. Assays were initiated by the addition of aliquots of a stock solution of 7,8-dihydroxyfluoranthene in ethanol (20 mM). The final substrate concentration ranged from 1 – 30 µM for PhdF reactions and 3 – 300 µM for 4413 reactions. The reaction was monitored by following an increase in absorbance at 488 nm (ε = 5490 M−1 cm−1). Initial rates were determined from the first 30 s of the reaction, plotted versus substrate concentration, and fit to the substrate inhibition or Michaelis-Menten equation to calculate the steady-state parameters k_{cat}, $K_{M,}$ and K_i using Grafit (Johnson, 2011; Haldane, 1930).

4.3 Results and Discussion

Reactions with Pyrenes

*Activity Assays using Dioxygenases with 1,2-Dihydroxypyrene (**3**) and 4,5-Dihydroxypyrene (**36**)*

All five dioxygenase enzymes were assayed for activity with 1,2-dihydroxypyrene (**3**) and 4,5-dihydroxypyrene (**36**). When 1,2-dihydroxypyrene (**3**) or 4,5-dihydroxypyrene (**36**) was incubated with each enzyme for >30 min no spectral changes were observed suggesting that these compounds might not be substrates for any of the five enzymes. The absorbance spectrums for 1,2-dihydroxypyrene (**3**) and 4,5-dihydroxypyrene (**36**) without enzyme are given in Figure 4.2.

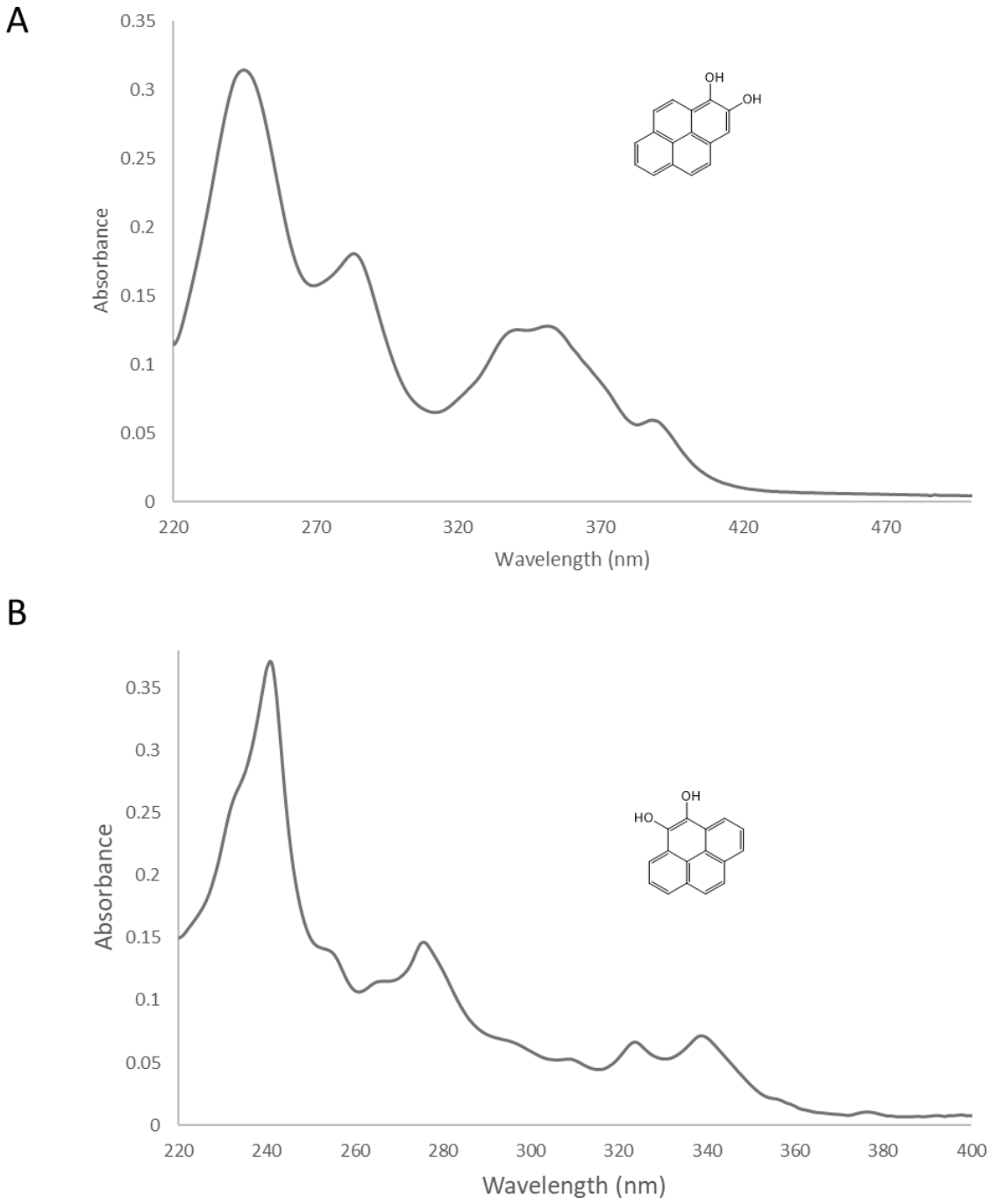

Figure 4.2: Absorbance spectrum of A) 1,2-dihydroxypyrene without enzyme and B) 4,5-dihydroxypyrene without enzyme.

Reactions with Fluoranthenes

*Activity Assays using Dioxygenases with 1,2-Dihydroxyfluoranthene (**40**), 2,3-Dihydroxyfluoranthene (**41**), and 7,8-Dihydroxyfluoranthene (**42**)*

All five dioxygenase enzymes were assayed for activity with 1,2-dihydroxyfluoranthene (**40**), 2,3-dihydroxyfluoranthene (**41**), and 7,8-dihydroxyfluoranthene (**42**). When 2,3-dihydroxyfluoranthene (**41**) was incubated with each enzyme for >30 min no spectral changes were observed suggesting that this compound might not be a substrate for any of the five enzymes. The absorbance spectrum for 2,3-dihydroxyfluoranthene (**41**) without enzyme is given in Figure 4.3. When 7,8-dihydroxyfluoranthene was incubated with PhdI, 2891 or 5306 for >30 min no spectral changes were observed suggesting that 7,8-dihydroxyfluoranthene might not be a substrate for PhdI, 2891 or 5306. 7,8-Dihydroxyfluoranthene was processed by PhdF and 4413 and the absorbance spectra for the reaction with PhdF is shown in Figure 4.4.

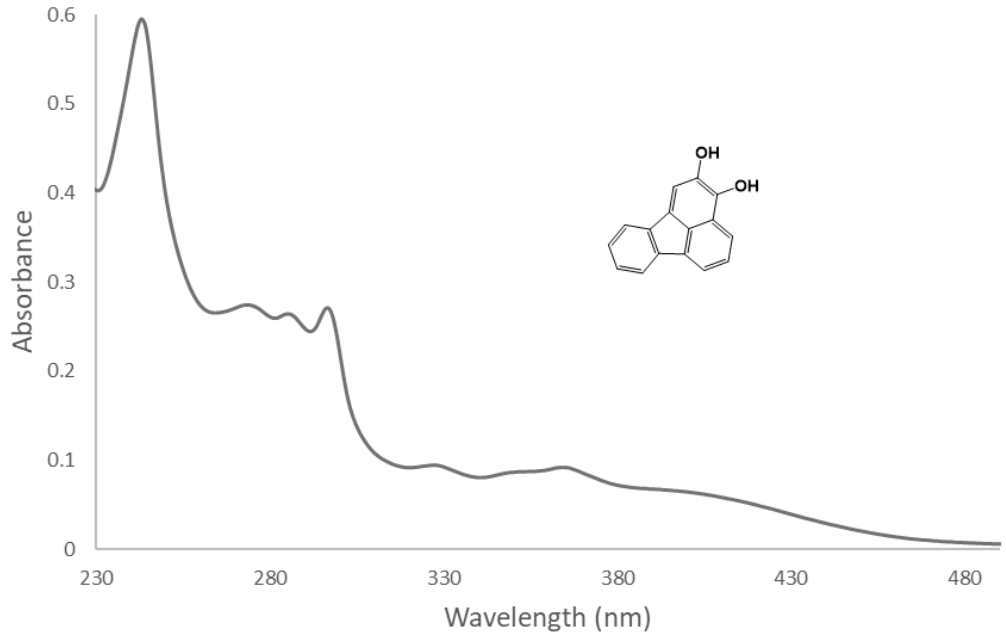

Figure 4.3: Absorbance spectrum for 2,3-dihydroxyfluoranthene without enzyme.

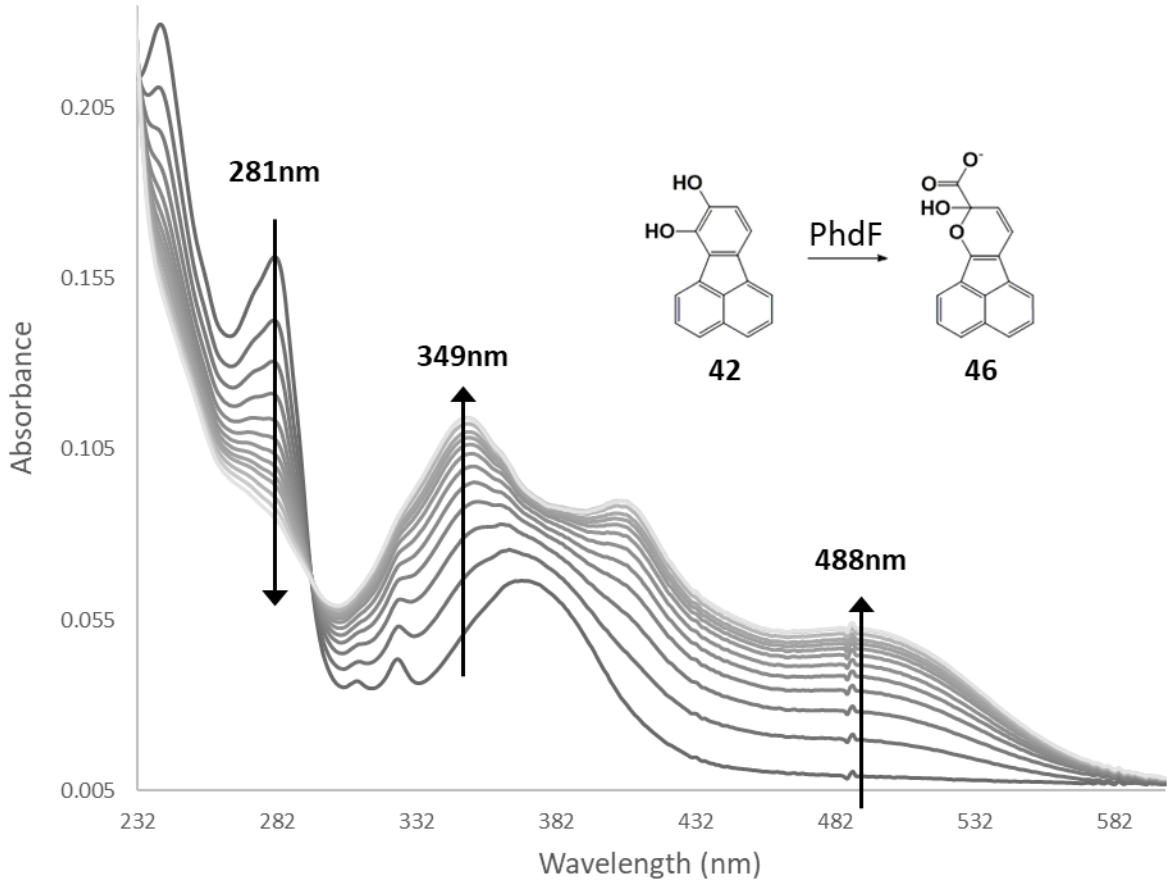

Figure 4.4: Absorbance spectra for the reaction of PhdF and 7,8-dihydroxyfluoranthene (**42**). The structure of **46** was inferred from a ^{1}H NMR spectrum of the crude reaction product. The compound will be unequivocally characterized in future work.

Identification of Dioxygenase Reaction Products

To determine whether cleavage of 7,8-dihydroxyfluoranthene (**42**) occurs at the ortho or meta position the product of the PhdF-catalyzed reaction was isolated and identified. 7,8-Dihydroxyfluoranthene (**42**) was treated with a whole cell suspension of PhdF. The structure of **46** was inferred from a ^{1}H NMR spectrum of the crude reaction product. It appears that PhdF and 4413 catalyze the ring-opening of 7,8-dihydroxyfluoranthene (**42**) at the meta position and the product is in the *cis* form as shown in Scheme 4.5. The compound will be further characterized in when more compound can be obtained.

Steady-State Kinetic Analysis Using Dioxygenases

The k_{obs} vs substrate concentration was plotted for the reactions of PhdF and 4413 with 7,8-dihydroxyfluoranthene (**42**) and are shown in Figure 4.5. The reaction using PhdF displays substrate inhibition and the data are fit using the substrate inhibition equation (Haldane, 1930). The reaction using 4413 appears to obey classic Michaelis-Menten kinetics and the data are fit using the Michaelis-Menten equation (Johnson, 2011). The measured k_{cat}/K_M for PhdF with 7,8-dihydroxyfluoranthene is nearly an order of magnitude greater than for the reaction using 4413. Kinetic parameters are summarized in Table 4.2.

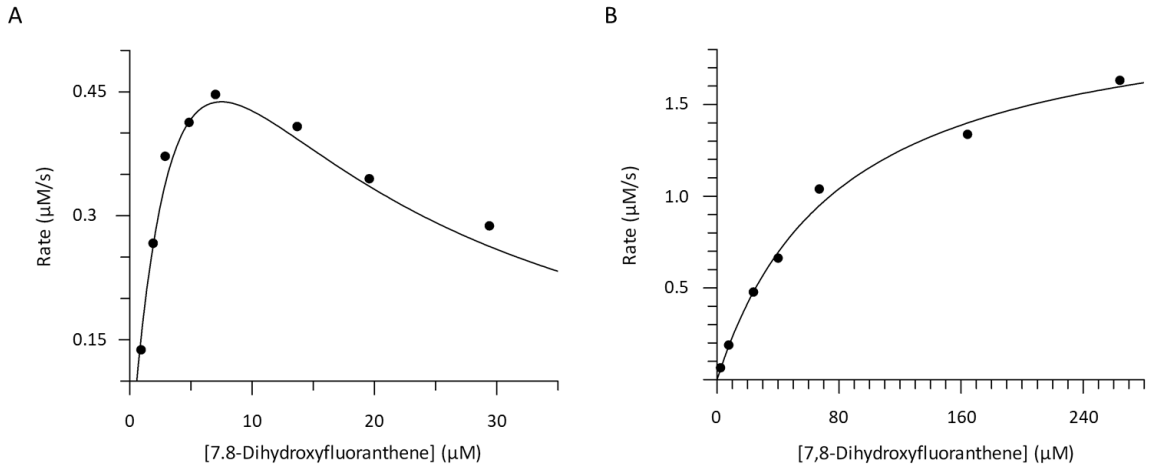

Figure 4.5: Plots of k_{obs} vs 7,8-dihydroxyfluoranthene concentration for the reaction with A) PhdF or B) 4413. The data are fit to the substrate inhibition or Michaelis-Menten equation (Haldane, 1930; Johnson, 2011).

Enzyme	Substrate	k_{cat} (s^{-1})	K_M (μM)	k_{cat}/K_M ($M^{-1}s^{-1}$)	K_i (μM)
PhdF	7,8-dihydroxyphenanthrene	3.9 ± 0.3	3.4 ± 0.4	(1.2 ± 0.2)E+06	18 ± 5
4413	7,8-dihydroxyphenanthrene	15.0 ± 0.6	81 ± 7	(1.9 ±0.2)E+05	—

Table 4.2: Kinetic parameters for the reaction of PhdF and 4413 with 7,8-dihydroxyfluoranthene.

*Activity Assays using PhdG with **46***

A coupled assay with PhdF, 7,8-dihydroxyfluoranthene (**42**), and PhdG was used to determine if PhdG can cleave the ring-opened product **46**. After **46** was generated using PhdF and 7,8-dihydroxyfluoranthene (**42**), PhdG was added. No spectral changes were observed. This suggests that **46** might not be a substrate for PhdG.

Summary

Overall, the work in this chapter addressed questions about the reactions and enzyme functions in the pyrene and fluoranthene catabolic pathways of *M. vanbaalenii* PYR-1. The major findings are 1) none of the dioxygenases assayed (designated PhdF, PhdI, 2891, 4413, and 5306) can ring-cleave the proposed pyrene catechol intermediates **3** or **36** or the proposed fluoranthene catechol intermediate **41**; 2) the dioxygenases designated PhdF and 4413 catalyze extradiol ring-cleavage of the fluoranthene catechol compound **42** to produce **46**; and 3) PhdG does not process **46** (see Scheme 4.4).

The inability of PhdF to catalyze ring-cleavage of either pyrene catechol compound (**3** or **36**, Scheme 4.4) is not surprising. During degradation of pyrene by *M. vanbaalenii* PYR-1, intermediate **3** is not ring-cleaved even though PhdF is upregulated in the presence of pyrene. However, **36** is cleaved at the ortho position, a reaction that the extradiol dioxygenase PhdF likely cannot catalyze (Kim, 2007). Three other annotated type I extradiol dioxygenases (designated 2891, 4413, and 5306) and one annotated as a type III extradiol dioxygenase (PhdI) were also unable to ring-cleave **3** or **36**. There are three other annotated type I extradiol dioxygenases in *M.*

vanbaalenii PYR-1 and one of these may have the ability to meta ring-cleavage of **3**, although none of these are upregulated in *M. vanbaalenii* PYR-1 in the presence of pyrene (Kim, 2008; Kim, 2007). The only intradiol dioxygenase that has been identified thus far in *M. vanbaalenii* PYR-1 is protocatechuate 3,4-dioxygenase (Kim, 2008). It is possible that this enzyme is responsible for the ortho cleavage of **36**. Future work on the reaction of protocatechuate 3,4-dioxygenase with **36** can clarify the issue.

None of the annotated type I extradiol dioxygenases (designated PhdF, 2891, 4413, 5306) or the annotated type III extradiol dioxygenase (PhdI) can ring-cleave the fluoranthene catabolic intermediate **41**. However, the dioxygenases designated PhdF and 4413 can cleave the fluoranthene catabolic intermediate **42** at the meta position to produce **46** (Scheme 4.4). The hydratase-aldolase PhdG does not process **46**. It is likely that an isomerization of **46** to the open *trans* form (Scheme 4.4) must take place before hydration and retro-aldol cleavage by PhdG can occur. This isomerization may happen non-enzymatically in the cellular environment of *M. vanbaalenii* PYR-1. There may also be an isomerase within *M. vanbaalenii* PYR-1 that has not yet been identified that can catalyze the isomerization of **46**. There are three other annotated type I extradiol dioxygenases in *M. vanbaalenii* PYR-1 (Kim, 2008). Although none of these dioxygenases are upregulated in the presence of fluoranthene, one of these may be able to catalyze both the ring-cleavage of **42** and the isomerization of **46** (Kweon, 2007). We are currently attempting to synthesize the proposed fluoranthene catechol intermediate **40**. We will investigate the activities of the dioxygenases described in this chapter (designated PhdI, PhdF, 2891, 4413, and 5306) with **40** as soon as the compound is available.

4.5 Supplemental

*1,2-Dihydroxypyrene (**3**) and 4,5-Dihydroxypyrene (**36**) Synthesis*

Oxidation of 1-hydroxypyrene to pyrene-1,2-dione was performed by following a published procedure (Wu, 2010). Esterification of pyrene-1,2-dione and pyrene-4,5-dione to pyrene-1,2-diyl diacetate and pyrene-4,5-diyl diacetate, respectively, were performed by following published procedures (Langvik, 2015). ^{1}H and ^{13}C NMR spectroscopy were used to verify the identity of these compounds. These stable compounds were stored at -20 °C. When needed, small amounts of the diacetates were hydrolyzed under argon to 1,2-dihydroxypyrene or 4,5-dihydroxypyrene using acetyl chloride and ethanol.

Pyrene-1,2-diyl diacetate: ^{1}H NMR ($(CD_3)_2CO$, 500 MHz) δ 1.6 (s, 3H), 2.6 (s, 3H), 7.4 (d, 1H, J = 9.2 Hz), 8.0 (d, 1H, J = 9.3 Hz), 8.1 (m, 1H), 8.3 (d, 2H, J = 8.9 Hz), 8.37 (s, 1H), 8.41 (m, 2H); ^{13}C NMR ($(CD_3)_2CO$, 125 MHz) δ 19.9, 20.5, 121.3, 124.0, 124.7, 124.9, 126.1, 126.2, 127.2, 127.3, 127.7, 129.1, 130.18, 130.21, 131.6, 131.8, 138.0, 141.1, 168.4, 139.5.

Pyrene-4,5-diyl diacetate: ^{1}H NMR ($CDCl_3$, 400 MHz) δ 2.6 (s, 6H), 8.0 (t, 2H), 8.1 (s, 2H), 8.17 (dd, 2H, J = 1.1 Hz, 7.9 Hz), 8.23 (dd, 2H, J = 1.1 Hz, 7.6 Hz); ^{13}C NMR ($CDCl_3$, 100 MHz) δ 20.6, 119.4, 123.6, 125.8, 125.9, 126.4, 127.6, 131.2, 136.7, 168.3

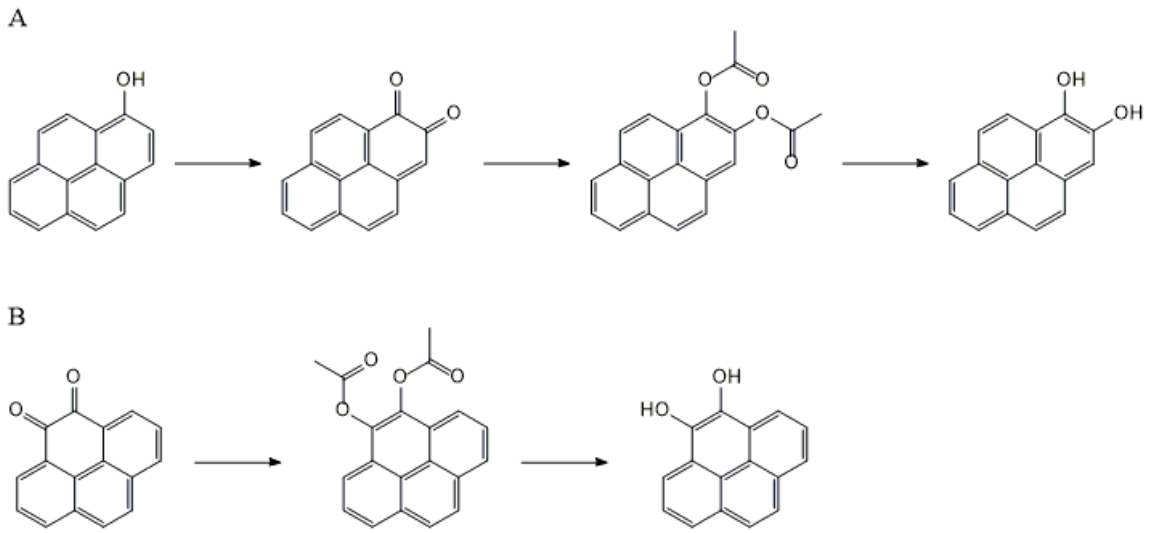

Scheme 4.6: Synthesis of A) 1,2-dihydroxypyrene and B) 4,5-dihydroxypyrene.

*2,3-Dihydroxyfluoranthene (**41**) Synthesis*

Fluoranthen-3-yl acetate was synthesized from fluoranthene following a published procedure (Shenbor, 1969). Transesterification using ethanol and acetyl chloride produced 3-hydroxyfluoranthene. Synthesis of 2,3-dihydroxyfluoranthene from 3-hydroxyfluoranthene followed the procedure described above for 1,2-dihydroxyfluoranthene synthesis from 1-hydroxyfluoranthene.

Fluoranthene-2,3-diyl diacetate: ^{1}H NMR ($CDCl_3$, 300 MHz) δ 2.4 (s, 3H), 2.5 (s, 3H), 7.4 (m, 2H), 7.65 (m, 1H), 7.8 (m, 5H); ^{13}C NMR ($CDCl_3$, 75 MHz) δ 20.5, 20.8, 116.5, 120.3, 121.4, 121.71, 121.73, 124.4, 127.9, 127.93, 129.0, 131.0, 135.7, 137.1, 137.6, 138.4, 139.7, 141.5, 168.4, 168.7.

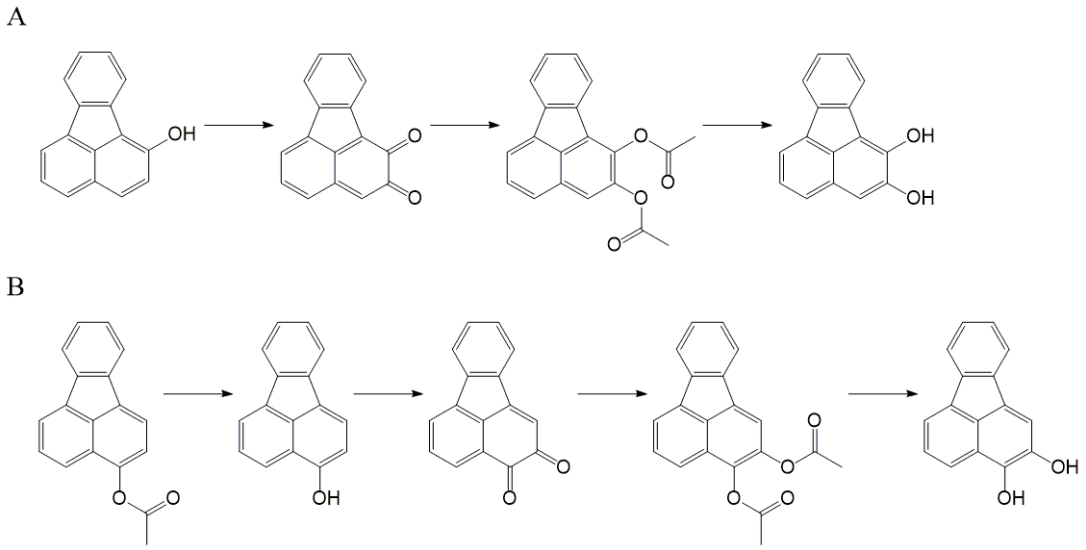

Scheme 4.7: Synthesis of A) 1,2-dihydroxyfluoranthene and B) 2,3-dihydroxyfluoranthene.

*7,8-Dihydroxyfluoranthene (**42**) Synthesis*

8-Methoxy-9-methylfluoranthene was synthesized using a published procedure (Yamaguchi, 2016). Demethylation using boron tribromide produced 8-hydroxy-9-methylfluoranthene. Oxidation to 9-methylfluoranthene-7,8-dione was performed following a published procedure (Wu, 2010). O-Methylation using dimethyl sulfate produced 7,8-dimethoxy-9-methylfluoranthene. Benzylic bromination using N-bromosuccinimide followed by hydrolysis produced 7,8-dimethoxyfluoranthene-8-carbaldehyde that was oxidized to 7,8-dimethoxyfluoranthene-8-carboxylic acid using the Jones reagent. Decarboxylation using copper in quinoline afforded 7,8-dimethoxyfluoranthene. ^{1}H and ^{13}C NMR spectroscopy were used to verify the identity of this compound. This stable compound was stored at -20 °C. When needed, small amounts of 7,8-dimethoxyfluoranthene were hydrolyzed under argon to 9,10-dihydroxyfluoranthene using boron tribromide.

7,8-dimethoxyfluoranthene: ^{1}H NMR ($CDCl_3$, 500 MHz) δ 4.0 (s, 3H), 4.1 (s, 3H), 7.0 (d, 1H, J = 8.1 Hz), 7.6 (m, 2H), 7.7 (m, 1H), 7.8 (d, 2H, J = 8.2 Hz), 7.9 (m, 2H), 8.19 (d, 1H, J = 6.9 Hz); ^{13}C NMR ($CDCl_3$, 125 MHz) δ 56.3, 60.3, 111.4, 117.3, 119.1, 123.3, 125.6, 126.4, 127.8, 128.2, 129.9, 132.4, 132.8. 133.4, 135.4, 136.9, 146.0, 153.0.

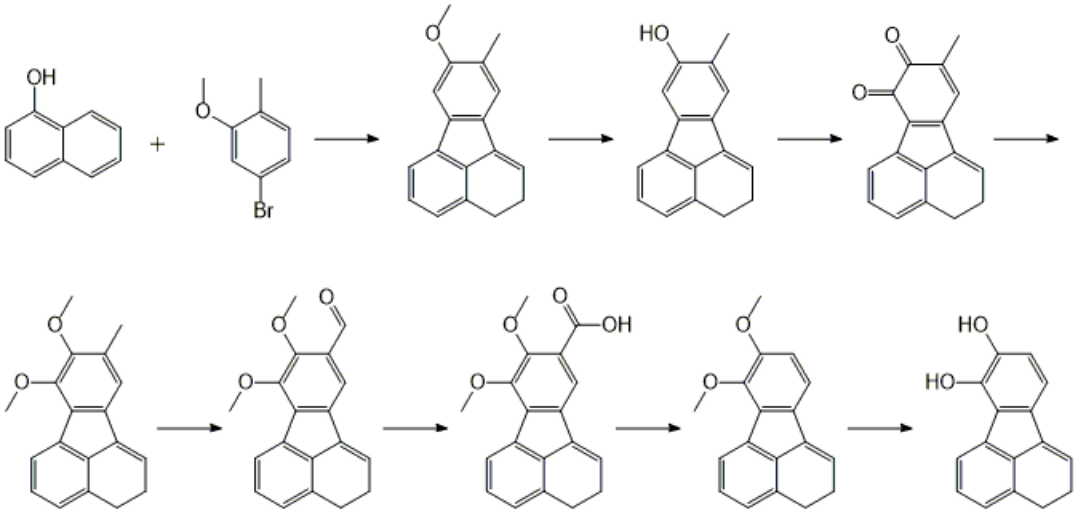

Scheme 4.8: Synthesis of 7,8-dihydroxyfluoranthene.

References

Acevedo, F., Pizzul, L., González, M., Cea, M., Gianfreda, L., and Diez, M. (2010). Degradation of polycyclic aromatic hydrocarbons by free and nanoclay-immobilized manganese peroxidase from *Anthracophyllum discolor*. Chemosphere *80*, 271-278.

Adachi, K., Iwabuchi, T., Sano, H., and Harayama, S. (1999). Structure of the Ring Cleavage Product of 1-Hydroxy-2-Naphthoate, an Intermediate of the Phenanthrene-Degradative Pathway of *Nocardioides sp*. strain KP7. Journal of Bacteriology *181*, 757-763.

Ali, M.A., Kondo, K., and Tsuda, Y. (1992). Synthesis and nematocidal activity of hydroxystilbenes. Chemical and Pharmaceutical Bulletin *40*, 1130-1136.

Anderberg, S.J., Newton, G.L., and Fahey, R.C. (1998). Mycothiol Biosynthesis and Metabolism: Cellular levels of potential intermediates in the biosynthesis and degradation of mycothiol in *Mycobacterium smegmatis*. Journal of Biological Chemistry *273*, 30391-30397.

Azubuike, C.C., Chikere, C.B., and Okpokwasili, G.C. (2016). Bioremediation techniques–classification based on site of application: principles, advantages, limitations and prospects. World Journal of Microbiology and Biotechnology *32*, 180.

Bailey, L.A., Nascarella, M.A., Kerper, L.E., and Rhomberg, L.R. (2016). Hypothesis-based weight-of-evidence evaluation and risk assessment for naphthalene carcinogenesis. Critical Reviews in Toxicology *46*, 1-42.

Bayly, R., Dagley, S., and Gibson, D. (1966). The metabolism of cresols by species of *Pseudomonas*. Biochemical Journal *101*, 293.

Boehm, P.D., Cook, L.L., and Murray, K.J. (2011). Aromatic hydrocarbon concentrations in seawater: Deepwater Horizon oil spill. Paper presented at: International Oil Spill Conference Proceedings (American Petroleum Institute).

Bogan, B., Lahner, L., Sullivan, W., and Paterek, J. (2003). Degradation of straight-chain aliphatic and high-molecular-weight polycyclic aromatic hydrocarbons by a strain of *Mycobacterium austroafricanum*. Journal of Applied Microbiology *94*, 230-239.

Bouchez, M., Blanchet, D., Bardin, V., Haeseler, F., and Vandecasteele, J.-P. (1999). Efficiency of defined strains and of soil consortia in the biodegradation of polycyclic aromatic hydrocarbon (PAH) mixtures. Biodegradation *10*, 429-435.

Bradford, M.M. (1976). A rapid and sensitive method for the quantitation of microgram quantities of protein utilizing the principle of protein-dye binding. Analytical Biochemistry *72*, 248-254.

Bugg, T.D. (2003). Dioxygenase enzymes: catalytic mechanisms and chemical models. Tetrahedron *59*, 7075-7101.

Cases, I., and de Lorenzo, V. (2005). Genetically modified organisms for the environment: stories of success and failure and what we have learned from them. International Microbiology *8*, 213-222.

Cebolla, A., Sousa, C., and de Lorenzo, V. (1997). Effector specificity mutants of the transcriptional activator NahR of naphthalene degrading *Pseudomonas* define protein sites involved in binding of aromatic inducers. Journal of Biological Chemistry *272*, 3986-3992.

Cho, H.J., Kim, K., Sohn, S.Y., Cho, H.Y., Kim, K.J., Kim, M.H., Kim, D., Kim, E., and Kang,

B.S. (2010). Substrate binding mechanism of a type I extradiol dioxygenase. Journal of Biological Chemistry *285*, 34643-34652.
de Souza Machado, A.A., Hoff, M.L.M., Klein, R.D., Cordeiro, G.J., Avila, J.M.L., Costa, P.G., and Bianchini, A. (2014). Oxidative stress and DNA damage responses to phenanthrene exposure in the estuarine guppy *Poecilia vivipara*. Marine Environmental Research *98*, 96-105.
Deininger, P. (1990). Molecular Cloning: A Laboratory Manual. Edited by J. Sambrook, EF Fritsch, and T. Maniatis. Cold Spring Harbor Laboratory Press, Cold Spring Harbor, NY, 1989 (in 3 volumes) (Academic Press).
DiBlasi, C.J., Li, H., Davis, A.P., and Ghosh, U. (2008). Removal and fate of polycyclic aromatic hydrocarbon pollutants in an urban storm water bioretention facility. Environmental Science & Technology *43*, 494-502.
Duan, L., Naidu, R., Thavamani, P., Meaklim, J., and Megharaj, M. (2015). Managing long-term polycyclic aromatic hydrocarbon contaminated soils: a risk-based approach. Environmental Science and Pollution Research *22*, 8927-8941.
Dupuy, J., Ouvrard, S., Leglize, P., and Sterckeman, T. (2015). Morphological and physiological responses of maize (*Zea mays*) exposed to sand contaminated by phenanthrene. Chemosphere *124*, 110-115.
Eibes, G., Arca-Ramos, A., Feijoo, G., Lema, J., and Moreira, M. (2015). Enzymatic technologies for remediation of hydrophobic organic pollutants in soil. Applied Microbiology and Biotechnology *99*, 8815-8829.
Farrington, J.W., and Takada, H. (2014). Persistent organic pollutants (POPs), polycyclic aromatic hydrocarbons (PAHs), and plastics: Examples of the status, trend, and cycling of organic chemicals of environmental concern in the ocean. Oceanography *27*, 196-213.
Fritzsche, C. (1994). Degradation of pyrene at low defined oxygen concentrations by a *Mycobacterium* sp. Applied and Environmental Microbiology *60*, 1687-1689.
Gavrilescu, M. (2010). Environmental biotechnology: achievements, opportunities and challenges. Dynamic Biochemistry, Process Biotechnology and Molecular Biology *4*, 1-36.
Gavrilescu, M., Demnerová, K., Aamand, J., Agathos, S., and Fava, F. (2015). Emerging pollutants in the environment: present and future challenges in biomonitoring, ecological risks and bioremediation. New Biotechnology *32*, 147-156.
Ge, Y., and Eltis, L.D. (2003). Characterization of hybrid toluate and benzoate dioxygenases. Journal of Bacteriology *185*, 5333-5341.
Ghosal, D., Ghosh, S., Dutta, T.K., and Ahn, Y. (2016). Current state of knowledge in microbial degradation of polycyclic aromatic hydrocarbons (PAHs): a review. Frontiers in Microbiology *7*.
Goldberg, E., Butler, P., Meire, P., Menzel, D., Risebrough, R., and Stickel, L. (1971). Chlorinated hydrocarbons in the marine environment. National Academy of Sciences, Washington, DC.
Haldane, J. (1930). Enzymes Longmans, Green, London.
Haworth, W.N. (1915). III.—A new method of preparing alkylated sugars. Journal of the Chemical Society, Transactions *107*, 8-16.
Heitkamp, M.A., and Cerniglia, C.E. (1988). Mineralization of polycyclic aromatic hydrocarbons

by a bacterium isolated from sediment below an oil field. Applied and Environmental Microbiology *54*, 1612-1614.
Hu, J., Sheng, L., Li, L., Zhou, X., Xie, F., D'Agostino, J., Li, Y., and Ding, X. (2014). Essential role of the cytochrome P450 enzyme CYP2A5 in olfactory mucosal toxicity of naphthalene. Drug Metabolism and Disposition *42*, 23-27.
Huang, L., Wang, C., Zhang, Y., Wu, M., and Zuo, Z. (2013). Phenanthrene causes ocular developmental toxicity in zebrafish embryos and the possible mechanisms involved. Journal of Hazardous Materials *261*, 172-180.
Iwabuchi, T., and Harayama, S. (1998). Biochemical and molecular characterization of 1-hydroxy-2-naphthoate dioxygenase from *Nocardioides* sp. KP7. Journal of Biological Chemistry *273*, 8332-8336.
Johnson, K.A., and Goody, R.S. (2011). The original Michaelis constant: translation of the 1913 Michaelis–Menten paper. Biochemistry *50*, 8264-8269.
Kaushik, C., and Haritash, A. (2006). Polycyclic aromatic hydrocarbons (PAHs) and environmental health. Our Earth *3*, 1-7.
Kelley, I., Freeman, J.P., and Cerniglia, C.E. (1990). Identification of metabolites from degradation of naphthalene by a *Mycobacterium* sp. Biodegradation *1*, 283-290.
Keum, Y.-S., Seo, J.-S., Hu, Y., and Li, Q.X. (2006). Degradation pathways of phenanthrene by *Sinorhizobium* sp. C4. Applied Microbiology and Biotechnology *71*, 935-941.
Kim, S.-J., Kweon, O., and Cerniglia, C. (2010). Degradation of polycyclic aromatic hydrocarbons by *Mycobacterium* strains. Handbook of Hydrocarbon and Lipid Microbiology, 1865-1879.
Kim, S.-J., Kweon, O., and Cerniglia, C.E. (2009). Proteomic applications to elucidate bacterial aromatic hydrocarbon metabolic pathways. Current Opinion in Microbiology *12*, 301-309.
Kim, S.-J., Kweon, O., Freeman, J.P., Jones, R.C., Adjei, M.D., Jhoo, J.-W., Edmondson, R.D., and Cerniglia, C.E. (2006). Molecular cloning and expression of genes encoding a novel dioxygenase involved in low-and high-molecular-weight polycyclic aromatic hydrocarbon degradation in *Mycobacterium vanbaalenii* PYR-1. Applied and Environmental Microbiology *72*, 1045-1054.
Kim, S.-J., Kweon, O., Jones, R.C., Edmondson, R.D., and Cerniglia, C.E. (2008). Genomic analysis of polycyclic aromatic hydrocarbon degradation in *Mycobacterium vanbaalenii* PYR-1. Biodegradation *19*, 859-881.
Kim, S.-J., Kweon, O., Jones, R.C., Freeman, J.P., Edmondson, R.D., and Cerniglia, C.E. (2007). Complete and integrated pyrene degradation pathway in *Mycobacterium vanbaalenii* PYR-1 based on systems biology. Journal of Bacteriology *189*, 464-472.
Kim, Y.-H., Freeman, J.P., Moody, J.D., Engesser, K.-H., and Cerniglia, C.E. (2005). Effects of pH on the degradation of phenanthrene and pyrene by *Mycobacterium vanbaalenii* PYR-1. Applied Microbiology and Biotechnology *67*, 275-285.
Kuppusamy, S., Thavamani, P., Megharaj, M., and Naidu, R. (2016). Biodegradation of polycyclic aromatic hydrocarbons (PAHs) by novel bacterial consortia tolerant to diverse physical settings–Assessments in liquid-and slurry-phase systems. International Biodeterioration & Biodegradation *108*, 149-157.
Kuppusamy, S., Thavamani, P., Venkateswarlu, K., Lee, Y.B., Naidu, R., and Megharaj, M.

(2017). Remediation approaches for polycyclic aromatic hydrocarbons (PAHs) contaminated soils: Technological constraints, emerging trends and future directions. Chemosphere *168*, 944-968.

Kweon, O., Kim, S.-J., and Cerniglia, C. (2010). Genomic view of mycobacterial high molecular weight polycyclic aromatic hydrocarbon degradation. Handbook of Hydrocarbon and Lipid Microbiology, 1165-1178.

Kweon, O., Kim, S.-J., Holland, R.D., Chen, H., Kim, D.-W., Gao, Y., Yu, L.-R., Baek, S., Baek, D.-H., and Ahn, H. (2011). Polycyclic aromatic hydrocarbon-metabolic network in *Mycobacterium vanbaalenii* PYR-1. Journal of Bacteriology, 00215-00211.

Kweon, O., Kim, S.-J., Jones, R.C., Freeman, J.P., Adjei, M.D., Edmondson, R.D., and Cerniglia, C.E. (2007). A polyomic approach to elucidate the fluoranthene-degradative pathway in *Mycobacterium vanbaalenii* PYR-1. Journal of Bacteriology *189*, 4635-4647.

Kweon, O., Kim, S.-J., Kim, D.-W., Kim, J.M., Kim, H.-l., Ahn, Y., Sutherland, J.B., and Cerniglia, C.E. (2014). Pleiotropic and epistatic behavior of a ring-hydroxylating oxygenase system in the polycyclic aromatic hydrocarbon metabolic network from *Mycobacterium vanbaalenii* PYR-1. Journal of Bacteriology *196*, 3503-3515.

Lamichhane, S., Krishna, K.B., and Sarukkalige, R. (2017). Surfactant-enhanced remediation of polycyclic aromatic hydrocarbons: A review. Journal of Environmental Management *199*, 46-61.

Li, L., Carratt, S., Hartog, M., Kovalchuk, N., Jia, K., Wang, Y., Zhang, Q.-Y., Edwards, P., Van Winkle, L., and Ding, X. (2017). Human CYP2A13 and CYP2F1 mediate naphthalene toxicity in the lung and nasal mucosa of CYP2A13/2F1-humanized mice. Environmental health perspectives *125*.

Liu, S.-H., Zeng, G.-M., Niu, Q.-Y., Liu, Y., Zhou, L., Jiang, L.-H., Tan, X.-f., Xu, P., Zhang, C., and Cheng, M. (2017). Bioremediation mechanisms of combined pollution of PAHs and heavy metals by bacteria and fungi: A mini review. Bioresource Technology *224*, 25-33.

Louvado, A., Gomes, N., Simões, M., Almeida, A., Cleary, D., and Cunha, A. (2015). Polycyclic aromatic hydrocarbons in deep sea sediments: Microbe–pollutant interactions in a remote environment. Science of the Total Environment *526*, 312-328.

Långvik, O., Sandberg, T., Wärnå, J., Murzin, D.Y., and Leino, R. (2015). One-pot synthesis of (R)-2-acetoxy-1-indanone from 1, 2-indanedione combining metal catalyzed hydrogenation and chemoenzymatic dynamic kinetic resolution. Catalysis Science & Technology *5*, 150-160.

M. Abdo, S.G., BJ Chou, R. Herbert, K (2001). Toxicity and carcinogenicity study in F344 rats following 2 years of whole-body exposure to naphthalene vapors. Inhalation Toxicology *13*, 931-950.

MacLeod, C., and Daugulis, A. (2003). Biodegradation of polycyclic aromatic hydrocarbons in a two-phase partitioning bioreactor in the presence of a bioavailable solvent. Applied Microbiology and Biotechnology *62*, 291-296.

Mallory, F.B., Rudolph, M.J., and Oh, S.M. (1989). Photochemistry of stilbenes. 8. Eliminative photocyclization of o-methoxystilbenes. The Journal of Organic Chemistry *54*, 4619-4626.

Martin, A., Little, C., Fraley, C., and Keyhan, M. (1995). Use of starvation promoters to limit

growth and select for trichlorethylene and phenol transformation activity in recombinant *Escherichia coli*. Applied and Environmental Microbiology *61*.
Mathew, B.B., Singh, H., Biju, V.G., and Krishnamurthy, N. (2017). Classification, source, and effect of environmental pollutants and their biodegradation. Journal of Environmental Pathology, Toxicology and Oncology *36*.
Megson, D., Reiner, E.J., Jobst, K.J., Dorman, F.L., Robson, M., and Focant, J.F. (2016). A review of the determination of persistent organic pollutants for environmental forensics investigations. Analytica Chimica Acta *941*, 10-25.
Mohan, S.V., Kisa, T., Ohkuma, T., Kanaly, R.A., and Shimizu, Y. (2006). Bioremediation technologies for treatment of PAH-contaminated soil and strategies to enhance process efficiency. Reviews in Environmental Science and Biotechnology *5*, 347-374.
Moody, J.D., Freeman, J.P., Doerge, D.R., and Cerniglia, C.E. (2001). Degradation of phenanthrene and anthracene by cell suspensions of *Mycobacterium* sp. strain PYR-1. Applied and Environmental Microbiology *67*, 1476-1483.
Mrdaković, M., Ilijin, L., Vlahović, M., Todorović, D., Gavrilović, A., Mrkonja, A., and Perić-Mataruga, V. (2015). Effects of fluoranthene on the fitness-related traits and antioxidative defense in *Lymantria dispar* L. Environmental Science and Pollution Research *22*, 10367-10374.
Nandakumar, M., Sankar, E., and Mohanakrishnan, A.K. (2014). Studies on the phthalidation of heteroarenes: A facile preparation of 3-(heteroaryl) phthalides via triflic acid mediated phthalidation. Synlett *25*, 0509-0514.
Nesnow, S., Davis, C., Padgett, W.T., Adams, L., Yacopucci, M., and King, L.C. (2000). 8, 9-Dihydroxy-8, 9-dihydrodibenzo [a, l] pyrene is a potent morphological cell-transforming agent in C3H10T1/2Cl8 mouse embryo fibroblasts in the absence of detectable stable covalent DNA adducts. Carcinogenesis *21*, 1253-1257.
Nikolaivits, E., Dimarogona, M., Fokialakis, N., and Topakas, E. (2017). Marine-derived biocatalysts: Importance, accessing, and application in aromatic pollutant bioremediation. Frontiers in Microbiology *8*.
Pampın, M.C., Estévez, J.C., Estévez, R.J., Maestro, M., and Castedo, L. (2003). Heck-mediated synthesis and photochemically induced cyclization of [2-(2-styrylphenyl) ethyl] carbamic acid ethyl esters and 2-styryl-benzoic acid methyl esters: total synthesis of naphtho [2, 1f] isoquinolines (2-azachrysenes). Tetrahedron *59*, 7231-7243.
Pedetta, A., Pouyte, K., Seitz, M.K.H., Babay, P.A., Espinosa, M., Costagliola, M., Studdert, C.A., and Peressutti, S.R. (2013). Phenanthrene degradation and strategies to improve its bioavailability to microorganisms isolated from brackish sediments. International Biodeterioration & Biodegradation *84*, 161-167.
Perpetuo, E.A., Souza, C.B., and Nascimento, C.A.O. (2011). Engineering bacteria for bioremediation. Molecular and Environmental Bioengineering-From Analysis and Modeling to Technology Applications (InTech).
Primm, T.P., Lucero, C.A., and Falkinham, J.O. (2004). Health impacts of environmental mycobacteria. Clinical microbiology reviews *17*, 98-106.
Ramos, J.L., Marqués, S., and Timmis, K.N. (1997). Transcriptional control of the *Pseudomonas* TOL plasmid catabolic operons is achieved through an interplay of host factors and plasmid-encoded regulators. Annual Reviews in Microbiology *51*, 341-373.

Rayu, S., Karpouzas, D.G., and Singh, B.K. (2012). Emerging technologies in bioremediation: constraints and opportunities. Biodegradation *23*, 917-926.
Rice, J.E., LaVoie, E.J., and Hoffmann, D. (1983). Synthesis of the isomeric phenols and the *trans*-2, 3-dihydrodiol of fluoranthene. The Journal of Organic Chemistry *48*, 2360-2363.
Roy, M., Khara, P., and Dutta, T.K. (2012). meta-Cleavage of hydroxynaphthoic acids in the degradation of phenanthrene by *Sphingobium* sp. strain PNB. Microbiology *158*, 685-695.
Saunders, C.R., Shockley, D.C., and Knuckles, M.E. (2003). Fluoranthene-induced neurobehavioral toxicity in F-344 rats. International Journal of Toxicology *22*, 263-276.
Sayler, G.S., and Ripp, S. (2000). Field applications of genetically engineered microorganisms for bioremediation processes. Current Opinion in Biotechnology *11*, 286-289.
Schell, M.A. (1983). Cloning and expression in *Escherichia coli* of the naphthalene degradation genes from plasmid NAH7. Journal of Bacteriology *153*, 822-829.
Seo, J.-S., Keum, Y.-S., Hu, Y., Lee, S.-E., and Li, Q.X. (2006). Phenanthrene degradation in *Arthrobacter* sp. P1-1: initial 1, 2-, 3, 4-and 9, 10-dioxygenation, and meta-and ortho-cleavages of naphthalene-1, 2-diol after its formation from naphthalene-1, 2-dicarboxylic acid and hydroxyl naphthoic acids. Chemosphere *65*, 2388-2394.
Seo, J.-S., Keum, Y.-S., Hu, Y., Lee, S.-E., and Li, Q.X. (2007). Degradation of phenanthrene by *Burkholderia* sp. C3: initial 1, 2-and 3, 4-dioxygenation and meta-and ortho-cleavage of naphthalene-1, 2-diol. Biodegradation *18*, 123-131.
Seo, J.-S., Keum, Y.-S., and Li, Q.X. (2009). Bacterial degradation of aromatic compounds. International Journal of Environmental Research and Public Health *6*, 278-309.
Services, U.D.o.H.a.H. (1995). Toxicological profile for polycyclic aromatic hydrocarbons. Agency for Toxic Substances and Disease Registry, Atlanta, Ge, USA, 19.
Shenbor, M., and Cheban, G. (1969). Preparation of 4-hydroxy-fluoranthene by the action of lead tetraacetate on fluoranthene. Russian Journal of Organic Chemistry *5*, 143-144.
Shuttleworth, K.L., and Cerniglia, E. (1995). Environmental aspects of PAH biodegradation. Applied Biochemistry and Biotechnology *54*, 291-302.
Sogin, M.L., Morrison, H.G., Huber, J.A., Welch, D.M., Huse, S.M., Neal, P.R., Arrieta, J.M., and Herndl, G.J. (2006). Microbial diversity in the deep sea and the underexplored "rare biosphere". Proceedings of the National Academy of Sciences *103*, 12115-12120.
Stingley, R.L., Khan, A.A., and Cerniglia, C.E. (2004). Molecular characterization of a phenanthrene degradation pathway in *Mycobacterium vanbaalenii* PYR-1. Biochemical and Biophysical Research Communications *322*, 133-146.
Straube, W., Jones-Meehan, J., Pritchard, P., and Jones, W. (1999). Bench-scale optimization of bioaugmentation strategies for treatment of soils contaminated with high molecular weight polyaromatic hydrocarbons. Resources, Conservation and Recycling *27*, 27-37.
Sugahara, Y., Kawaguchi, M., Itoyama, T., Kurokawa, D., Tosa, Y., Kitamura, S.-I., Handoh, I.C., Nakayama, K., and Murakami, Y. (2014). Pyrene induces a reduction in midbrain size and abnormal swimming behavior in early-hatched pufferfish larvae. Marine Pollution Bulletin *85*, 479-486.
Sun, G.-D., Xu, Y., Jin, J.-H., Zhong, Z.-P., Liu, Y., Luo, M., and Liu, Z.-P. (2012). Pilot scale ex-situ bioremediation of heavily PAHs-contaminated soil by indigenous microorganisms and bioaugmentation by a PAHs-degrading and bioemulsifier-producing strain. Journal of

Hazardous Materials *233*, 72-78.
Sun, Y., Yin, Y., Zhang, J., Yu, H., Wang, X., Wu, J., and Xue, Y. (2008). Hydroxyl radical generation and oxidative stress in *Carassius auratus* liver, exposed to pyrene. Ecotoxicology and Environmental Safety *71*, 446-453.
Thompson, L.C., Ladner, J.E., Codreanu, S.G., Harp, J., Gilliland, G.L., and Armstrong, R.N. (2007). 2-Hydroxychromene-2-carboxylic acid isomerase: a kappa class glutathione transferase from *Pseudomonas putida*. Biochemistry *46*, 6710-6722.
Timmis, K.N., and Pieper, D.H. (1999). Bacteria designed for bioremediation. Trends in Biotechnology *17*, 201-204.
Tomar, R.S., and Jajoo, A. (2015). Photomodified fluoranthene exerts more harmful effects as compared to intact fluoranthene by inhibiting growth and photosynthetic processes in wheat. Ecotoxicology and Environmental Safety *122*, 31-36.
Vaca, C., Törnqvist, M., Rannug, U., Lindahl-Kiessling, K., Ahnström, G., and Ehrenberg, L. (1992). On the bioactivation and genotoxic action of fluoranthene. Archives of Toxicology *66*, 538-545.
Vaillancourt, F.H., Bolin, J.T., and Eltis, L.D. (2006). The ins and outs of ring-cleaving dioxygenases. Critical Reviews in Biochemistry and Molecular Biology *41*, 241-267.
Vila, J., Nieto, J.M., Mertens, J., Springael, D., and Grifoll, M. (2010). Microbial community structure of a heavy fuel oil-degrading marine consortium: linking microbial dynamics with polycyclic aromatic hydrocarbon utilization. FEMS Microbiology Ecology *73*, 349-362.
Vinson, R., and Garret, K. (2000). Enzyme-enhanced bioremediation at Thule Air Base, Greenland. Federal Facilities Environmental Journal *10*, 39-49.
von Kleist, L., Michaelis, S., Bartho, K., Graebner, O., Schlief, M.n., Dreger, M., Schrey, A.K., Sefkow, M., Kroll, F., and Koester, H. (2016). Identification of potential off-target toxicity liabilities of catechol-O-methyltransferase inhibitors by differential competition capture compound mass spectrometry. Journal of Medicinal Chemistry *59*, 4664-4675.
Walter, U., Beyer, M., Klein, J., and Rehm, H.-J. (1991). Degradation of pyrene by *Rhodococcus* sp. UW1. Applied Microbiology and Biotechnology *34*, 671-676.
Wasilkowski, D., Swedziol, Z., and Mrozik, A. (2012). The applicability of genetically modified microorganisms in bioremediation of contaminated environments. Chemik *66*, 817-826.
Wessel, N., Ménard, D., Pichavant-Rafini, K., Ollivier, H., Le Goff, J., Burgeot, T., and Akcha, F. (2012). Genotoxic and enzymatic effects of fluoranthene in microsomes and freshly isolated hepatocytes from sole (*Solea solea*). Aquatic Toxicology *108*, 33-41.
Wick, L., De Munain, A., Springael, D., and Harms, H. (2002). Responses of *Mycobacterium* sp. LB501T to the low bioavailability of solid anthracene. Applied Microbiology and Biotechnology *58*, 378.
Wild, S.R., and Jones, K.C. (1995). Polynuclear aromatic hydrocarbons in the United Kingdom environment: a preliminary source inventory and budget. Environmental Pollution *88*, 91-108.
World Wide Fund (2018). Toxic Chemicals. WWF.panda.org.
Wu, A., Duan, Y., Xu, D., Penning, T.M., and Harvey, R.G. (2010). Regiospecific oxidation of polycyclic aromatic phenols to quinones by hypervalent iodine reagents. Tetrahedron *66*, 2111-2118.

Wu, Y., Teng, Y., Li, Z., Liao, X., and Luo, Y. (2008). Potential role of polycyclic aromatic hydrocarbons (PAHs) oxidation by fungal laccase in the remediation of an aged contaminated soil. Soil Biology and Biochemistry *40*, 789-796.

Yamaguchi, M., Higuchi, M., Tazawa, K., and Manabe, K. (2016). Three-step synthesis of fluoranthenes through Pd-catalyzed inter-and intramolecular C–H arylation. The Journal of Organic Chemistry *81*, 3967-3974.

Zhang, X.-J., Shi, Z., Lyv, J.-X., He, X., Englert, N.A., and Zhang, S.-Y. (2015). Pyrene is a novel constitutive androstane receptor (CAR) activator and causes hepatotoxicity by CAR. Toxicological Sciences *147*, 436-445.

Zhang, Y., Huang, L., Wang, C., Gao, D., and Zuo, Z. (2013). Phenanthrene exposure produces cardiac defects during embryo development of zebrafish (*Danio rerio*) through activation of MMP-9. Chemosphere *93*, 1168-1175.

Zhang, Y., Wang, C., Huang, L., Chen, R., Chen, Y., and Zuo, Z. (2012). Low-level pyrene exposure causes cardiac toxicity in zebrafish (*Danio rerio*) embryos. Aquatic Toxicology *114*, 119-124.